SPRINGER BRIEFS IN ENVIRONMENTAL SCIENCE

Sima Bagheri

Hyperspectral Remote Sensing of Nearshore Water Quality

A Case Study in New York/New Jersey

Springer

SpringerBriefs in Environmental Science

SpringerBriefs in Environmental Science present concise summaries of cutting-edge research and practical applications across a wide spectrum of environmental fields, with fast turnaround time to publication. Featuring compact volumes of 50 to 125 pages, the series covers a range of content from professional to academic. Monographs of new material are considered for the SpringerBriefs in Environmental Science series.

Typical topics might include: a timely report of state-of-the-art analytical techniques, a bridge between new research results, as published in journal articles and a contextual literature review, a snapshot of a hot or emerging topic, an in-depth case study or technical example, a presentation of core concepts that students must understand in order to make independent contributions, best practices or protocols to be followed, a series of short case studies/debates highlighting a specific angle.

SpringerBriefs in Environmental Science allow authors to present their ideas and readers to absorb them with minimal time investment. Both solicited and unsolicited manuscripts are considered for publication.

More information about this series at http://www.springer.com/series/8868

Sima Bagheri

Hyperspectral Remote Sensing of Nearshore Water Quality

A Case Study in New York/New Jersey

Springer

Sima Bagheri
Department of Civil and Environmental
Engineering
New Jersey Institute of Technology
Newark, NJ
USA

ISSN 2191-5547 ISSN 2191-5555 (electronic)
SpringerBriefs in Environmental Science
ISBN 978-3-319-46947-8 ISBN 978-3-319-46949-2 (eBook)
DOI 10.1007/978-3-319-46949-2

Library of Congress Control Number: 2016953642

Printed on acid-free paper

This Springer imprint is published by Springer Nature
The registered company is Springer International Publishing AG
The registered company address is: Gewerbestrasse 11, 6330 Cham, Switzerland

Preface

This monograph presents the results of the assessment of the water quality conditions in the Hudson/Raritan Estuary and the New Jersey coastal waters, Two decades of research venture utilizing remotely sensed data. Components of the concept of assessment of water quality conditions using multispectral satellite, videography and imaging spectroscopy data in coordination with in situ measurements are discussed and results of such analysis are presented.

The focus of the study is the New Jersey estuarine and nearshore waters which is considered as a valued ecological, economic and recreational resource within the New York metropolitan area. These waters are enriched by increased nutrient loading from point, non-point sources such as agricultural and urban run-off causing eutrophication and pollution. Water pollution is a major global problem that requires continuing evaluation and revision of water resources policies at all levels. Moreover we are heading towards a water crisis, caused by climate change with significant impact on coastal environment; home to majority of population worldwide. To improve the quality of water and control the problem of excessive fertilization, regular monitoring of water quality is required. Currently there is no systematic management tool for operational monitoring and prediction of spreading of pollution in this area. Conventional shipboard sampling is both time consuming and labor intensive while there is a critical need for an economical management system for the estuary and its high susceptibility to the various sources of pollution and environmental hazards. Remote sensing can provide greater economy in many types of hydrologic surveys than using conventional methods. This is possible since certain bio–and geochemical constituents of surface/near-surface water produce changes in reflectance which can be measured by optical remote sensors.

The monograph details the development of a remote sensing water quality monitoring/management system with emphasis on the discrimination between organic and inorganic turbidity promoting eutrophication. It demonstrates the use of bio-optical modeling and retrieval techniques to derive the concentrations of important water quality parameters (chlorophyll, color dissolved organic matter and suspended sediments) in the study area. It illustrates methods and analysis approaches that have been used in the datasets to improve detection and

characterization of nearshore water quality issues in order to provide the managers and planners how to improve the conditions for reducing the frequency and extent of algal blooms and eutrophication. The work should further research and potentially lead to improved understanding of the characteristics of algal blooms important in global climate change studies.

The monograph is aimed at a wide audience, ranging from the graduate students and the working scientists to policy makers and managers. Efforts have been made to highlight general principles as well as the site-specific application. It also provides a detailed bibliography at the end of each chapter for those wishing to delve deeper into the field.

Newark, USA Sima Bagheri

Acknowledgments

This monograph was based on the research project funded by the National Science Foundation (BES-9806982) (1998–2001). Support of the NASA Head quarters and the AVIRIS Science Team for multiyear data acquisitions of the AVIRIS over the study site was greatly appreciated. Support of NOAA J.J. Howard Sandy Hook Laboratory and Marine Academy of Science and Technology (MAST) Vocational school in Fort Hancock, NJ for providing ship time and access to the laboratory facility is much appreciated.

This monograph was prepared during my sabbatical leave from teaching in academic year 2015–2016. Funding support during sabbatical leave was provided by the New Jersey Institute of Technology.

My sincere thanks to Dr. Steef Peters from Water Insight and Mary Balogh, from USFWS for their expert reviews of the monograph. They graciously made time in their incredibly busy schedules to provide significant feedback and comments to improve the monograph. The invaluable contributions of Dr. Anatoly Gitelson, from the University of Nebraska, Lincoln and Dr. Zoe-Helen Michalopoulou from New Jersey Institute of Technology in Chap. 6 of the monograph is greatly appreciated.

Contents

Chapter 1
Introduction

Abstract Currently there are numerous efforts underway to improve the understanding of physical, chemical and biological characteristics of waters including remote sensing techniques. Remotely sensed data give information on the interaction between solar radiation, sea water and the different substances contained within it. Remote sensing methods can be used to determine water quality parameters, such as the trophic state, Secchi depth, turbidity, concentration of chlorophyll-a or suspended inorganic matter. The study area—Hudson/Raritan Estuary is one of the most productive regions in the world and it is declared as a major natural and scenic resource to both NY and NJ. At the same time, it is one of the most intensively developed and industrialized estuaries in the world. With increasingly sophisticated sensors, better data, and improved algorithms, water quality parameters–phytoplankton detection and species identification can be accurately determined. Remote sensing as a monitoring/management tool can complement the local and state government efforts in combating the factors attributed to water pollution control infrastructure.

Keywords Remote sensing techniques · Water quality parameters · Trophic state · Secchi depth · Turbidity · Phytoplankton · Chlorophyll-a · Total suspended matter (TSM) · Colored dissolve organic matter (CDOM) · Monitoring · Inherent optical properties (IOP) · Electromagnetic energy · Algal bloom · Case 1 and case 2 waters · Videography · Multispectral data · Imaging spectroscopy

1.1 Overview

Hudson/Raritan Estuary is a component of the New York Harbor (NYH) which is formed by a network of interconnected tidal waterways along the shores of New York and northern New Jersey. NYH is bounded by the Hudson River to the north, Long Island Sound to the east, and the Atlantic Ocean to the south. It's comprised of (1) The Hudson/Raritan Estuary, and (2) NY/NJ Bight area extending from Montauk Point in Long Island to Cape May, New Jersey as shown in Fig. 1.1.

S. Bagheri, *Hyperspectral Remote Sensing of Nearshore Water Quality*,
SpringerBriefs in Environmental Science, DOI 10.1007/978-3-319-46949-2_1

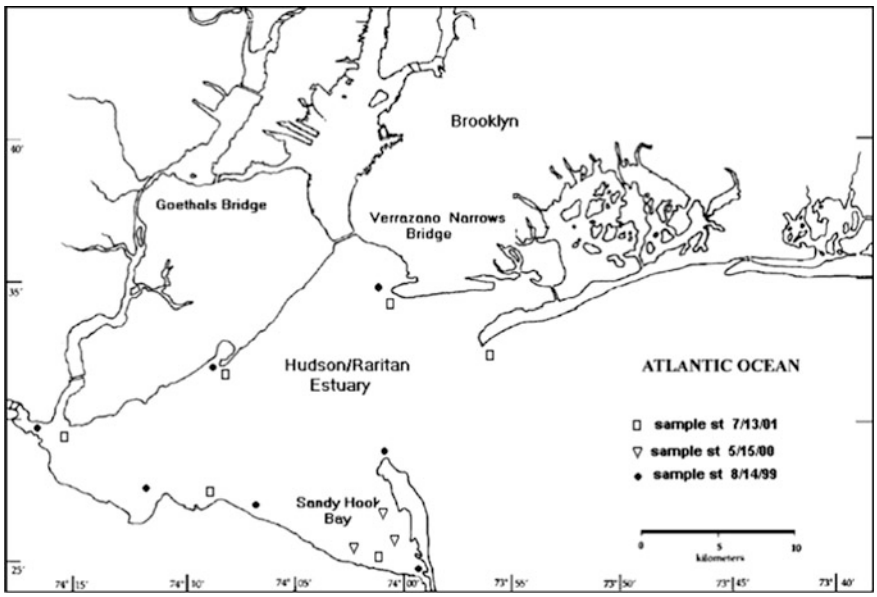

Fig. 1.1 The Map of the study area with locations of sample points surveyed

The study area, Hudson-Raritan Estuary forms at the confluence of the Hudson and Raritan rivers with the Atlantic Ocean. It is one of the most productive regions in the world (Marshall and Cohn 1987) and it is declared as a major natural and scenic resource to both NY and NJ (Sieburth et al. 1988). At the same time, it is one of the most-trafficked and most intensively developed and industrialized estuaries in the world. The waters are enriched by increased nutrient loading from point, non-point sources such as agricultural and urban run-off creating eutrophication and pollution. The industrial wastewater discharges and combined sewer outflows contributed to low dissolved oxygen. Pollution from ships routinely spills into the Hudson-Raritan Estuary, as well as the debris (i.e., fuel, garbage, sewage, and ballast) and industrial waste and pesticides which travel downstream and settle in the water and sediment of the estuary (http://education.nationalgeographic.com/education/encyclopedia/estuary/?ar_a=1).

Long-term water quality records for most locations in the estuary illustrate degradation from population growth and inadequate sewage treatment through the mid-1960s with gradual improvement following construction of wastewater treatment plants and implementation of secondary treatment (O'Shea and Brosnan 1997).

Historically, water quality problems in the estuary have included severe oxygen depletion and closure of shellfish beds and recreational beaches due to bacterial contamination. More recently, nutrient enrichment, algal blooms, heavy metals, sediment contamination, and bioaccumulation of toxins such as PCBs in striped bass (Thomann et al. 1992) degraded estuarine water quality.

To protect and preserve the New York/New Jersey estuarine and coastal environment, state and federal programs including the NY/NJ Harbor Estuary Program (HEP) (Walker et al. 1999), NY/NJ Clean Ocean and Shore Trust (COAST) (Wright and Bartlett 2000), and the NJ Coastal Management Program (CMP) (Randle 1982) have been established. The National Estuary Program which is designed to encourage local communities to take responsibility for managing their own estuaries has designated the Hudson/Raritan Estuary as an Estuary of National Significance in 1988 (Walker et al. 1999). The program focuses on improving water quality in an estuary, and maintaining the integrity of the whole system—its chemical, physical, and biological properties, as well as its economic, recreational, and aesthetic values (EPA 2002). New Jersey Department of Environmental protection (NJDEP) has monitored water quality as part of the cooperative monitoring program since 1985. NJDEP monitors the condition of the State's coastal waters by measuring basic water quality (dissolved oxygen, nutrients and water clarity) on a quarterly basis. EPA's National Coastal Assessment (NCA) research program is performed in partnership with NJDEP and includes measurements of sediment chemistry, sediment toxicity and the benthic community annually in New Jersey's estuarine waters. NJDEP also performs a coastal surveillance program using helicopter surveys to identify floatables, oil slicks and algae blooms as well as the dredging projects within the state. Using the NCA ranking indices of estuarine condition, the HEP has found that, although some measures of estuarine health in the study area have demonstrated improvements over time (including increases in dissolved oxygen levels, reductions in nutrient loadings and the decline in bacterial levels attributed to water pollution control infrastructure improvements), other trends, such as ongoing fish consumption advisories and declines in some fish and wading bird populations, have not been as positive. The inadequate availability of data is still a significant barrier to properly interpreting indicators in this estuarine system (EPA 2007).

1.1.1 Review of Water Quality Basics and Importance of Monitoring

According to the European Union Water Framework Directives 2000/60/EC and 2006/7/EC, the assessment of water quality in coastal and inland areas is a priority.

The major factors which can influence the quality of coastal water (excluding the aquatic macro-fauna) are: suspended sediments (turbidity), phytoplankton and cyanobacteria (i.e., chlorophylls, carotenoids), dissolved organic matter (DOM), organic and inorganic nutrients, pesticides, metals, thermal releases, macrophytic algae, pathogens, and oils. With the exception of chemicals and pathogens, the above mentioned factors affect the optical and/or thermal properties of waters thus directly changing the signal acquired by optical sensors over water bodies. For this reason they are also called optically active parameters. While much progress has

been made with the new technology using appropriate optical sensors, the study of coastal and inland waters that mixes suspended mineral particles, dissolved organic matter, organic and inorganic pollutants, is still challenging because, it is complicated by a high spatio-temporal variations.

The absence of comprehensive and integrative strategic planning within the NY/NJ coastal area have resulted in poor coordination and limited enforcement of policies and laws. There is no comprehensive or cohesive management plan dealing with coastal areas. Institutional management is similarly fragmented with a plethora of agencies having concurrent responsibility for managing aspects of the resources of the coastal zone.

Currently there are numerous efforts underway to improve the understanding of physical, chemical and biological characteristics of waters including remote sensing techniques. Remote sensing methods can be used in order to determine water quality parameters, such as the trophic state, Secchi depth, turbidity, concentration of chlorophyll-a or suspended organic matter. Typically, a single indicator will allow us to determine the total impact of various pollutants on the overall status of water. With increasingly sophisticated sensors, better data, and improved algorithms, phytoplankton detection and species identification can be accurately determined using remote sensing data. Remotely sensed data give information on the interaction between solar radiation, sea water and the different substances contained within it. The main processes involved are absorption, scattering and transmission of electromagnetic energy (Aguirre-Gomez et al. 1995). Absorption of light within the marine environment is carried out by four different components: the water itself, phytoplankton, colored dissolved organic matter (CDOM) and total suspended matter (TSM).

This monograph describes the development of a well-calibrated nearshore/coastal water quality model using remote sensing data focusing on Hudson/Raritan Estuary of NY/NJ in United States. The objective is to assess the environmental characteristics of estuarine water in order to understand the complex interactions between the physical, chemical and biological elements of nearshore ecosystem and develop methods to predict/prevent algal blooms in order to preserve the quality of nearshore waters (Bagheri et al. 1999).

1.1.1.1 Definitions of Case 1 and Case 2 Oceanic Water Types

The optical classification of waters is based on a commonly-used method of classifying oceanic waters into one of two types: Case 1 or Case 2 (Morel and Prier 1977; Gordon and Morel 1983). In “Case 1”, scattering in the water arises mainly from organic (phytoplankton) particle, while in “case 2” inorganic particles are significant.

Coastal waters are often referred to as Case 2 water, where the marine phytoplankton is not the dominant, optically active water substance. Particulate matter and colored dissolved organic matter (CDOM), which do not always co-vary with chlorophyll, also affect case 2 water optical properties. Case 2 water can be referred

to as multiparameter water. It must be acknowledged that this classification concept is somewhat idealized because, in reality, all waters belong to an intermediate case (Gordon et al. 1975).

1.1.1.2 Complexity of Case 2 Water

According to Mobley et al. (2004), the definitions of Case 1 and Case 2 were originally developed for optically deep waters. "***If only the Inherent Optical Properties (IOPs) of the water itself is considered, then the bottom is irrelevant. We are unable to formulate well-defined and scientifically justified quantitative criteria for unambiguously classifying a water body or optical property as either Case 1 or Case 2. Therefore it's suggested to drop the Case 1–Case 2 classification and focus on modeling water bodies according to whatever constituents are in the water column and whatever the bottom boundary is when describing the water as Case 1 or 2***". So in that sense, all optically shallow waters are Case 2, even if the water IOPs themselves are Case 1 (Mobley et al. 2004).

In ocean color data, water leaving radiance reaching a remote sensor results from a mixture of optically active substances including phytoplankton chlorophyll, detritus, suspended sediments, and color dissolved organic materials. The presence of several non-correlated constituents makes nearshore (Case 2) waters optically complex than most oceanic (Case 1) waters. The color of Case 1 waters quantified by the subsurface reflectance R(0-) and is a function of absorption and scattering by algal pigments, algal detritus and water itself. In Case 2 waters the combined effects of particulate backscattering and high absorption introduce complex interacting relations between the water constituents and subsurface reflectance (Mobley et al. 2004).

Remote sensing data offers unique advantages for the study of recurrent hydrological/morphological phenomena on regional and local scales. This case study presents results of multispectral data (i.e., Landsat TM, MSC-02 videography (in brief)) and imaging spectroscopy—**NASA**/Airborne Visible Infra Red Imaging Spectrometer (AVIRIS) with emphasis on the latter since high resolution remote sensing data enable us to systematically detect and document the time and space dimensions of water ecosystems. In particular, imaging spectroscopy, with high spatial/spectral resolution can help to derive water quality parameters such as the type and size of suspended particles, toxic algal blooms, and other phytoplankton species that serve as a marker of eutrophication. These parameters are of great interest for various applications such as the determination of primary production in coastal/nearshore waters.

For the purpose of ocean color remote sensing, the nearshore waters of the Hudson/Raritan Estuary are optically classified as Case 2 waters. This means that water leaving radiance reaching a remote sensor results from a mixture of optically active substances, in addition to pure water itself, (IOCCG 2000) including:

- ❖ Phytoplankton. This component also includes phytoplankton and other microscopic organisms with major influence on optical properties of water.
- ❖ Suspended material (inorganic). Even though microscopic organisms are also "suspended" material, we use this term here to represent only suspended material of inorganic nature.
- ❖ Color Dissolved Organic Materials (Yellow Substances). It also includes "detrital" particulate material, which generally has absorption characteristics similar to yellow substances.

1.1.2 Water Quality Monitoring Basics

Water quality is a measure of the suitability of water for a particular use based on selected physical, chemical, and biological characteristics (EPA).

Water-Quality Properties includes:

Color, Temperature, Electric conductivity, Dissolved oxygen, Hardness, pH, Salinity, Suspended sediment and Turbidity.

1.1.2.1 Conventional Water Quality Surveys

There are many ways to monitor water quality conditions. Conventional monitoring includes sampling the chemical condition of water, sediments, and fish tissue to determine levels of key constituents such as dissolved oxygen, nutrients, metals, oils, and pesticides. The method includes monitoring physical variables such as temperature, flow rate, sediments and potential erosion from the banks and shoreline. Monitoring for biological variables includes the abundance and variety of aquatic plant and animal life and the ability of test organisms to survive in the sample water (EPA 2002).

Standards and guidelines are established to protect water for designated uses such as drinking, recreation, agricultural irrigation, or protection and maintenance of aquatic life. The U.S. Environmental Protection Agency (USEPA) and the States are responsible for establishing the standards for constituents in water that have been shown to pose a risk to human health. Other standards protect aquatic life, including fish, and fish-eating wildlife such as birds.

1.1.2.2 Remote Sensing Basics and Its Use as a Monitoring Tool

Overhead sensors record the color of natural water as spectral reflectance, determined by the composition of the upwelling underwater light field. The greater the amount and specificity of color information available, the better a remote hydrological application will generally perform. This is particularly true for estuarine

applications, where independent variations of optically important water quality parameters (WQP), bottom cover types, and water depths can all occur simultaneously. At the same time, all hydrological targets share general characteristics induced by the water medium itself. For example, there is a strong absorption of light with wavelengths shorter than those of blue light or with wavelengths longer than those of near-infrared light. Outside these limits, signals within or beneath any hydrological volume are attenuated so much, that the signals are negligible for practical remote detection.

Measurements of the spectral distribution of light intensity can be obtained by optical remote sensing, a technique to collect color data by detection of upward radiance at a distance (Bagheri et al. 2005). The intensity of reflected light increases with the amount of scattering and decreases by absorption. Parameters related to water color and recorded by ocean color sensors are used to study environmental processes like the primary production of biomass and the distribution of suspended matter. Remotely sensed data can provide greater economy in many types of hydrologic surveys than using conventional methods. This is possible since certain biological and geochemical constituents of surface/nearsurface water produce changes in reflectance that can be measured by the remote sensing sensors (Bagheri et al. 2005).

Remote sensing of coastal waters has developed since the early seventies from an empirically based method producing qualitative water quality maps to more quantitative methods such as semi-analytical and analytical methods, which produce thematic maps of spatial and temporal distribution patterns of parameters of water quality based on the image interpretation and calibration (Morel and Gordon 1980).

Three important optical properties used for monitoring water quality are the concentrations of chlorophyll (CHL_a), color dissolved organic matter (CDOM) and total suspended matter (TSM). In coastal water, the major constituents are the CHL_a, CDOM, TSM and the water itself causing absorption and scattering of light.

Ocean color remote sensing is defined as the study of the interaction between the visible light and aquatic environments from Earth-orbiting satellites. This has opened the way for studying ocean phenomena and processes at finer spatial scales, such as the interactions at the land-sea interface, trends in coastal water quality and algal blooms.

Recent advances in satellite and airborne remote sensing, such as improvements in sensor, algorithm calibrations and processing techniques have provided for increased coverage of remotesensing, ocean-color products for coastal regions. Human population growth and changes in coastal management practices have brought about significant changes in the concentrations of organic and inorganic particulate and dissolved substances entering the coastal waters. There is increasing concern that these inputs have led to declines in water quality and have increased local concentrations of phytoplankton, which cause harmful algal blooms (HABs).

In ocean color remote sensing, the airborne/satellite sensor records the color of natural water as spectral reflectance, which is determined by changes in the spectral composition of the underwater light field (Kirk 1994). In a natural color satellite

imagery, the clear waters of the open ocean look dark blue. Chlorophyll and other pigments in phytoplankton can color the water bright blue, green, and even reddish-brown. Sediment can turn the water milky blue. Organic matter can turn the water tea-colored. For analysis and interpretation of the ocean color, whether observed from just beneath the sea surface or at satellite altitudes, Morel and Gordon (1980) describe three approaches: (i) an empirical method, relying completely on statistical relationships between the upward radiance at the sea surface and the quantity of interest; (ii) a semi-analytical method, in which the spectral characteristics of the parameters of interest are known and some modeling of the physics is introduced; and (iii) an analytical method, in which radiative transfer models are used to extract the inherent optical properties (IOPs).

Ocean color, detected from both aircraft and satellite remote sensing platforms, has the capability to quantitatively measure water column phytoplankton biomass if the signals can be quantitatively interpreted (Figs. 1.2 and 1.3). When coupled with appropriate in situ measurements, ocean color data can be used to estimate water column primary productivity (NOAA 2010) http://www.lib.noaa.gov/about/news/fan_04152010.pdf. Figure 1.3a, b show the measurements of ocean color based on electromagnetic energy of 400–700 nm wavelengths. This energy is emitted by the sun, transmitted through the atmospher and reflected by the earth surface.

Determination of chlorophyll-a concentration, as an indication of phytoplankton photosynthesis (primary production), is the main objective of the remote monitoring of estuarine/nearshore waters. Such measurements can give information about the biology of the oceans/coastal zones, which plays an important role in the exchange of carbon dioxide between ocean and atmosphere critical in global change investigations. Using remote sensing data, changes in bio/geochemical constituents of surface waters can be monitored and analyzed.

This monograph describes the construction of a bio-optical water quality model (Gordon et al. 1975) linking the water constituent concentrations to (i) the inherent

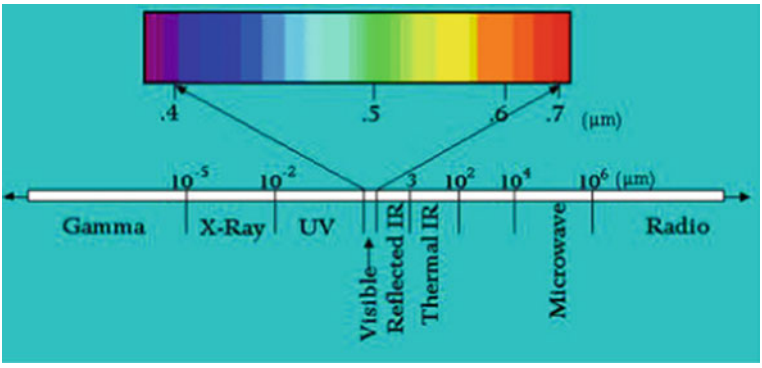

Fig. 1.2 The measurements of ocean color based on electromagnetic energy of 400–700 nm wavelengths (*Source* NASA Earth Observatory)

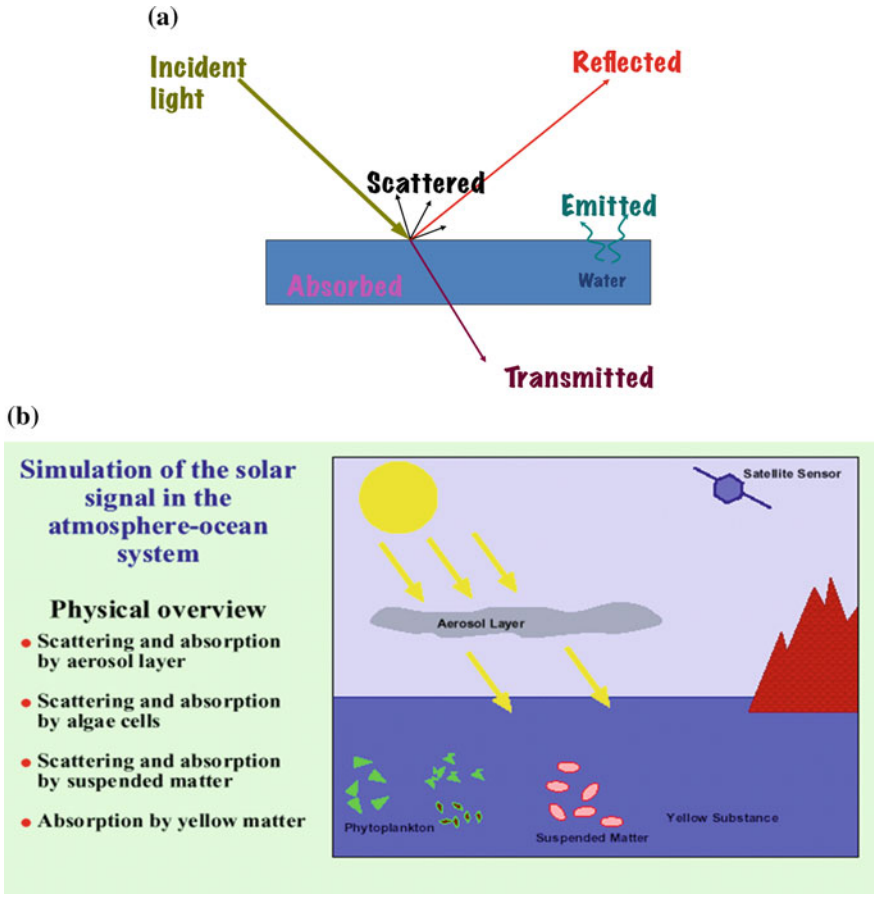

Fig. 1.3 EMR interactions with coastal water (**a**) and with water constituents (**b**)

optical properties (IOPs) , using the specific inherent optical properties (SIOP), and (ii) to the subsurface light levels (Dekker et al. 2011). Generation of accurate reflectance (R(0)) from radiance recorded by the NASA/AVIRIS sensor is the key parameter for input into inverse modeling for estimation of constituent concentrations. In conjunction with bio-optical model, the linear matrix inversion technique (Hoge et al. 1996) is used for retrieval of estuarine water constituents in terms of chlorophyll, colored dissolved organic matter and inorganic material. The long term goal is the establishment of a monitoring/management system for retrieval of estuarine water constituents using remotely sensed data. Subsequently, the results can be integrated into a computer-based geospatial database for use as a management tool for monitoring of water quality conditions of the estuary. Such efforts are complementary to the development of interactive maps at local and global scales and establishment of a spectral library for detection/identification of harmful algal blooms (HABs) causing eutrophication and pollutions in the coastal and estuarine waters.

1.1.3 Introduction to Hyperspectral Remote Sensing—Historical Perspective

Remote sensing of ocean color from space began in 1978 with the launch of NASA's Coastal Zone Color Scanner (CZCS). For detailed description of all sensors (IOCCG 2000) listed the readers are referred to (NASA/GSFC website).

Although CZCS was an experimental mission, the sensor continued to generate a valuable data until early 1986. CZCS had six spectral bands, four of which were used primarily for ocean color. These were of a 20 nm bandwidth centered at 443, 520, 550, and 670 nm. Band 5 had a 100 nm bandwidth centered at 750 nm and a dynamic range more suited to land. Band 6 operated in the 10.5–12.5 μm region and sensed emitted thermal radiance for derivation of equivalent black body temperature.

Ten years later, with the launch of a new generation of ocean color sensors—MOS, OCTS and POLDER in 1996 and SeaWiFS in 1997 the ocean color data became available to the science community. See Tables 1.1 and 1.2 for historical and current Ocean Color Sensors.

In reference to the international ocean color missions, the Japanese Space Agency, NASDA launched the Advanced Earth Observing Satellite (ADEOS) On August 17, 1996. Among the instruments carried aboard the ADEOS spacecraft was the Ocean Color and Temperature Scanner (OCTS). OCTS is an optical radiometer with 12 bands covering the visible, near infrared and thermal infrared regions (Eight of the bands in the VIS/NIR are used for oceanographic research).

SeaWiFS provided quantitative data on global ocean bio-optical properties to the science community. SeaWiFS had 8 spectral bands from 412 to 865 nm. It collected global data at 4 km resolution, and local data at 1 km. The mission and sensor were optimized for ocean color measurements, with a local noon (descending) equator crossing time orbit, fore-and-aft tilt capability, full dynamic range, and low polarization sensitivity. Detailed description is available on: http://oceandata.sci.gsfc.nasa.gov.

Several new ocean color sensors have recently been launched and still more are planned for the near future by various space agencies. These sensors capture continuous global ocean color data (e.g. chlorophyll concentration) providing significant benefits for research in areas of biological oceanography and climate change studies. The missions listed below (Table 1.2) were developed and launched with the same objective to optimize the ocean color measurements:

MODIS (Moderate Resolution Imaging Spectroradiometer) is a key instrument aboard the Terra (EOS AM) and Aqua (EOS PM) satellites. Terra MODIS and Aqua MODIS are viewing the entire Earth's surface every 1 to 2 days, acquiring data in 36 spectral bands. MODIS scans the ocean in the infrared and the visible portions of the spectrum. It can detect extremely subtle changes in the temperature and color of the water.

MERIS (lunched by the European Space Agency) is a programmable, medium-spectral resolution, imaging spectrometer operating in the solar reflective

Table 1.1 Historical ocean color sensors

Sensor/data source	Agency	Satellite	Operating dates	Swath (km)	Spatial resolution (m)	# of bands	Spectral coverage (nm)	Orbit
CZCS	NASA	Nimbus-7	24/10/78–22/6/86	1556	825	6	433–12,500	Polar
	(USA)	(USA)						
CMODIS	CNSA	SZ-3	25/3/02–15/9/02	650–700	400	34	403–12,500	Polar
	(China)	(China)						
COCTS	SOA	HY-1A	15/5/02–1/4/04	1400	1100	10	402–12,500	Polar
CZI	(China)	(China)		500	250	4	420–890	
GLI	NASDA	ADEOS-II	14/12/02–24/10/03	1600	250/1000	36	375–12,500	Polar
	(Japan)	(Japan)						
HICO	ONR, DOD and NASA	JEM-EF	18/09/09–4/12/14	50 km	100	124	380–1000	51.6°
		Int. Space Stn.		Selected coastal scenes				15.8 orbits p/d
MERIS	ESA	ENVISAT	1/3/02–9/5/12	1150	300/1200	15	412–1050	Polar
	(Europe)	(Europe)						
MOS	DLR	IRS P3	21/3/96–31/5/04	200	500	18	408–1600	Polar
	(Germany)	(India)						
OCI	NEC	ROCSAT-1	27/01/99–16/6/04	690	825	6	433–12,500	Polar
	(Japan)	(Taiwan)						
OCM	ISRO	IRS-P4	26/5/99–8/8/10	1420	360/4000	8	402–885	Polar
	(India)	(India)						
OCTS	NASDA	ADEOS	17/8/96–29/6/97	1400	700	12	402–12,500	Polar
	(Japan)	(Japan)						

(continued)

Table 1.1 (continued)

Sensor/data source	Agency	Satellite	Operating dates	Swath (km)	Spatial resolution (m)	# of bands	Spectral coverage (nm)	Orbit
OSMI	KARI (Korea)	KOMPSAT-1/Arirang-1 (Korea)	20/12/99–31/1/08	800	850	6	400–900	Polar
POLDER	CNES (France)	ADEOS (Japan)	17/8/96–29/6/97	2400	6 km	9	443–910	Polar
POLDER-2	CNES (France)	ADEOS-II (Japan)	14/12/02–24/10/03	2400	6000	9	443–910	Polar
POLDER-3	CNES (France)	Parasol	Dec 2004–Dec 2013	2100	6000	9	443–1020	Polar
SeaWiFS	NASA (USA)	OrbView-2 (USA)	01/08/97–14/02/11	2806	1100	8	402–885	Polar

Source International Ocean Color Coordinating Group (IOCCG)
Website: http://www.ioccg.org/sensors/

Table 1.2 Current ocean color sensors

Sensor/data link	Agency	Satellite	Launch date	Swath (km)	Spatial resolution (m)	Bands	Spectral coverage (nm)	Orbit
COCTS	SOA	HY-1B	11-Apr-07	3000	1100	10	402–885	Polar
CZI	(China)			500	250	4	433–695	
GOCI	KARI/KIOST	COMS	26-Jun-10	2500	500	8	400–865	Geostationary
	(South Korea)							
MERSI	CMA	FY-3A	27-May-08	2900	250/1000	20	402–2155	Polar
	(China)							
MERSI	CMA	FY-3B	5-Nov-10	2900	250/1000	20	402–2155	Polar
	(China)							
MERSI	CMA	FY-3C	23-Sep-13	2900	250/1000	20	402–2155	Polar
	(China)							
MODIS-Aqua	NASA	Aqua	4-May-02	2330	250/500/1000	36	405–14,385	Polar
	(USA)	(EOS-PM1)						
MODIS-Terra	NASA	Terra	18 Dec. 1999	2330	250/500/1000	36	405–14,385	Polar
	(USA)	(EOS-AM1)						
OCM-2	ISRO	Oceansat-2	23 Sept. 2009	1420	360/4000	8	400–900	Polar
	(India)	(India)						
OLCI	ESA/EUMETSAT	Sentinel 3A	16-Feb-16	1270	300/1200	21	400–1020	Polar
VIIRS	NOAA	Suomi NPP	28 Oct. 2011	3000	375/750	22	402–11,800	Polar
	(USA)							

Source International Ocean Color Coordinating Group (IOCCG)
Website: http://www.ioccg.org/sensors/

spectral range. 15 spectral bands can be selected by ground command. The instrument scans the Earth's surface by the "push-broom" method. MERIS is designed to acquire data over the Earth whenever illumination conditions are suitable.

MODIS has daily repeat cycles whereas MERIS had a 1–2 day revisit cycle. MERIS has also collected data at 300 × 300 m pixel resolution whereas MODIS has several bands at 250 and 500 m resolution for use in coastal waters. The two sensors provide important information on the global aspects of water quality.

The Aquarius/SAC-D mission was developed collaboratively between NASA and Argentina's space agency. It is the first space-based global observations of ocean surface salinity with a resolution of 150 km (93 miles) showing the variations in salinity changes from month to month, season to season and year to year. Aquarius data combined with in-water measurements generate operational maps of ocean salinity distributions with climate change implications.

NOTE. Although it is considered that MODIS and MERIS both are part of the Hyperspectral Remote Sensing (HRS) activities in space, but in terms of both spatial and spectral resolutions, these sensors and projects still lag behind the ideal HRS sensor with high spectral resolution, more than 100 narrow bands, and high spatial resolution with less than 30 m ground sample distance (GSD). The data are complimentary to MODIS and MERIS data.

1.1.3.1 Space-Borne Hyperspectral Missions

Recent advances in sensor technology have led to the development of hyperspectral sensors (also known as imaging spectrometers) capable of collecting imagery containing several hundred bands over the electromagnetic spectrum.

The concept of hyperspectral remote sensing began in the mid-1980s and has been used most widely by geologists for identification and mapping of minerals. Spectroscopy can be used to detect individual absorption features due to specific chemical bonds in a solid, liquid, or gas (Lee and Landgrebe 1993).

Today, these sensors greatly expand the potential of remote sensing to assess, map, and monitor the characteristics of all natural resources including marine coastal zones.

Hyperspectral data are particularly useful in marine coastal zones because of the spectral complexity of suspended as well as benthic features found in these environments (Richardson 2000). Hyperspectral data from a satellite can also provide the best information, with current technology, on how the global carbon budget is changing (Ustin et al. 2011).

The launch of NASA's EO-1 Hyperion sensor in 2000 marked the establishment of a spaceborne hyperspectral sensor with mineral mapping capabilities. The Hyperion senor covers the 0.4–2.5 μm spectral range with 242 spectral bands at approximately 10 nm spectral resolution and 30 m spatial resolution from a 705 km orbit (Pearlman et al. 1999). Although designed for land applications, Hyperion was tested for its capabilities over a range of water targets in Eastern Australia,

including Moreton Bay. This region was selected due to its spatial gradients in optical depth, water quality, bathymetry, and substrate composition (Brando et al. 2003).

(HICO™) Hyperspectral Imager for the Coastal Ocean is the first spaceborne imaging spectrometer designed to sample the coastal ocean. HICO samples selected coastal regions at 90 m with full spectral coverage (380–960 nm sampled at 5.7 nm) and has a very high signal-to-noise ratio to resolve the complexity of the coastal ocean. HICO demonstrates coastal products including water clarity, bottom types, bathymetry and on-shore vegetation maps. The current focus is on providing HICO data for scientific research on coastal zones and other regions around the world (http://oceancolor.gsfc.nasa.gov/cms/data/hico).

Future planned ocean color satellite missions include:

(a) EnMAP (Environmental Mapping and Analysis Program) is a German hy-perspectral satellite mission providing high-quality hyperspectral image data on a timely and frequent basis. Its main objective is to investigate a wide range of ecosystem parameters including coastal zones and inland waters. The launch of the EnMAP satellite is envisaged for 2015.

(b) HySPIRI is a new NASA initiative to place a HRS sensor in orbit and is intended to complement EnMAP, as its data acquisition covers the globe periodically. The HyspIRI mission will study the world's ecosystems and provide critical information on natural disasters such as volcanoes, wildfires and drought. The HyspIRI mission includes two instruments—an imaging spectrometer measuring from the visible to short wave infrared (VSWIR: 380 nm–2500 nm) in 10 nm contiguous bands and a multispectral imager measuring from 3 to 12 um in the mid and thermal infrared (TIR). The VSWIR and TIR instruments both have a spatial resolution of 60 m at nadir. The VSWIR will have a revisit of 19 days and the TIR will have a revisit of 5 days. HyspIRI also includes an Intelligent Payload Module (IPM) which will enable direct broadcast of a subset of the data file://localhost/ (http/:: hyspiri.jpl.nasa.gov).

It is important to mention that other national agencies are working to place HRS sensor in orbit as well. A good example is PRISMA of the Italy's space agency. PRISMA is a push broom sensor with swath of 30–60 km, GSD of 20–30 m (2.5–5 m PAN) with a spectral range of 0.4–2.5 μm. The satellite launch was set for the end of 2013 and the new lunch date is unknown.

ISIS (International Satellite Imaging Spectrometry, http://www.isiswg.org) group provides a forum for technical and programming discussions and consultation among national space agencies, research institutions and other spaceborne HRS/IS data providers.

The main goals of the group are to share information on current and future spaceborne IS ("hyperspectral") missions, and to seek opportunities for new international partnerships to the benefit of the global user community.

WorldView 2 is operating at an altitude of 770 km. WorldView 2 enables DigitalGlobe to offer half-meter panchromatic resolution and 1.8 m multispectral resolution. The WorldView 2 system allows DigitalGlobe to substantially expand its imagery product offerings to both commercial and international customers with a more commercially desirable, higher performance product. Added spectral diversity provides the ability to perform precise change detection and mapping. WorldView 2 incorporates the industry standard four multispectral bands (red, blue, green and near-infrared) and also includes four new bands (coastal, yellow, red edge, and near-infrared).

The WorldView 2 telescope has a 110 cm aperture and flys at a higher altitude of 770 km. It provides the same panchromatic half-meter resolution imagery as WorldView 1, in addition to 1.8 m multispectral resolution imagery.

A mostly identical WorldView 3 earth observation satellite was launched in 2014. This satellite has an additional infra-red capability. From its lower orbit of 617 km, it has a ground resolution of 0.31 m.

1.1.3.2 Airborne Hyperspectral Remote Sensing

Numerous airborne systems have been developed and flown over the past three decades. Recent review papers (i.e., Ben Dor 2012) list over twenty airborne imaging spectrometers.

The first Airborne Imaging Spectrometer (AIS) developed in 1983 was followed by the Airborne Visible/infrared Imaging Spectrometer (AVIRIS) in 1987. AVIRIS has gone through numerous upgrades and it is proved to be the prime provider of high quality hyperspectral data. Improvements have come in signal-to-noise ratio, radiometric and spectral calibration accuracy (Green et al. 2001). Since the focus of the case study in this monograph is the application of the AVIRIS data, the emphasis is placed on the characteristics of the AVIRIS as compared to other airborne hyperspectral data. For a detailed description on other airborne imaging spectrometers the readers are referred to Ben Dor (2012).

AVIRIS is a 224-channel imaging spectrometer with approximately 10 nm spectral resolution covering the 0.4–2.5 μm spectral range. The sensor is a whiskbroom system utilizing scanning foreoptics to acquire cross-track data. The instantaneous field of view (IFOV) is 1 milliradian. Four off-axis double-pass Schmidt spectrometers receive incoming illumination from the foreoptics using optical fibers. Four linear arrays, one for each spectrometer, provide high sensitivity in the 0.4–0.7 μm, 0.7–1.2 μm, 1.2–1.8 μm, and 1.8–2.5 μm regions respectively. (Green et al. 2001).

AVIRIS is flown by NASA Jet Propulsion Laboratory (JPL) as a research instrument on the NASA ER-2 aircraft at an altitude of approximately 20 km, resulting in approximately 20-m pixels and a 10.5-km swath width. Since 1998, it has also been flown on a Twin Otter aircraft at low altitude, yielding 2–4 m spatial resolution.

The main objective of the AVIRIS project is to identify, measure, and monitor constituents of the Earth's surface and atmosphere based on molecular absorption and particle scattering signatures. Research with AVIRIS data is predominantly focused on understanding processes related to the global environment and climate change http/:aviris.jpl.nasa.gov:index.html.

References

Aguirre-Gomez R, Boxal SR, Weeks AR (1995) Identification of algal pigments using high order derivatives. IEEE Proc 2084–2086

Bagheri S, Zetlin C, Dios R (1999) Estimation of optical properties of nearshore waters. Int J Remote Sensing 20:3393–3397

Bagheri S, Peters S, Yu T (2005) Retrieval of marine water constitutes from AVIRIS data in the Hudson/Raritan Estuary. Int J Remote Sens 26(18):4013–4027

Ben Dor E, Malthus T, Plaza A, Schläpfer D (2012) Hyperspectral remote sensing. Wiley, New York, pp 1160

Brando Vittorio E, Dekker Arnold G (2003) Satellite hyperspectral remote sensing for estimating estuarine and coastal water quality. IEEE Trans Geosci Remote Sens 41(6):1378

Dekker AG, Stuart RP, Anstee J, Bissett P, Brando VE, Casey B, Fearns P, Hedley J, Klonowski W, Lee ZP, Lynch M, Lyons M, Mobley M, Roelfsem C (2011) Intercomparison of shallow water bathymetry, hydro-optics, and benthos mapping techniques in Australian and Caribbean coastal environments. www.aslo.org/lomethods/free/2011/0396.html

Gordon HR, Morel AY (1983) Remote assessment of ocean color for interpretation of satellite visible imagery, a review, in lecture notes on coastal and estuarine studies. Springer, New York, pp 144

Gordon HR, Brown OB, Jacobs MM (1975) Computed Relationships between inherent and apparent optical properties of a flat homogeneous ocean. Appl Optics 14:417–427

Green and Betina Pavri (2001) AVIRIS Inflight calibration experiment results for 2001. NASA/JPL, AVIRIS Workshop

Hoge FE, Wright CW, Lyon PE, Swift RN, Yungel JK (1999) Satellite retrieval of inherent optical properties by inversion of an oceanic radiance model: A preliminary algorithm. Appl Opt 38 (3):495–504

EPA (2002) http://water.epa.gov/polwaste/wastewater/treatment/upload/2002_06_28_wquality_chap06.pdf. http://water.epa.gov/type/watersheds/monitoring/bioassess.cfm

IOCCG (2000) Remote sensing of ocean colour in coastal, and other optically-complex, waters. Sathyendranath, S. (ed.), *Reports of the International Ocean-Colour Coordinating Group*, No. 3, IOCCG, Dartmouth, Canada

Kirk J (1994) Light and photosynthesis in aquatic ecosystems. Cambridge University Press

Lee C, Landgrebe DA (1993). Feature extraction based on decision boundaries. IEEE Trans Geosci Remote Sensing 15(4):388–400

Marshall H, Cohn M (1987) Phytoplankton composition of the New York bight and adjacent waters. J Plankton Res 9(2):267–276

Mobley CD, Stramski D, Bissett WP, Boss E (2004) Optical modeling of ocean waste—Is case 1 case 2 classification still useful? Oceanography 65

Morel A, Prieur L (1997) Analysis of variations in ocean color. Limnol Oceanogr 22:709–722

Morel A, Gordon HR (1980) Report of the working group on ocean color. Boundary Layer Meteoroid 18:343–355

NationalGeographic: (http://education.nationalgeographic.com/education/encyclopedia/estuary/?ar_a=1)

O'Shea ML, Brosnan TM (1997) New York harbor water quality survey. Main report and appendices 1995. New York Department of Environmental Protection, Bureau of Wastewater Pollution Control, Division of Scientific Services, Marine Sciences Section, Wards Island, NY

Pearlman J, Carman S, Lee P, Liao L, Segal C (1999) Hyperion imaging spectrometer on the new millennium program earth orbiter-1 system. In: Proceedings of International Symposium on Spectral Sensing Research (ISSSR), Systems and Sensors for the New Millennium, published on CD-ROM, International Society for Photogrammetry and Remote Sensing (ISPRS)

Randle E (1982) National reserve system and transferable development rights: is the New Jersey Pinelands Plan an unconstitutional taking? BC Envtl Aff L Rev 10:183

Richardson L (2000) Hyperspectral remote sensing of the ocean; Volume 4154; 115–123; (SEE 20010092254). NOAA: http://www.lib.noaa.gov/about/news/fan_04152010.pdf

Sieburth J, Johnson P, Hargraves P (1988) Ultrastructure and ecology of *Aureococcus anophageferens* gen. et sp. nov. (Chrysophyceae): the dominant picoplankter during a bloom in Narragansett Bay, Rhode Island, Summer 1985. J Phycol 24(3):416–425

Thomann et al (1992) Environmental toxicology and risk assessment, 3(1218)

Ustin SL, Zarco-Tejada PJ, Asner GP (2011) The role of hyperspectral data in understanding the global carbon cycle NASA/JPL, Aviris Workshop

Walker W, McNutt R, Maslanka C (1999) The potential contribution of urban runoff to surface sediments of the Passaic River: sources and chemical characteristics. Chemosphere 38(2): 363–377

Wright D, Bartlett D (2000) Marine and coastal geographical information systems. CRC

Chapter 2
New York/New Jersey Nearshore Waters—A Case Study in NY/NJ

Abstract The study area is the New York/New Jersey estuarine and nearshore waters. These waters are enriched by increased nutrient loading from point, non-point sources such as agricultural and urban run-off causing eutrophication and pollution. Eutrophication disrupts the pre-existing natural balance of the system, resulting in phytoplankton blooms of both increased frequency and intensity in response to the over-enrichment. Dense and accelerated phytoplankton blooms ultimately increase oxygen demand on the system leading to episodes of hypoxia. To improve the quality of water and control the problem of excessive fertilization, regular monitoring of water quality is required.

Keywords Airborne Visible Infrared Imaging Spectrometer (AVIRIS) · Hudson/Raritan Estuary · Marine geology · Ecology · Hypoxia · Harmful algal blooms · Bioindicator · Nanoplankton · Netplankton · Chlorophyta · Diatoms · Cyanobacteria · Brown tides · Marine geology · Estuarine waters · Polychaetes · Phytoplankton · Zooplankton · Eutrophication

2.1 Environmental Setting of NY/NJ Nearshore Waters

Hudson/Raritan Estuary of NewYork/New Jersey is a complex estuarine system where tidal and wind-driven currents are modified by freshwater discharges from the Hudson, Raritan, Hackensack, and Passaic rivers. These waters are enriched by increased nutrient loading from point and non-point sources such as agricultural and urban run-offs (e.g. agricultural herbicides, toxic discharges, suspended sediments and nutrients), causing pollution. Development along the shoreline has caused much pollution to build up in the estuary over time, particularly from the large cities around the estuary, including New York City and Newark, New Jersey. Sources of pollutants include municipal treatment plants, industrial discharges, combined sewer overflows, storm water tributaries, landfill leachate, navigable vessels, and atmospheric deposition. The estuary is used for many recreational activities including swimming, boating and sport fishing, which are now one of the biggest industries of the area.

S. Bagheri, *Hyperspectral Remote Sensing of Nearshore Water Quality*,
SpringerBriefs in Environmental Science, DOI 10.1007/978-3-319-46949-2_2

2.1.1 Physical Characteristics

The study area is the Hudson/Raritan Estuary south of the Verrazano Narrows, and bordered by western Long Island, Staten Island and New Jersey (Fig. 2.1).

The partially mixed drowned river estuary is relatively shallow (<8 m) (Oey et al. 1985). It is connected to the Atlantic Ocean through the Sandy Hook Rockaway Point transect and to Long Island Sound through the East River. The Estuary constitutes an extremely complex system involving the interaction of tidal and wind-driven currents modified by the freshwater discharges from Hudson, Raritan, Hackensack, and Passaic rivers.

The freshwater discharge from the Hudson River contributes a monthly average discharge ranging from about 100 m^3/s in dry seasons to about 1800 m^3/s in spring, while the combined monthly average discharges of the Raritan, Passaic and Hackensack rivers ranges from 10 to 100 m^3/s. The number of wastewater inputs include 26 major waste treatment plants, about 100 point sources of industrial and municipal origin and in excess of 700 combined storm drains and sewer outflows. There are four major sewage sources; two with a combined mean discharge of 11 m^3/s are located near the mouth of the Passaic River and near the mouth of Kill Van Kull which opens to the Upper Bay. A third in the East River has a mean discharge of 42 m^3/s, and the fourth sewage source is Jamaica Bay with a mean discharge of 14 m^3/s (Oey et al. 1985).

The volume discharged into the system from Staten Island, New Jersey and the Raritan River is small compared to these sources. Conditions in the Raritan-Lower Bay part of the estuary can be quite variable due to its shallowness and the speed with which it can change in response to factors such as tide, rain and wind. However, the net movement of water within the estuary is counter-clockwise. The following two factors influence the circulation patterns in the estuary: (1) the geometry of the estuary with open boundaries (Sandy Hook connection with the Atlantic Ocean and East

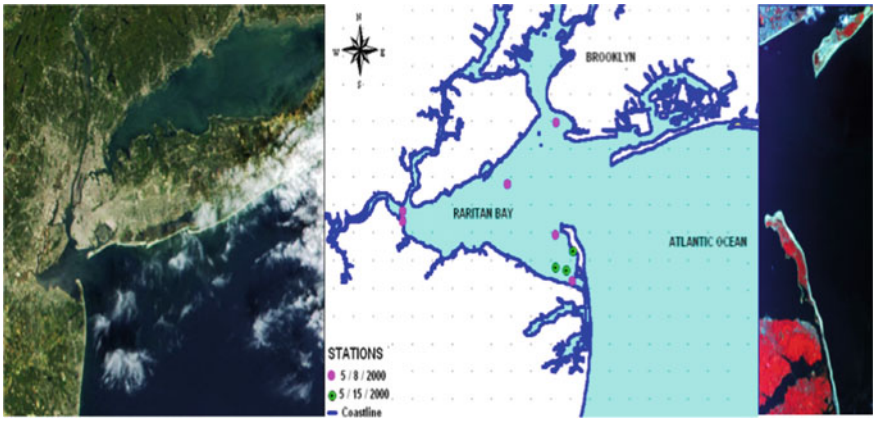

Fig. 2.1 Map of the study area with the locations of sample points

River Strait connection with Long Island Sound) and, (2) surface wind stress which is considered part of the surface boundary conditions. The estimated flushing time of the estuary, 16–21 days or 32–42 tidal cycles (Jeffries 1962), tends to retain pollutants entering the system and delay dilution with receiving waters.

2.1.2 Marine Geology/Ecology

The geologic characteristics of the Hudson/Raritan estuarine floor, are comprised of four major sedimentary regions: the Sandy Hook Bay Muds, the West Raritan Bay Muds, the Keansburg Sands, and the Lower Bay Sands (Nagle 1967). Accumulation of fine-grained sediments is usually indicative of lower energy conditions and protected environment. In contrast, the presence of sand often characterizes high energy conditions and an environment exposed to vigorous waves or strong tidal currents. The principal area of mud accumulation extends from west–Raritan Bay into east–Sandy Hook Bay. The sediment generally becomes finer westward towards the mouth of the Raritan River (Coch 1986) and sandy along the New Jersey coast south of the mud deposit. This sand, derived from the erosion of the Cretaceous beds of sand at the New Jersey shore, persist due to prevailing north-westerly winter winds that raise waves of sufficient energy to prevent the deposition of fine-grained sediment near this coast (Mutler et al. 1984). Extensive sand banks are located to the north of the muds of Raritan Bay and Sandy Hook Bay (Coch 1986; Kastens et al. 1978; Jones et al. 1979). These sediments are primarily relic glacial sands and they cover almost the entire floor of the Lower Bay. Strong tidal currents at the mouth of the Lower Bay have reworked these deposits into large shoals and the penetration of the ocean waves into the Lower Bay prevent the retention of the fine-grained sediment except at a few small but significant sites (Mutler et al. 1984). These sites are borrow pits that were produced by sand mining operations. Within the pits, mud accumulates at rapid rates, even though conditions prevent its deposition on the surrounding sand banks (Olsen et al. 1984).

The Hudson/Raritan Estuary is a complex ecosystem and it is considered “the most intensively developed and industrialized estuary on the U.S. east coast” (Pearce 1988). Many diverse organisms continue to use the estuary for part or all of their lives. These organisms include commercially valuable shellfish and finfish, and lower organisms such as polychaetes, phytoplankton and zooplankton that are basic to the estuarine food web. Many fish depend on the estuary as a nursery and critical stages of their life cycle occur in these waters, while others use it as a key migration route between fresh and sea water. At one time both shell- and fin-fish fisheries thrived in the estuary. Some, such as oyster, hard clam and soft clam shellfisheries collapsed or were reduced because of bacterial contamination. The commercial fin-fishery was relocated offshore due to legislation preventing fishing in the estuary. Today, outside of a few pound nets in the Raritan Bay part of the estuary, most fin-fishing has been reduced to sport activity, although some clams are harvested for depuration or transfer to cleaner waters (MacKenzie 1990).

However the estuary is used for many recreational purposes including swimming, boating and sport fishing, which is now one of the biggest industries.

Over the last century the quality of the estuarine water has degraded in part due to eutrophication. Eutrophication disrupts the pre-existing natural balance of the system, resulting in algal blooms of both increased frequency and intensity in response to the over-enrichment. Blooms are population booms of phytoplankton, tiny organisms that live in water, photosynthesize and form the base of the ocean food chain (Table 2.1). They're like the plants of the deeper ocean, except that unlike plants, some species are able to swim.

Some species also eat other organisms in addition to getting energy from photosynthesis.

There are several causes that can contribute to an algal bloom. These blooms can occur seasonally, after an upwelling of nutrient-rich water, or due to pollution such as agricultural/urban runoff. In both cases, the water becomes saturated with nutrients, creating an ideal environment for phytoplankton productivity. Even natural causes can trigger an algal bloom, such as a rainstorm followed by warm, sunny weather (EPA 2000). While phytoplankton are an important aspect of a healthy body of water and help to provide oxygen and food for aquatic organisms, an imbalance of phytoplankton levels can cause major problems. Noxious phytoplankton blooms are among the potential negative impacts, as are shifts to less desirable species of phytoplankton, diminished aesthetics, and changes in phytoplankton cell size. Dense and accelerated phytoplankton blooms ultimately increase oxygen demand on the system leading to episodes of hypoxia (Bagheri et al. 2005). Hudson/Raritan Estuary together with majority of the world's coastal zones are subject to recurrent outbreaks

Table 2.1 Phytoplankton in Hudson/Raritan Estuary

Divisions/classes	Species	References
Diatom	*Rhizosoplenia delicatula*, *Asterionella glacialis*, *Skeletonema costatum*, *Thalassiosira* sp.	Schuster et al. (2000)
	Asterionella glacialis, *Leptocylindrus danicus*, *Skeletonema costatum*, *Rhizosoplenia delicatula*, *Nitzschia pungerns*	Marshall et al. (1987)
Dinoflagellate	*Prorocentrum* sp., *Katodinium* sp.	Schuster et al. (2000)
	Ceratium fusus, *C. lineatum*, *C. longipes*, *C. tripos*, *Prorocentrum*, *P. minimum*, *P. balticum*	Marshall et al. (1987)
Chrysophyceae	*Calycomonas gracillis*, *Calycomonas ovalis*, *Dictyocha fibula*, *Distephanus speculum*	Marshall et al. (1987)
Cyptophytes		Marshall et al. (1987)
Euglenophyceans		Marshall et al. (1987)
Haptophyceae	*Emiliania huxleyi*	Marshall et al. 1987

Source https://palebluedotreview.wordpress.com/a-closer%C2%A0look/what-are-phytoplankton/

of toxic phytoplankton or harmful algal blooms (HABs) triggered by the combined effect of particular meteorological forcing and nutrient fields. The harmful algal blooms (HABs), which have been observed in every coastal state of the US (Boesch 1997), are formed through dispersal of HAB organisms, nutrient enrichment, and introduction and transport of cysts via ballast water transfers (Hallegraeff 1993). Algal blooms have been recorded over the last 40 years (Olsen 1989). As early as 1960s, red tides were documented to be caused by several species of phytoflagellates, such as *Olishthodiscus leteus*, *Katodinium rotundatum*, and Prorocentrum spp. (Mahoney and McLaughlin 1977). The major phytoflagellate red tides were confined primarily to the Hudson/Raritan Estuary (Olsen 1989). In 1985, the brown tide caused by *Aureococcus anophagefferens* was first observed in the Long Island Sound (Sieburth et al. 1988). In New Jersey, brown tides were first confirmed in lower Barnegat Bay and adjacent Little Egg Harbor Bay in 1995 (Nuzzi et al. 1996). Negative impacts of these exceptional blooms as opposed to the annual spring blooms are associated with the presence of toxins secreted by various species of dinoflagellates, diatoms and cyanobacteria and are documented as a byproduct of shellfish bed closures, public health reports as noxious aerosols and aquatic mortality events and environmental conditions. HABs pose a serious threat to ecosystems and public health, as well as to the economy, as they are responsible for fish kills, shellfish poisoning, and human illness (Table 2.2).

While reports of toxic outbreaks are escalating worldwide, early detection remains elusive, impeding progress towards understanding the forces responsible for bloom initiation, development and advection. It is imperative, because of the damage to aquatic ecosystems, fisheries and tourism, that the environmental conditions that trigger and control harmful algal blooms be sufficiently understood in order to predict occurrences and mitigate potential effects (Bagheri et al. 1999). Annual average monitoring and management costs for HABs are estimated at $2 million, distributed among twelve states: Alaska, California, Connecticut, Florida, Maine, Massachusetts, New Hampshire, North Carolina, New Jersey, New York, Oregon, and Washington. These costs include the routine operation of shellfish toxin monitoring programs, plankton monitoring, and other management activities (Anderson et al. 2000).

Utilizing ocean color remote sensing offers an effective tool to locate areas rich in phytoplankton concentrations. Phytoplankton, as revealed by ocean color remote sensing, frequently show scientists where ocean currents provide nutrients for plant growth and where fishing industry can find good fishing spots by looking at ocean color images. ln addition, phytoplankton show where pollutants poison the ocean and prevent plant growth, and where subtle changes in the climate affect phytoplankton growth. Since phytoplankton depends upon specific conditions for growth, they frequently become the first indicator of a change in their environment: Increases in temperature due to global climate change can contribute to important changes in phytoplankton composition and abundance. This is considered to be a major pathway of carbon cycling in the ocean and thus essential to global change studies. Since phytoplankton depends upon specific conditions for growth, they

Table 2.2 HABs observed in the New York/New Jersey coastal water, 1959–2010

Division/classes	Species	Tides
Diatoms		
	Asterionella	
	Cerataulina pelagica	
	Chaetoceros sp.	
	Cylindrotheca closterium Leptocylindrus sp.	
	Pseudonitzschia delicatissima Pseudonitzschia seriata	
	Pseudonitzschia pungens multiseries Pseudonitzschia	
	(*Nitzschia*) spp. *Rhizosolenia* sp.	
	Skeletnema costatum	
	Thalassiosira spp.	
	Ceratium tripos Red *Gyrodinium aureolum Green*	
	Katodinium rotundatum Red *Pfiesteria piscicida*	
	Prorocentrum lima	
	Prorocentrum micans Red *Prorocentrum redfieldi*	Red
	Scripsiella trochoidea	
	Aureococcus anophagefferens	Brown
	Olisthodiscus luteus	Red
	Didymocystis sensu Green Nannochloris atomus	Green
	Eutreptia lanowii	Red
Dinoflagellates Pelagophyceae Raphidophy Chlorophytes		
Euglenids		

Source http://nj.gov/dep/dsr/raritanbay/RaritanBib_authorA-Z_4-14-2015.pdf

frequently become the first indicator of a change in their environment. Phytoplankton communities can be used both, as a sensitive bioindicator for water quality regarding nutrients load and as a water quality parameter, which dictate the euthrophication level and toxicity (derived from toxic algae) of the water.

Phytoplankton population in the Hudson/Raritan estuary, the Bight Apex and coastal waters of New Jersey is dominated by netplankton diatoms (e.g., speletonema costatum) during the unstratified winter/spring months (November–April) and by nanoplankton chloropyta (e.g., Nannochloris atomus) during the stratified summer/fall months (May–October). Diatoms typically dominate at all times in the offshore waters of the Bight (Fig. 2.2 and Table 2.1). Dinoflagellate blooms off the

Fig. 2.2 Species of phytoplankton. *Source* http://www1.whoi.edu/images/jgofs_brochure.pdf

New Jersey coast are recurrent events during the summer. Since 1968, red tides have been associated with *Olisthodiscus luteus* (1976, 1978, 1979) and *Prorocentrum micanas* (1968, 1972, 1983). The bloom of *Gyrodinium aureolum* off the coast of southern New Jersey in 1984–85 was termed "green tide" because of it's brilliant green color. *Nannochloris atomus* is another common species that causes green tides in New Jersey waters (USEPA 1986).

Brown tides are caused by the bloom of the *Aureococcus anophageffereus*. It had first appeared in Narragansett Bay, Rhode Island and Long Island's Peconic and Great South Bays. The brown tides occur in the summer months. They can kill shellfish and block sunlight to the underwater plants destroying the habitat of many marine resources. The brown tides have a major effect on the shell fishing industry. In 1985 a brown tide in Peconic Bay reduced a $2 Million scallop industry to a few thousand dollars. Research has shown that iron can stimulate growth of brown tides. Environmental factors such a warmer climate, increased salinity of water and lack of rainfall could contribute to the bloom formations, but the exact causes or cure are not known yet (NY Sea Grant 1998).

In the three centuries since the Governor of New York ordered a sewer system to be constructed in Lower Manhattan, New York City has made considerable progress in protecting public health and improving the water quality of the harbor. Today, strict regulations and community activities are working to protect and restore the Hudson-Raritan Estuary. The restoration of oyster beds is an important part of many projects.

http://www.fondriest.com/environmental-measurements/parameters/water-quality/algae-phytoplankton-chlorophyll/#algae10.

As a result of the clean-up efforts to date, the public has enjoyed greatly increased opportunities for recreational uses such as swimming, boating, and fishing. The improvements in water quality also provide substantial benefits to the local economy through commercial fishing and other water-based revenue-generating activities. Although tremendous ecological improvements have resulted from water pollution control efforts implemented since the 1970s, a number of environmental problems remain to be solved for the Hudson-Raritan Estuary. Some contemporary concerns and issues include, for example, contamination of sediments and restrictions on dredge spoil disposal, remaining fish advisories for human consumption, episodic

low dissolved oxygen, the occurrence of nuisance algal blooms and effluent controls on nitrogen discharged to the estuary, and increasing nonpoint source runoff from overdevelopment in the drainage basin of the estuary (NYCDEP 1999).

References

Anderson DM, Hoagland P, Kaoru Y, White AW (2000) Estimated Annual Economic Impacts from Harmful Algal Blooms (HABs) in the United States WHOI September 2000 Technical Report. 89 p

Bagheri S, Zetlin C, Dios R (1999) Estimation of optical properties of nearshore waters. Int J Remote Sensing 20:3393–3397

Bagheri S, Peters S, Yu T (2005) "Retrieval of water quality constituents concentrations from AVIRIS data in Hudson/Raritan Estuary. Int J Remote Sensing 26(18):4013–4027

Boesch D (1997) Harmful algal blooms in coastal waters: Options for prevention, control and mitigation. US Dept. of Commerce, National Oceanic and Atmospheric Administration, Coastal Ocean Office

Coch NK (1986) Sediment characteristics and facies distribution in the Hudson System. J NE Geol 8:109–129

EPA (2000) Progress in water quality—Hudson/Ratitan Estuary Case Study. rpt 832-R-00-008 Chapter 6, pp 1–32

Hallegraeff GM (1993) A review of harmful algal blooms and their apparent global increase. Phycologia 32(2):79–99

Kastens KA, Fray CT, Schubel JR (1978), Environmental effects of sand mining in the Lower Bay of New York Harbor. Marine Sciences Research Center, Special report, 15, State University of New York, Stony Brook, New York

Jeffries HP (1962) Environmental characteristics of Raritan Bay A polluted estuary. Limnol Oceangr 7:21–31

Jones CR, Fray CT, Schubel JR (1979) Textural properties of properties of surficial sediments of Lower Bay of New York Harbor. Marine Science Research Center, Special report 21, State University of New York, Stony Brook, New York

MacKenzie CL Jr (1990) History of the Fisheries of Raritan Bay, New York and New Jersey. Mar Fish Rev 52(4):1–45

Mahoney J, McLaughlin J (1977) The association of phytoflagellate blooms in Lower New York Bay with hypertrophication. J Exp Marine Biol Ecol 28

Mutler HG, Staiken DM, McCormick JM, Berger KJ (1984) Sediments in the Raritan Bay—Lower New York Bay complex. Bull NJ Acad Sci 29:79–96

Nagle JS (1967) Geology of Raritan Bay. In: The report for the conference on pollution of raritan bay and adjacent interstate waters, Third Session Volume III - appendices. Federal Water Pollution Control Administration

New York Sea Grant (1998), NJ StarLedger 10, June, 1990. Coastline, 1998 l NY Sea Grant Institute, 27(1):10–11

Nuzzi R, Olsen P, Mahoney J, Zodl G (1996) The first *Aureococcus anophagefferens* brown tide in New Jersey. Harmful Algae News, IOC Newsletter

Oey L-Y, Mellor GL, Hires RI (1985) A three-dimensional simulation of the Hudson/Raritan Estuary. Part I & II. J Geop Oceanogr 15:12:1676–1709

Olsen P (1989) Development and distribution of a brown-water algal bloom in Barnegat Bay, New Jersey with perspective on resources and other red tides in the region. Novel Phytoplankton Blooms: Causes and Impacts of Recurrent Brown Tides and Other Unusual Blooms 35:189–212

Olsen CR, Larsen IL, Brewster RH, Cutshall NH, Bopp RF, Simpson HJ (1984) A geochemical assessment of sedimentation and contaminant distributions in the Hudson-Raritan Estuary. NOAA, Technical report. nos OMS2.

Pearce J (1988) Changing patterns of biological responses to pollution in the New York Bight. Hudson/Raritan Estuary Issues, Resour Status Manage 9:1–26 (NOAA Estuary-of-the-month seminar series)

Schuster R, Feerst E, Olsen P (2000) Annual summary of phytoplankton blooms and related conditions in the New Jersey coastal water summer of 1999. NJDEP.

Sieburth J, Johnson P, Hargraves P (1988) Ultrastructure and ecology of *Aureococcus anophageferens* gen. et sp. nov. (Chrysophyceae): the dominant picoplankter during a bloom in Narragansett Bay, Rhode Island, Summer 1985. J Phycol 24(3):416–425

USEPA (1986) US environmental protection agency region II, 1986, Green Tide Environmental Inventory. http://www.state.nj.us/dep/bmw/Reports/phytorpt99.pdf, www.state.nj.us/dep/bmw/Reports/Phyto2005Final.pdf

Chapter 3
In-Situ Measurements to Establish the Bio-optical Model

Abstract To develop ocean color model for Case 2 waters; it is required to develop an appropriate bio-optical model in order to link the water constituent concentrations to the inherent optical properties (IOPs) and to link the IOPs to the subsurface irradiance reflectance R(0−) recorded by remote sensors. As part of this bio-optical modeling efforts, biweekly field campaigns were carried out in the Hudson/Raritan Estuary of New York-New Jersey during the course of the project (1998–2001) to obtain in-situ measurements of subsurface irradiance reflectance R(0−), together with in situ samples, that were later analyzed in the laboratory for their inherent optical properties and bio-optical modeling. The results of the field campaign with emphasis on August 1999 are presented in this chapter.

Keywords Ocean color · Subsurface irradiance reflectance R(0−) · Bio-optical modeling · Insitu measurements · Fluorescence · Pigments · Absorption · Attenuation · Scattering · Spectroradiometer · Upwelling · Downwelling · FWHM · Spectrophotometer · Ac-9

3.1 Introduction

Efforts at modeling ocean color data in water quality application revolve around two major issues: (1) Development of theoretical models for presentation of ocean color data as a function of inherent optical properties (IOPs); and (2) Categorizing the inherent optical properties of water constituents encountered in water bodies and their variations as a function of constituents concentrations (IOCCG 2000). For Case I water, the absorption of phytoplankton, total suspended material (TSM), and colored dissolved organic matter (CDOM) are directly proportional to CHL_a concentration (Morel and Prieur 1977; Prieur and Sathyendranath 1981). However, variation in the shape and magnitude of the absorption coefficients are poorly documented for coastal waters including the East Coast of the United States—the geographic location of the study site (Babin et al. 2003; D'Sa and Del Castillo 2006; Groom et al. 2009). The aim of the research in Hudson/Raritan Estuary was

S. Bagheri, *Hyperspectral Remote Sensing of Nearshore Water Quality*,
SpringerBriefs in Environmental Science, DOI 10.1007/978-3-319-46949-2_3

to built ocean color remote sensing models based on the extensive multidate field measurements often coordinated with overflights of multispectral and hyperspectral sensors to establish inherent optical properties for this geographic location (Bagheri et al. 1993, 1999, 2000). The measured IOPs were then used as default input into bio-optical model to model reflectance and to estimate water quality parameters in terms of total chlorophyll (TCHL), CDOM and TSM using inverse modeling as detailed in Chaps. 5 and 6. Two systems of in situ measurements were used during the course of the research coordinated with multispectral and hyperspectral sensors as outlined below:

(1) **Shipboard Automated Sampling**. Sea truth data were collected using a shipboard automated sampling system coordinated with Landsat-5 TM, MSC-02 Videography and GER Imaging Spectrometer (Bagheri et al. 1993, 1999). Water was pumped continuously through the sampling system from a depth of 1 m below surface. Temperature, conductivity and fluorescence of water passing through the system were monitored and averaged for each minute during this period. The corresponding year, month, day, time, latitude and longitude using Loran C unit also were recorded. A continuous-flow fluorometer set-up for chlorophyll-a analysis was used to measure pigment fluorescence. Periodically water samples were collected for phytoplankton speciation. At five minute intervals, water was collected from the automated system effluent for turbidity, salinity and chlorophyll pigment analysis. Chlorophyll-a and phaeopigment concentrations in these samples were determined according to Evans et al. (1987). Discrete samples collected for chlorophyll pigment analysis were used to determine if fluorescence recorded by the continuous-flow fluorometer was representative of actual pigments concentrations in the water passing through.

Since the continuous-flow fluorometer measures the combined fluorescence of both chlorophyll-a and phaeopigments and cannot distinguish between the two, chlorophyll-a and phaeopigment concentrations determined from discrete samples were added, using molecular weights, to estimate the concentration of chlorophyll-a derived pigments that would be responsible for fluorescence recorded from corresponding water passing through the underway fluorometer. Because of the greater number of observations obtained using the underway system and the high degree of correlation between the two sets of data, fluorescent data generated from the continuous-flow fluorometer was used to develop and test algorithms. Figure 3.1 shows estimation of cholorophyll concentration using the band ratio (NIR and Green) of Landsat 5 TM versus fluorescence concentration measured by continuous-flow fluorometer along one of the transect surveyed in the estuary by shipboard automated sampling during TM overpass on August 30, 1990.

(2) **In Situ Measurements**. To develop ocean color model for Case 2 waters; it is required to develop an appropriate bio-optical model in order to link the water constituents to the inherent optical properties (IOPs) and to link the IOPs to the subsurface irradiance reflectance R(0−). Thus the measurement of subsurface irradiance reflectance is the key modeling parameter for deriving atmospherically corrected remote sensing data (Kirk 1984; Dekker et al. 1997). The in situ measurements during 1999–2001 field survey and coordinated with AVIRIS overflights

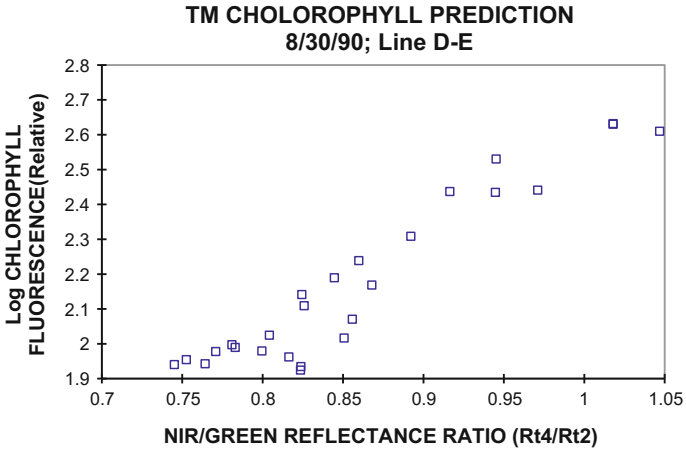

Fig. 3.1 TM band ratio NIR/Green versus log chlorophyll fluorescence for estimation of chlorophyll concentration

included collection of in situ samples, that were later analyzed in the laboratory for their IOPs together with in situ measurement of subsurface irradiance reflectance R(0−) as described below:

3.2 Subsurface Irradiance Reflectance R(0−)

Spectral subsurface irradiance reflectances R(0−)s for all stations marked in Fig. 1.1 were obtained using the field spectroradiometers. The goal is to parameterise the bio-optical model relating the CDOM, TSM and algal pigment concentration, to the light absorption and scattering and to the water leaving radiance, through direct and laboratory based optical measurements. In short, the link between remotely sensed upwelling radiance and underwater inherent optical properties is made through R(0−). During August 1999 field campaign, three field spectrometers with different designs deployed simultaneously for intercomparison process during the course of the research: The OL754 is purpose built for underwater measurements of up and downwelling irradiance; the PR650 is purpose built for radiance measurements in above surface applications and the Ocean Optics 2000 system is a modular spectrophotometric/spectroradiometric system relying on optical fibers and fore-optics to enable it to carry out a variety of optical measurements. The methods of dispersing the incoming lightfield is different as well as the optical detectors registering the number of photons. The specifications of the field spectroradiometers used in the intercomparison process are as follows:

3.2.1 OL 754

The OL 754 is a scanning submersible spectroradiometer. The OL 754-O-PMT Spectrometer Optics Head (Fig. 3.2) uses a double monochromator for low stray light and measures spectral data over 300–850 nm. Three sets of fixed slits are provided with the PMT Optics Head enabling the user to vary the FWHM from 1 to 10 nm, for computation of normalized percentage reflectance curves. The OL IS-470-WP Submersible Sphere Assembly (4-inch integrating sphere) has dual port design with the ports located 90° apart. The sphere contains an internal baffle before the exit port to permit only integrated light from exiting the sphere. The integrating sphere is connected via a waterproof fiber optic to the entrance port of the monochromator. The design of the sphere and the geometries of its components (entrance port, baffle, etc.) enable the WP submersible sphere assembly to achieve a near-perfect cosine response. The OL 730-7Q-WP Quartz Fiber Optic Probe provides a mechanism for mounting the input optics (i.e., cosine receptor, integrating sphere etc.) to the entrance port of the monochromator. Other peripherals of OL 754 includes:

1. The OL 754-C Spectroradiometer Controller links all components to a shipboard computer where the spectroradiometric data is stored.
2. The OL 752-10 is a NIST traceable lamp to calibrate the spectrometer for spectral irradiance response measurement.
3. The OL 65A is a precision current power supply, specifically designed for operation of standard lamps such as the OL 752-10.

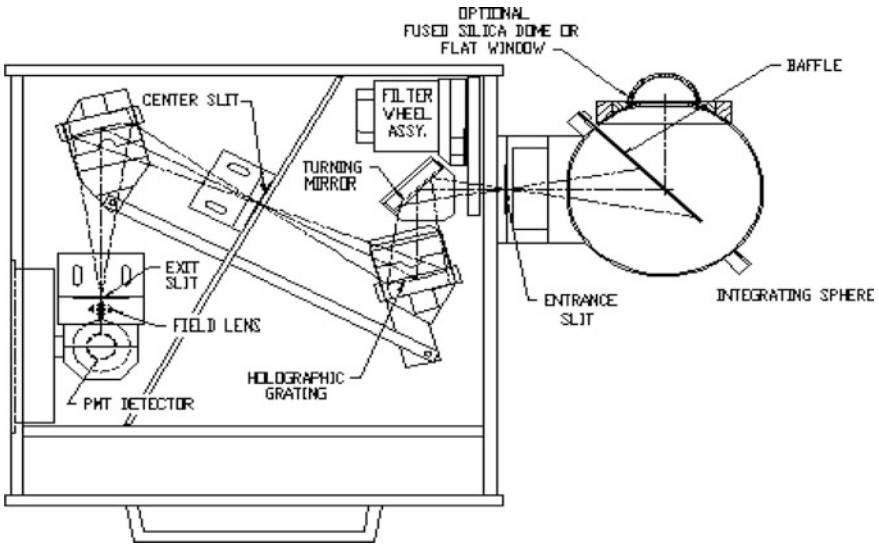

Fig. 3.2 Configuration of the OL754 PMT optics head. *Source* Optronic Laboratory User's Manual (1998)

4. The OL-752-150 Dual Check source module checks the wavelength and gain calibrations. The accuracy of these parameters is verified quickly in the lab/field to ensure that the system has not been adversely affected by shipping, handling or change in environment.

The software provides flexibility to accommodate different field conditions. The Quick Scan^{TM} feature of the software allows scanning of sources that are changing with time by scanning much faster than conventional methods. This feature takes into account such important factors as automatic gain changes and blocking filter changes.

The necessary parameters needed to determine the irradiance of a test source (Optronic Laboratories 1998):

i	dark reading (measured while source is shuttered before scan) [A].
λ	wavelength [nm].
K(λ)	system spectral irradiance response calibration factor [W cm^{-2} nm^{-1} A^{-1}].
E(λ)	standard lamp spectral irradiance [W cm^{-2} nm^{-1}].
T(λ)	test source irradiance [W cm^{-2} nm^{-1}].
$S_E(\lambda)$, $S_T(\lambda)$	average signal reading [A] with dark current (i [A]) subtracted.

The system spectral irradiance response, K(λ), is calculated as follows:

$$K(\lambda) = E(\lambda)/S_E(\lambda)$$

The test source spectral irradiance, T(λ), is calculated as follows:

$$T(\lambda) = K(\lambda) * S_T(\lambda)$$

Upwelling ($E_u(\lambda)$) and downwelling ($E_d(\lambda)$) irradiances were obtained by deploying the submersible sphere assembly in direct and reverse modes into the water at 3 feet below the surface (Fig. 3.3). This depth was generally deeper than the maximum wave amplitude to negate the effects of waves. The subsurface

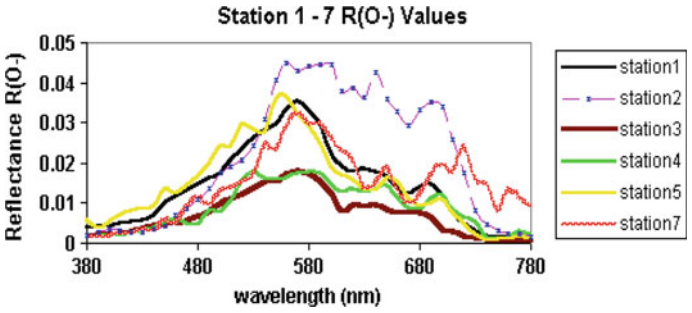

Fig. 3.3 R(0−) Data for all stations using OL 754

irradiance reflectance R(0−) in percentage was calculated as a ratio of $E_u(\lambda)$ to $E_d(\lambda)$ irradiance in units of (W/(cm^2 nm)) for intercomparison process.

3.2.2 PR 650

The PR-650 portable telephotometer/colorimeter (Photo Research) with 1° measuring optics, holographic grating, 128-element diode-array spectrometer covering the spectra from 380 to 780 nm with a FWHM of 8 nm was used for spectral radiance measurements above the water surface. The integration time was automatically selected. At each measurement cycle a dark measurement of equal duration was automatically subtracted as detailed in Gons (1999). The method of measurement is geared fully towards above surface measurements, with the advantage of not having to deal with variable watercolumn heights due to waves, no selfshading, rapid measurements etc.

The water-leaving radiance (L_{au}) and the downward radiance of skylight (L_{sky}) were scanned at a nadir and a zenith angle of 42°, respectively. The angle of 42° was used in order to avoid influence by reflection and shading from the boat. The measured water-leaving radiance included reflected sky light, which can be subtracted after also measuring the sky radiance at the relevant angle (Eq. 3.1). In order to calculate downward radiance (E_{ad}) and discriminate between direct sunlight and the diffuse irradiance, the radiance was measured from a calibrated reflectance panel before (L_{rp}) and after shading (Lr_{pd}) (Eq. 3.1). For both practical and theoretical reasons the chosen direction of observation was 90° to the plane of the sun. Each scan involved 10 measurement cycles of which the average was filed (Fig. 3.4). Three up to 5 complete series of scans were done, which in general took less than 3 min.

From the light measurements obtained above the water surface, the subsurface irradiance reflectance R(0−), i.e. the ratio of upward (E_{wu}) and downward irradiance (E_{wd}) just beneath the water surface was computed, as described in Gons (1999).

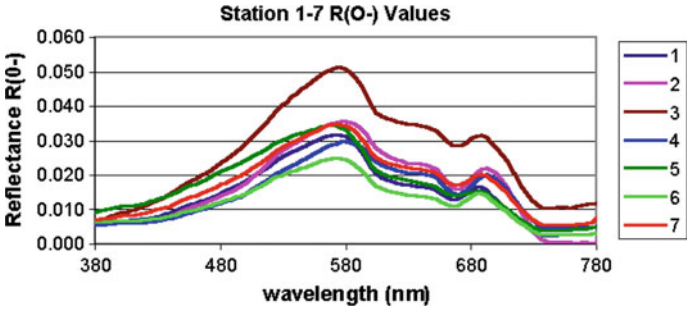

Fig. 3.4 R(0−) Data for all stations using PR 650

$$R(0-) = \frac{Qf(L_{au} - r_{sky}L_{sky})}{[\{E_{ad} - r_{\Theta}(1-F)E_{ad} - r_{dif}FE_{ad}\} + (0.5E_{wu})]} \quad (3.1)$$

where

Q the conversion coefficient for L_{wu} to E_{wu},
f the conversion constant of L_{au} to L_{wu},
L_{au} the upward radiance above the water at nadir angle of 42°,
L_{sky} the radiance of skylight at zenith angle of 42°,
r_{sky} the Fresnel reflectance coefficient at zenith angle of 42°,
E_{ad} the downward irradiance just above the water,
r_{θ} the Fresnel reflectance coefficient for sunlight,
r_{dif} the Fresnel reflectance coefficient for diffuse light,
F the fraction diffuse light of E_{ad},
E_{wu} the upward irradiance just below the water surface.

The following values were applied. The value of the geometric parameter Q while still being a point of discussion in literature was calculated according to Gons (1999). Whereby Q depends on solar angle and the ratio between total and diffuse downwelling light. Here Q varied between 2.8 and 3.4. For the value of r_{sky} the modeled value of 0.0293 was used (Gons 1999), only in case of a flat water surface (no waves) the theoretical value of 0.0256 (Kirk 1984) may be used. Further the values f = 1.84 for salt water (Austin 1980), and r_{dif} = 0.06 (Jerlov 1976) were applied. The Fresnel reflectance coefficient for sunlight (r_{θ}) was calculated from Julian day, time and geographical position. The downward irradiance just above the water (E_{ad}) was obtained by measuring the radiance from a calibrated reflectance panel. The fraction diffuse light (F) was the ratio between E_{ad} measurements obtained from the reflectance panel before (Lr_p) and after shading (Lr_{pd}).

The reflectance spectra were stored in a Spectral Library database only if they satisfied the following criteria:

(1) R(0−) > 0 for the spectral wavelength range between 440 and 780 nm, and
(2) R(0−) < 0.33 for the spectral wavelength range between 440 and 780 nm.

In case one of the triple R(0−) spectra differed more than the standard deviation from the average, the spectrum was rejected. The two remaining R(0−) spectra were then averaged as input into intercalibration.

3.2.3 Ocean Optics 2000

The SD2000 Fiber Optic Spectrometer is a low-cost, high-performance system that is easily configured. The SD2000 has a high-sensitivity linear CCD array that provides high response and good optical resolution. The design is based on a S2000 grating (600 lines/mm), with an entrance slit of 50 mm. The 2050 wavelength

bands range from 350–900 nm, with a FWHM of approximately 1.5 nm. The spectrometer was directly linked to a laptop on-board. At all stations, measurements of the under-water irradiance reflectance were made. The downwelling and upwelling irradiance was measured simultaneously by connecting cosine collectors to the fibers. Then one sensor was directed upwards, and the fiber was connected to one channel of the Ocean Optics (Master) the other sensor was directed downwards and the fiber was connected to the other channel of the Ocean Optics (Slave). Both sensors were attached to a heavy frame and were lowered into the water using a crane, positioned at the rear of the ship, which for all stations were directed towards the sun. To avoid resuspension of bottom material, ship engines were shut off at all stations except station 7.

For all measurements a running average of ~ 10 nm was applied to reduce noise and a spectrally flat dark current correction applied by assuming a zero irradiance for wavelengths larger then 950 nm, due to the large absorption of pure water in that spectral region. The irradiance reflectance at a certain depth was then calculated by dividing the upwelling and downwelling irradiance and applying a spectral correction for the difference in sensitivity of the two sensors. The correction was established one day before the field-campaign, using a calibration lamp, but without the cosine collectors. After rejection of inconsistent measurements the remaining measurements were averaged (Fig. 3.5).

The subsurface irradiance reflectance R(0−) was calculated as a ratio of $E_u(\lambda)$ to $E_d(\lambda)$ irradiance. For direct comparison radiance data of PR650 was converted to irradiances and data from different spectrometers were plotted for all stations (see Figs. 3.2, 3.3 and 3.4). Intercomparison of different types of field spectroradiometers (i.e., OL 754, PR 650 and Ocean Optics 2000) were established using the spectral position and magnitude of subsurface reflectance peaks. Comparing the reflectance spectra (Figs. 3.6 and 3.7) show that there are some differences between the results of the different spectroradiometers. The range of reflectance values, however is, quite consistent (i.e., 1–5 % R(0−) over the wavelength range of 480–700 nm). However the spectral shape varies as seen in Fig. 3.7. Several reflectance features are prominent in the spectra depicted on Figs. 3.6 and 3.7 which support earlier research results that information extraction in inland and turbid estuarine and coastal waters should be limited to spectral green to infrared

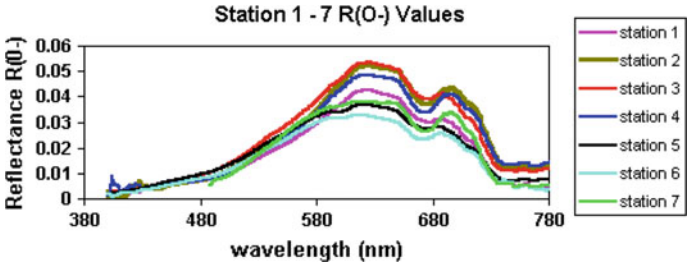

Fig. 3.5 R(0−) Data for all stations using ocean optics 2000

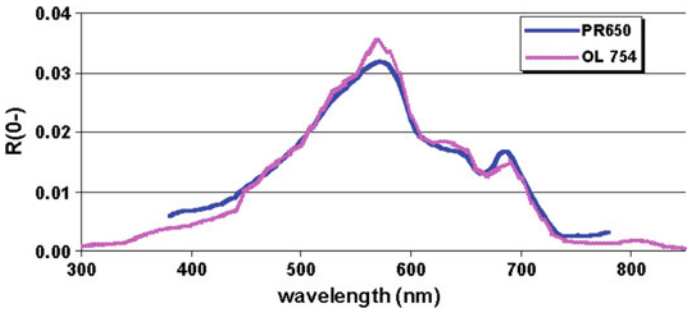

Fig. 3.6 Comparison of OL 754 and PR 650 spectral features

Fig. 3.7 Comparing OL 754, PR650, Ocean 2000

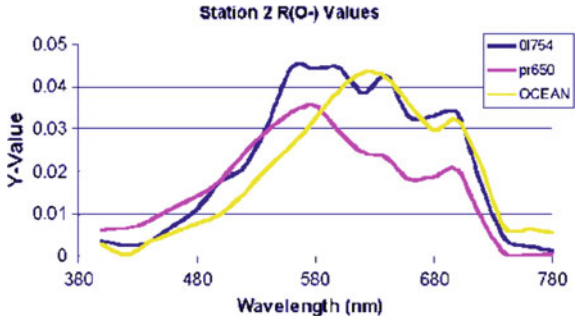

part of the spectrum (Dekker 1993; Gitelson and Kondratyev 1991). These features are the absorption by CDOM, TSM and the first CHL_a absorption peak causing low reflectance. Beyond 500 nm overall absorption decreases and reflectance increases allowing a better discrimination on local spectral features in the spectra, such as the red chlorophyll a absorption peak at 676 nm.

In conclusion over most of the stations measured the influence of the wave propagations were shown in the spectra acquired by OL 754. Generally, wave refraction problem result from the modulation of light by alternating focusing and defocusing cycles produced by the motion and shape of the waves. With the other systems averages of many scans were taken but, because of time constraints, only one upwelling and one scan was taken with the OL 754 at each station and the influence of waves can be seen in the results.

3.3 Inherent Optical Properties (IOPs)

The spectral absorption and backscattering are the inherent optical properties (IOP). The spectral absorption will cause reduction in R(0−) and the spectral scattering causes an increase in R(0−). Laboratory based spectrophotometric measurements of

spectral attenuation and spectral absorption were performed. From these measurements spectral scattering was deduced. Absorption spectra of seston (phytoplankton and TSM) and TSM were determined using the filterpad method (Truper and Yentsch 1967) with 0.45 μm Whatman GF/F filters (Figs. 3.8, 3.9 and 3.10). The absorption was calculated on a basis of a calibrated relationship between the optical density of a suspension in a sample cell and the optical density on a filter (Weidemann and Cleveland 1993). The absorption spectra of color dissolved organic matter (CDOM) and the seston beam attenuation were determined spectrophotometrically according to the methods described in Rijkeboer et al. (1998).

Additional measurements of spectral absorption and beam attenuation coefficients were made using the ac-9 instrument. The ac-9, with one absorption flow tube and one attenuation flow tube, measures beam absorption (a) and attenuation (c) coefficient at 9 wavelengths (412, 440, 488, 510, 532, 555, 650, 676, 715 nm). Ac-9 measures vertical profiles of upwelling radiance, downwelling irradiance,

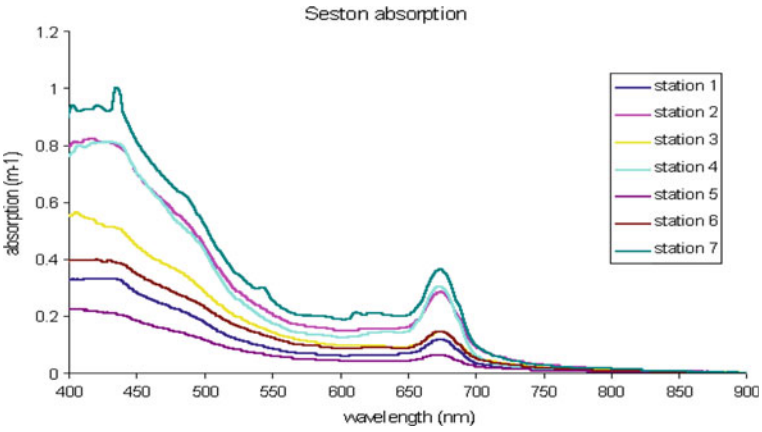

Fig. 3.8 Absorption spectra of seston (organic and non-algal inorganic material)

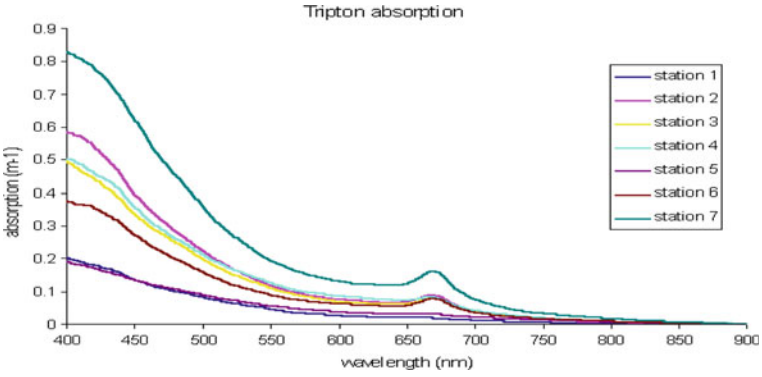

Fig. 3.9 Absorption spectra of TSM (non-fraction of seston)

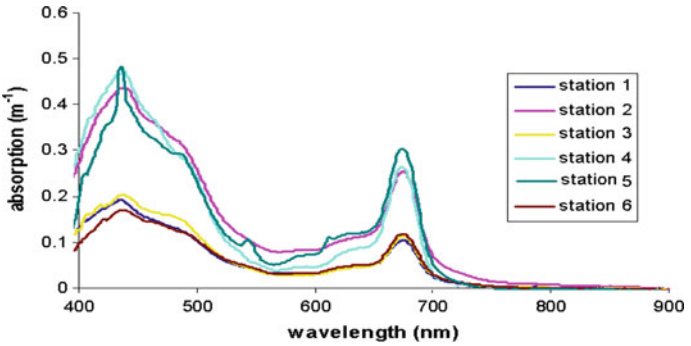

Fig. 3.10 Phytoplankton absorption spectra

absorption and scattering. The chlorophyll-a absorption peak at 670 nm were used to get an independent estimate of phytoplankton biomass to separate it from the total particulate absorption. At the time there was no commercially available total scattering meter to measure the total scattering coefficient, b. However, the value of b was obtained by measuring the beam attenuation coefficient, c, in a specified wavelength. Since c = a + b, the value of b could be calculated (IOCCG 1999). Use of the ac-9 has enabled us to model the backscattering coefficient (b_b), which is an important input parameter for establishing the IOPs of the estuary. Figure 3.11

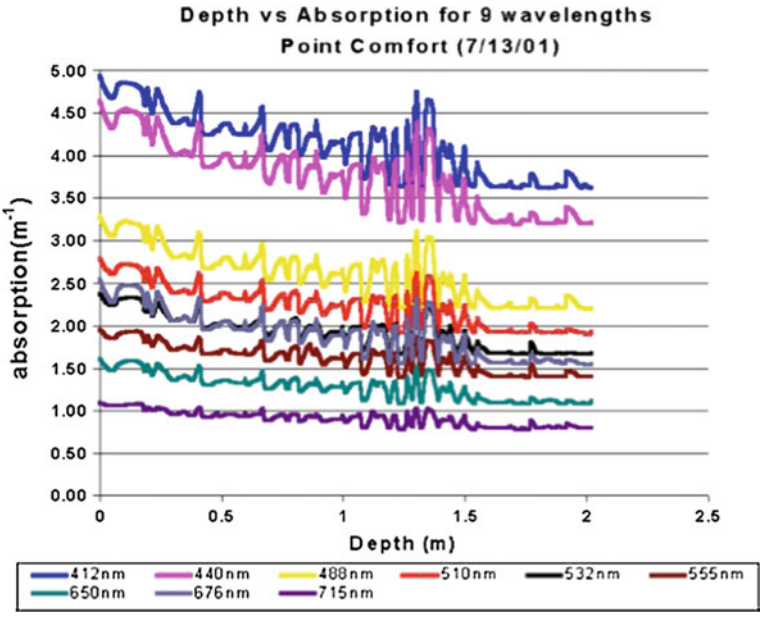

Fig. 3.11 The absorption spectra for 9 wavelengths recorded by ac-9 at station 5

shows the absorption spectra recorded by ac-9 at station 5 (Point Comfort) on July 13, 2001. The primary advantage being that the ac-9 is an in situ instrument that can be used on profiling systems, flow-through systems and moorings.

3.4 Optical Water Quality Concentrations (WQP)

To develop bio-optical model, it is essential that the specific absorption and scattering of the major constituents of the estuarine water are known. The specific absorption and scattering are the per unit concentration absorption and scattering properties. Once these are known spectral irradiance reflectances of any range of concentrations potentially present in the waters may be modeled. To estimate optical water quality concentrations coinciding with the spectral reflectance measurements subsurface water samples (0.2–0.5 m depth) were taken in 1-1 bottles and placed in a cooler with melting ice before transport to the laboratory for analysis.

Standard procedures as described by Rijkeboer et al. (1998) were used to determine the concentrations of total chlorophyll-a (TCHL) defined as the sum of chlorophyll-a and phaeopigment (as indication of concentration of phytoplankton) and total suspended matter (TSM). The TCHL concentration was determined according to the Dutch standard norm (NEN 6520 1981). This method is based on the extraction of chlorophyll-a pigments from the phytoplankton using hot ethanol (80 %, at 75 °C). The TCHL is then determined spectrophotometrically, using the extinction of the solvent at 665 and 750 nm. The phaeopigment concentration is determined similarly after acidification of the sample. All analysis were performed in duplicates to verify the result. Additional chlorophyll measurements have been performed using extraction in cold acetone (Strickland and Parson 1972). The TSM concentrations were determined according to the Dutch standard norm (NEN 6484 1982), by filtering samples over 0.45 μm Whatman GF/F filters and drying the filters at 80 °C. Ignition loss was determined by washing the filters with TSM at 550 °C. The filters were flushed with 10 ml tap water to prevent overestimation of the TSM concentration due to remaining salt left on the filter. Filtered volumes range from 50 to 200 ml. All analyses were performed in triplicates. Both methods are reproducible within 5 % (Pasterkamp et al. 1999). see Table 3.1 for the concentrations per sampling point. The TSM ranges (6.44–25.74 g m^{-3}) are within the range expected for this time of year (1999), but the measurements are not representative of maximum concentrations for the estuary. The TCHL concentrations are low (6.33–47.79 mg m^{-3}), since measurements did not coincide with any major outbreaks of phytoplankton blooms at the time of survey. Table 3.1 lists the sampling stations selected in diverse parts of the estuary (Fig. 1.1—Chap. 1) with maximum taxonomic variability in phytoplankton community with IOPs and concentrations data obtained on August 1999, May 2000 and July 2001 in conjunction with simultaneous AVIRIS overflights. These sampling stations were sampled repeatedly during the multiyear field campaigns outside of the AVIRIS data acquisition.

Table 3.1 Sample locations and local observations recorded onboard R/V Walford on August 14, 1999, May 15, 2000 and July 13, 2001 field campaigns

Date	St	Location	Lat	Long	S.D. (m)	TCHL (mg m^{-3})	TSM (g m^{-1})
8/14/1999	1	Comptons/PewsCreek	40.45	74.08	1.3	15	6
	2	Keyport Harbor	40.47	74.19	0.8	32	26
	3	Traid Bridge	40.50	74.28	0.9	17	13
	4	Crookes Pt State Isl.	40.54	74.14	0.6	37	15
	5	Coney Isl. Pt	40.57	74.02	1.8	6	11
	6	Sandy Hook Tip	40.49	74.02	0.9	22	12
	7	Shrewbury River	40.38	73.98	0.5	48	21
5/15/2000	1	Buoy2	40.42	74.01	1.25	31	8
	2	Atlantic Highlands	40.47	74.03	1.25	46	11
	3	Horseshoe Cove	40.59	74.03	1.37	22	7
7/13/2001	1	Tip of Sandy Hook	40.55	73.93	1.3	38	23
	2	Ambrosa Channel	40.54	74.02	0.8	17	8
	3	Great Kills	40.52	74.13	0.9	36	23
	4	Raritan River	40.49	74.24	0.6	32	21
	5	Point Comfort	40.46	74.14	1.8	73	5
	6	Sandy Hook Bay	40.42	74.03	0.9	38	8

Note All data collected during outgoing tides

References

Austin RW (1980) Coastal zone color scanner radiometry. Ocean Opt VI SPIE 208:170–177

Babin M, Stramski D, Ferrari GM, Claustre H, Bricaud A, Obolensky G, Hoepffner N (2003) Variations in the light absorption coefficients of phytoplankton, nonalgal particles, and dissolved organic matter in coastal waters around Europe. J Geophys Res C Oceans 108(7):4–1

Bagheri S, Stein M, Zetlin C (1993) Use of integrated remotely sensed data in water quality assessment of Hudson/Raritan estuary. J Mar Environ Eng 1:53–63

Bagheri S, Zetlin C, Dios R (1999) Estimation of optical properties of nearshore water. Int J Remote Sens 20(17):3393–3397

Bagheri S, Pasterkamp R, Rijkeboer M (2000) Comparison of spectroradiometers in preparation of bio-optical modeling. In: JPL/AVIRIS workshop, Pasadena, CA

Dekker AG (1993) Detection of optical water quality parameters for eutrophic waters by high resolution remote sensing. Ph.D. Thesis, Fac. Earth Sciences, Vrije Universiteit, Amsterdam, The Netherlands, p 240

Dekker AG, Hoogenboom HJ, Goddijn LM, Malthus TJM (1997) The relationship between inherent optical properties and reflectance spectra of turbid inland waters. Remote Sens Rev 15 (1–4)

D'Sa EJ, Del Castillo C (2006) Bio-optical properties and ocean color algorithms for coastal waters influenced by the Mississippi river during a cold front. Appl Opt 45:7410–7428

Evans CA, O'Relilly JE, Thomas JP (1987) A handbook for the measurement of chlorophyll-a and primary productivity. Biomass Scientific Series No. 8. SCAR, SCOR, IABO, ACMRR AND NOAA/NMFS

Gitelson AA, Kondratyev KY (1991) Optical models of water bodies. Int J Remote Sens 12 (3):373–385

Gons HJ (1999) Optical teledetection of chlorophyll a in Turbid Inland waters. Environ Sci Technol 6

Groom S, Martinez-Vicente V, Fishwick J, Tilstone, Gerald Moore G (2009) The western english channel observatory: optical characteristics of station L4. J Mar Syst 77:278–295

IOCCG (1999) In: JA Yoder (ed) Status and plans for satellite ocean-colour missions: considerations for complementary missions, Reports of the International Ocean-Colour Coordinating Group, Dartmouth, Canada, p 43

IOCCG (2000) In: Sathyendranath S (ed) Remote sensing of ocean colour in coastal, and other optically-complex, waters

Jerlov NG (1976) Marine optics. Elsevier, Amsterdam, The Netherlands

Kirk JTO (1984) Dependence of relationship between inherent and apparent optical properties of water on solar altitude. Limnol Oceanogr 29:350–356

Morel A, Prieur L (1977) Analysis of variations in ocean color. Limnol Oceanogr 22:709–722

NEN 6520 (1981) Water: spectrophotometric determination of chlorophyll a content. Nederlands Normalisatie-instituut, Delft, The Netherlands (in Dutch)

NEN 6484 (1982) Water: determination of the content of not dissolved material and its ignition residue. Nederlands Normalisatie-instituut, Delft, The Netherlands (in Dutch)

Optronic Laboratories Inc (1998) User manual. Orlando, Florida

Pasterkamp R, Rijkeboer M, Dekker A (1999) Specific inherent optical properties of Dutch inland waters and estuaries. W99/10, IVM/VU, Amsterdam, The Netherlands (in press)

Prieur L, Sathyendranath S (1981) An optical classification of coastal and oceanic waters based on the specific spectral absorption curves of phytoplankton pigments, dissolved organic matter, and other particulate materials. Limnol Oceanogr 26(4):671–689

Rijkeboer M, Dekker AG, Hoogenboom HJ (1998) Reflectance spectra with associated water quality parameters measured in Dutch waters (Speclib-TK-database). Institute for Environmental Studies, E98/12, The Netherlands

Strickland JDH, Parson TR (1972) A practical handbook of seawater analysis. Fisheries Research Board of Canada, Ottawa, p 163

Truper HG, Yentsch CS (1967) Use of glass fiber filters for the rapid preparation of in vivo absorption spectra of photosynthetic bacteria. J Bacteriol 94:1255–1256

Weidemann AD, Cleveland JS (1993) Quantifying absorption by aquatic particles: a multiple scattering correction for glass-fiber filters. Limnol Oceanogr 38:1321–1327

Chapter 4
Application of Hyperspectral Data

Abstract Three decades of airborne imaging spectroscopy have demonstrated the added value of this remote sensing technique to improve the understanding of Earth's functioning. With the advent of airborne imaging spectroscopy, the specialized image processing system has made the generation of quantitative methods such as semi-analytical and analytical methods possible. Producing thematic maps depicting spatial and temporal distribution patterns of optical water quality parameters are based on the image interpretation and calibration for better monitoring and management of water resources.

4.1 Introduction

Remote sensing of coastal waters has developed since the early seventies from an empirically based method producing qualitative water quality maps to more quantitative methods such as semi-analytical and analytical methods, which produce thematic maps of spatial and temporal distribution patterns of optical water quality parameters based on the image interpretation and calibration. The current discussion deals with the imaging spectroscopy/hyperspectral data emphasizing the use of the NASA/Airborne Visible Infrared Imaging Spectrometer (AVIRIS) data acquired over the study site in water quality application. Spectroscopy is based on the accurate measurement of spectra emitted by samples under controlled, experimental conditions, and comparison of such spectra to known standards (USGS). Spectroscopy has been an accepted science in analytical laboratories for many years in many disciplines. Imaging spectroscopy on a small scale is performed routinely with scanning electron microscopes. On a large scale, spectral images from satellites of the planet earth provide both regional and global perspectives to scientists. In conjunction with the advent of airborne imaging spectrometers, the specialized image processing system moves spectroscopy from the analytical laboratory to the field of remote sensing. Three decades of airborne imaging spectroscopy have clearly demonstrated the added value of this remote sensing technique to improve the understanding of Earth's functioning (Carrere et al. 2013).

S. Bagheri, *Hyperspectral Remote Sensing of Nearshore Water Quality*,
SpringerBriefs in Environmental Science, DOI 10.1007/978-3-319-46949-2_4

Present spaceborne sensors like Hyperion (Pearlman et al. 2003) or HICO (Lucke 2011) have opened up the way for new studies of surface chemistry. Furthermore, the growing number of scheduled spaceborne missions like EnMAP (Kaufmann 2006), PRISMA (Galeazzi et al. 2009) or future sensor like HyspIRI (Green 2007) prove that the scientific community is highly motivated to extend the range of applications using such a technique (Carrere et al. 2013).

4.2 AVIRIS Imaging Spectrometer and Its Characteristics

AVIRIS data in conjunction with simultaneous in-water measurements were collected in Hudson/Raritan Estuary of NY–NJ (1998–2001). AVIRIS has 224 spectral channels covering the 400–2500 nm spectral region with 10 nm spectral and 20 m spatial resolutions (Table 4.1; Fig. 4.1a, b). AVIRIS Records the radiance leaving (and influenced by) the targeted surface plus additional diffuse radiation contributed by atmospheric scattering and direct reflected solar radiation. Above the atmosphere, the water leaving reflectance is often less than 1–2 % of the total signal. AVIRIS data is collected as a data cube with spatial information collected in the X-Y plane, and spectral information represented in the Z-direction. Figure 4.1b depicts the data characteristcs in AVIRIS hyperspectral data cube over Moffett Field, CA.

To develop analytical algorithms for case 2 waters, an optical model is used to link the water quality parameters (WQP) to the (specific inherent optical properties ((SIOP), linking these in turn to apparent optical properties (AOP) such as the remote sensing reflectance or the subsurface irradiance reflectance (R(0−)). In situ measurements of remote sensing reflectance and derived R(0−) are used to validate model simulations of R(0−). They are also used to calibrate and validate the atmospheric correction of observations from high platform—aircraft. Thus R(0−) is the key modeling parameter to translate remote observations of water leaving radiance into, for example, a thematic map of total chlorophyll (TCHL) concentration which, subsequently, can be used as input into a geographical information system (GIS) database of the study area to monitor and manage the estuarine water resources.

Table 4.1 Specification of AVIRIS

Sensor design	Whisk broom, 4 spectrometers
Platform	Airborne ER-2 @ ~20 km
Spectral characteristics	224 bands, $\Delta\lambda$ ~10 nm, FWHM ~10 nm
Typical GSD	~20 m from ER-2
Full field of view	30° (~12 km at ER-2 altitude)
SWIR characteristics	Relatively high SNR

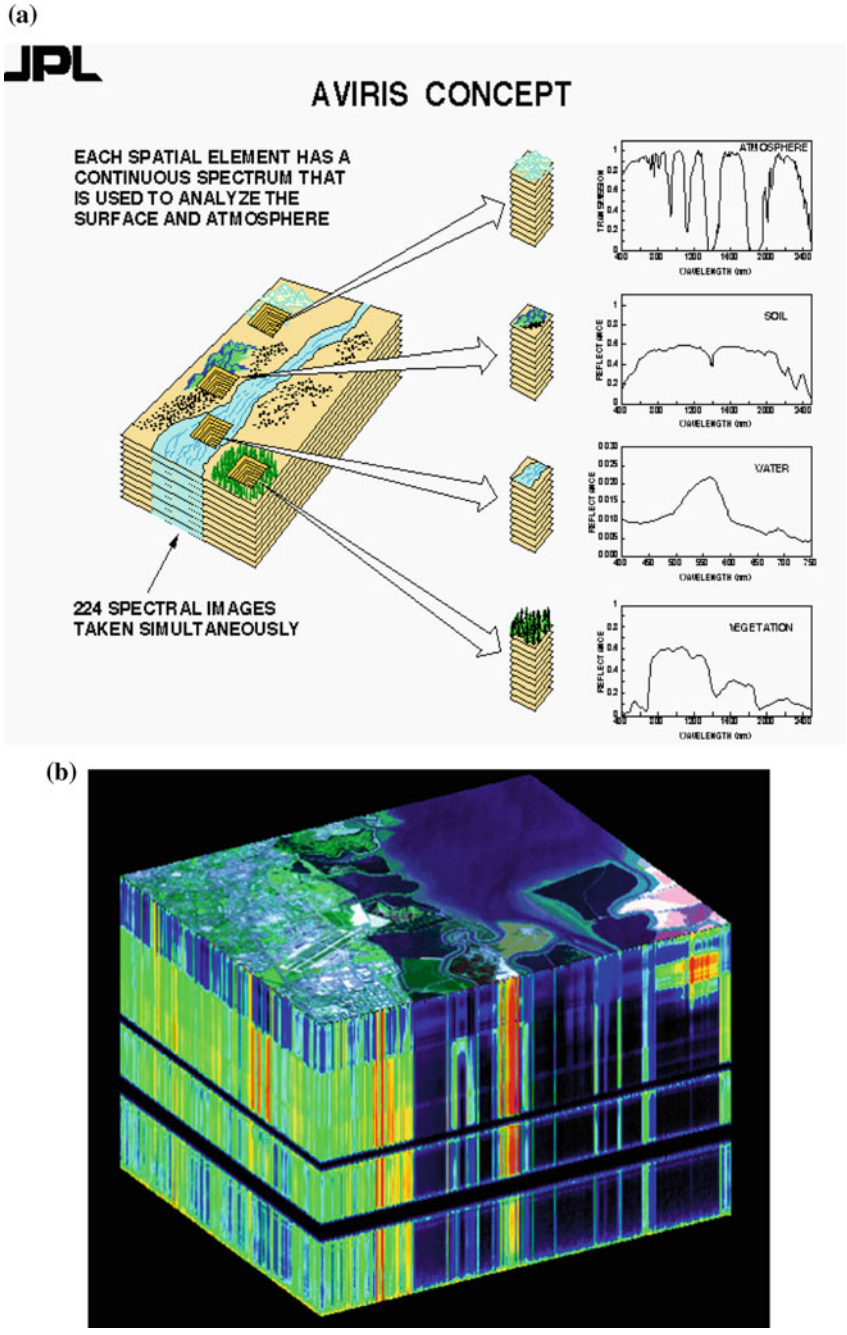

Fig. 4.1 **a** AVIRIS Imaging Spectrometer. *Source* http://aviris.jpl.nasa.gov. **b** AVIRIS datacube of Moffet Field, CA http://aviris.jpl.nasa.gov/data/images/avcubebig.gif

4.3 Geometric/Radiometric Correction

The Jet Propulsion Laboratory AVIRIS Data Facility delivers numerous engineering, aircraft state, and Global Positioning System (GPS) data sets that can be used to facilitate geometric rectification of the imagery. Calibrated AVIRIS data processed at the NASA Jet Propulsion Laboratory AVIRIS Data Facility was used in this research. The AVIRIS scanner, similar to other "push broom" scanners has a relatively geometrically correct scan line that wanders around with the roll, pitch yaw, velocity and direction changes in the moving aircraft (USGS). The cross-track scan line dimension is geometrically accurate because the scan time is fast (8.3 ms) compared to plane motions. This speed makes the AVIRIS scan line similar to that in a "push broom" satellite sensor such as Landsat (USGS). Using the JPL data, combined with ancillary data including Digital Elevation Models (DEM), geometric correction was performed utilizing ENVI software.

4.4 Radiative Transfer (RT) Code Applications

Understanding the relationship between reflectance, absorption and backscattering of water is essential for developing the analytical and multitemporal algorithms necessary to use remote sensing as a management tool in the nearshore/estuarine environment. The goal was to calibrate the AVIRIS data spectrally and radiometrically to radiance/reflectance for bio-optical and inverse modelings and generation of thematic maps of water quality parameters. Deriving water quality information at the water surface requires an accurate measure of the spectrum at the water surface, either remote sensing reflectance, normalized water leaving radiance or subsurface irradiance reflectance. Quantitative spectral measurements at the water surface form the basis for algorithms developed for CZCS (coastal Zone Color Scanner), SeaWiFS (the Sea-viewing Wide Field-view Sensor), MODIS (the Moderate-Resolution Imaging Spectroradiometer) and others (IOCCG 1999). These algorithms usually include two steps. The first step is to separate the atmospheric radiance from the radiance that comes from the water. The next step is to relate the water-leaving radiance to the water constituent concentration using a bio optical model (IOCCG 1999). Because the water-leaving radiance typically comprises at most about 10 % of the total radiance at the top of the atmosphere (TOA), the key to reliable retrieval of the water-leaving radiance from the measured total radiance is an accurate correction of the effects of aerosol scattering and absorption (Bagheri et al. 2001). Most of the atmospheric correction algorithms are designed for case 1 (oceanic) water and are based on the assumption that the water-leaving radiances are close to zero in the spectral range 760–870 nm. Thus, an aerosol/aerosol optical depth model can be derived from the bands located in that region of the spectrum. Subsequently, the aerosol information can be extrapolated into the visible range for retrieval of the water-leaving radiance and the water constituent concentration.

Unfortunately, these algorithms are not directly applicable to case 2 (turbid coastal) waters because of the presence of suspended materials which cause strong scattering in the spectral range 760–870 nm Further discussion on the utility of NIR for detection of water quality parameters—Chlorophyll a is given in Chap. 6.

Based on the findings of (Bagheri et al. 2003; Bagheri 2011) two promising methods for atmospheric corrections were tested and applied to the AVIRIS data to infer the water-leaving radiance: (1) Coupled Atmosphere Ocean (CAO) system based on discrete ordinate method (DISORT) and; (2) Tafkka.

4.4.1 Discrete Ordinate (DISORT)

The remote sensing signal received by the AVIRIS is the sum of the water-leaving radiance and contribution from atmospheric aerosols and molecules. Comparison of the AVIRIS measured radiance and in situ reflectance measurements reveals the effect of the atmosphere on the total upwelling spectral radiance measured by AVIRIS (Green et al. 1996). In atmospheric correction, the most challenging issue is to remove the impact of the highly variable aerosol component top of the atmosphere (TOA) to convert remote sensing measured radiance into normalized water leaving radiance. This is the required input to algorithms designed to retrieve phytoplankton pigments or total suspended material (TSM) concentrations. A comprehensive radiative transfer model for the coupled atmosphere-ocean (CAO) system based on the discrete-ordinate method (DISORT) computes the radiance within and backscattered from the atmosphere-ocean system (Jin and Stamnes 1994; Thomas and Stamnes 1999). The CAO-DISORT model, in which multiple scattering by water particles are properly treated, was suitable for constructing an atmospheric correction algorithm, for SeaWIFS to calculate the amount of light incident above the water surface (downwelling irradiance) for a given geographic location and a chosen atmosphere. Using SeaWiFS channels 765 and 865 nm the retrieval of aerosol optical depth and aerosol model was possible due to the small contribution from the case I water in the NIR. Then, the retrieved aerosol model and optical depth was used to predict the water leaving radiance in the visible, and subsequently to retrieve the chlorophyll concentration from the SeaWiFS channels at 490 nm and 555 nm. This approach provided simultaneous retrieval of atmospheric aerosol properties and chlorophyll concentrations in Case I waters. This algorithm was modified for use with the AVIRIS data to retrieve marine parameters for coastal waters (Bagheri et al. 2002). The AVIRIS data were ideal for coastal water retrieval because of the hyperspectral design, and the wide spectral range covering from 400 to 2500 nm. The channels at 765 nm and 865 nm are no longer suitable for aerosol retrieval in the coastal water, because of the strong scattering of coastal water. The longer wavelength channels, (1040 and 1240 nm) were selected to retrieve aerosol properties.

In contrast to Case I waters where the optical properties are assumed to covary with the chlorophyll concentration, a bio-optical model for coastal waters including

3 different components: chlorophyll, CDOM and suspended material were used. Because the different components have different spectral scattering/absorption characteristics, the wide spectral range of the AVIRIS instrument provided a good opportunity for retrieval of multiple components. Other feasibility studies based on a three-component model (Frette et al. 1998, 2001) showed promising results. Using hyperspectral instrument allows the inversion to be based on the full spectral form of the SIOP's especially the specific phytoplankton absorption. This might make a hyperspectral inversion more accurate and might provide information on accessory pigments etc.

A three-component bio-optical model in conjunction with the CAO-DISORT code was used to compute the radiance both at the surface and at the top of the atmosphere using the field measurements obtained over the Hudson/Raritan Estuary. Figure 4.2 shows a comparison of reflectance measured and computed

AVIRIS 2000_CAODisort values	
Station 3	
412	4.65E-03
443	9.19E-03
490	1.30E-02
510	1.78E-02
555	3.27E-02
670	9.33E-03
765	2.63E-03
865	1.69E-03

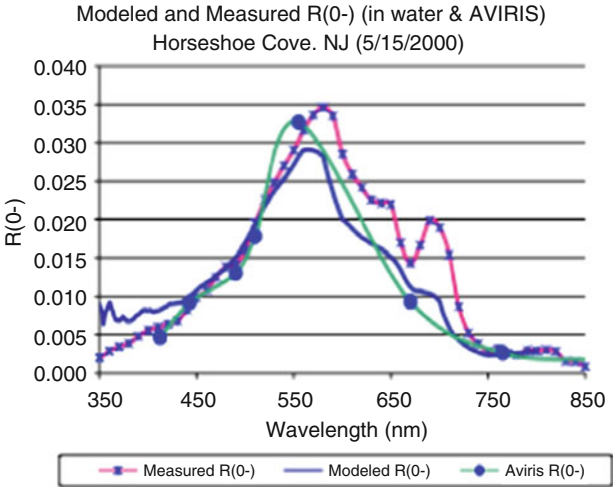

Fig. 4.2 Modeled, Measured R(0−) (in water) and CAO-DISORT R(0) for AVIRIS data collected (5/15/2000) over Station 3—Horseshoe Cove, NJ

from CAO-DISORT code based on a bio-optical model consistent with the field measurements. As depicted in the Fig. 4.2 there is a general agreement on the overall shape of the spectrum. But coupled atmosphere-ocean (CAO) system based on the discrete-ordinate method (DISORT) and partially the model seem to miss the distinct chl absorption peak (reflectance valley at 676 nm which is very profound in the measured spectra). The differences between CAO DISORT and the measured spectrum can be traced back to the calibration of the AVIRIS instrument which may not be calibrated as well over water bodies. It is important to note that AVIRIS is predominantly used for land applications. Nevertheless, the high spatial resolution of the AVIRIS data was a key in coastal water property retrieval and estimation since coastal waters usually have high spatial and temporal variations.

4.4.2 Tafkaa

Tafkaa is an extensively modified version of the Atmospheric REMoval algorithm (ATREM; Gao and Davis 1997) that has been specifically adapted to address the confounding variables associated with aquatic remote sensing applications (Gao et al. 2000; Montes et al. 2001). Atmospheric correction algorithm, Tafkaa, was used to remove the effects of the atmosphere so as to infer the water-leaving radiance. Tafkaa is used to calculate the amount of light incident above the water surface (downwelling irradiance) for AVIRIS using a coastal aerosol model. Tafkaa input parameters derived from the AVIRIS metadata files are listed in Table 4.2. A full description of these and other input parameters (i.e., solar and viewing geometry) can be found in Tafkaa User's Guide (Montes et al. 2004).

Tafkaa was run with a mid-latitude summer atmospheric model, using the 940 and 1140 nm bands to derive water vapor, and allowing the model to estimate atmospheric visibility based on image characteristics. Options were also selected to reduce the effects of spectral mismatch and minimize the errors associated with the water vapor bands and other smaller spectral artifacts.

The earlier atmospheric correction algorithms derive aerosol information from channels in the 660–870 nm spectral range. These algorithms cannot be easily adapted for the retrieval of water-leaving radiances over coastal waters. To derive aerosol information it is required to use these channels in addition to channels in longer wavelengths. An updated and modified version of TAFKAA (Montes et al. 2001), that uses the correct geometry on a pixel-by-pixel basis, and an improved treatment of the solar and view geometry is used here to process the hyperspectral data of Hudson/Raritan Estuary (Fig. 4.3a–d).

Table 4.2 Tafkaa atmospheric parameters applied to AVIRIS (5/15/2000)

Parameter	Parameterization	Source
Input radiance data cube	Image centre latitude = 40° 44′ 00″	AVIRIS Jet Propulsion Laboratory
	Image centre longitude = 73° 53′ 50″	
Cloud mask	NDVI > 0.05	AVIRIS Input data cube
Atmospheric model	Mid-Latitude summer	Selected from MODTRAN standard models on the basis of surface temperatures
Ozone	0.325	Acquired from Earth Probe TOMS (Total ozone mapping radiometer)
Atmospheric gases	H_2O, CO_2, O_3, CO, CH_4, O_2	Tafkaa options
Geometry	Single nadir viewing: Image centre zenith angle = 45° 00′ 00″	Calculated from AVIRIS header data
	Image centre azimuth angle = 194° 00′ 00″	
Aerosol method	Pixel-by-pixel	Tafkaa options
Aerosol model	Coastal	Selected from MODTRAN standard models based on geography of the scene
Relative humidity	80 %	Tafkaa options (selection on the basis of weather of the day)
Aerosol wavelengths	0.86, 1.04	Tafkaa options (selection based on the quality of the radiance cube. Noisy bands cannot be used)
Exclude aerosol model	None	Tafkaa options (selection based on the geography of the scene)
Exclude relative humidity	90, 98 %	Tafkaa options (selection based on the geography of the scene)
Sensor altitude	20.16 (km)	Acquired AVIRIS header data
Image centre date	5-15-200 (mm:dd:yyyy)	Acquired from AVIRIS header data
Image centre time	14:10:50 (hh:mm:ss)	Calculated from AVIRIS header data
Wind speed	2 (m/s)	

TAFKAA is used to provide the link between the spectra measured by the AVIRIS spectrometers and the in situ measurements of spectral reflectance in the water using OL754 spectroradiometer by considering the following:

The strength of the 760 nm oxygen absorption band measured in AVIRIS spectrum through characterization of surface pressure height.

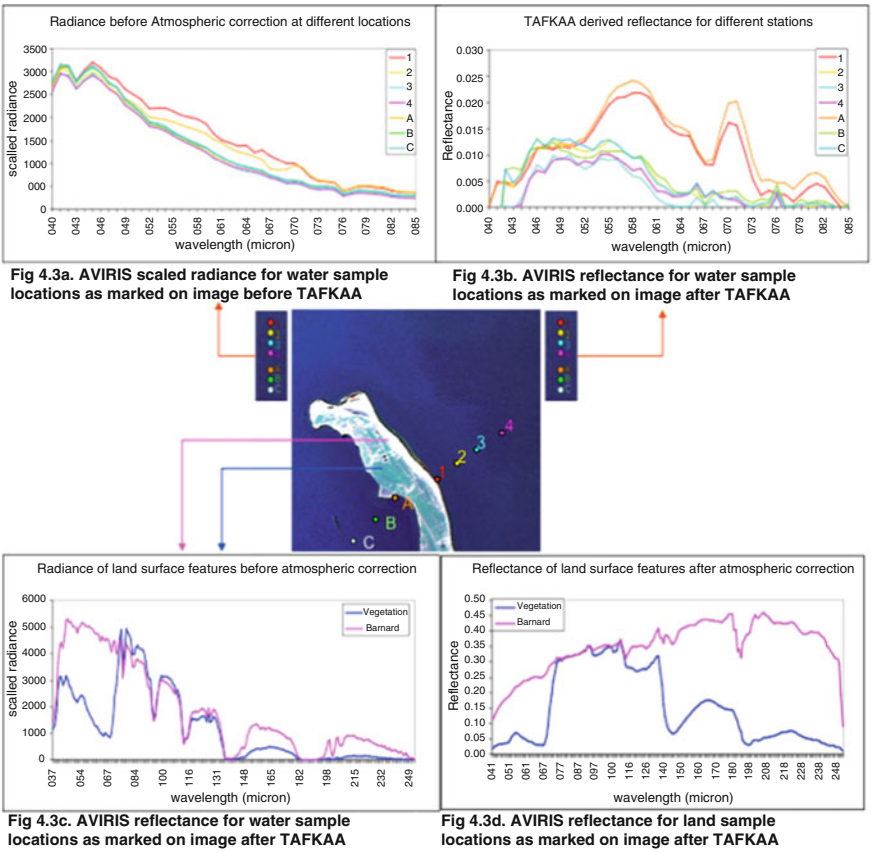

Fig 4.3a. AVIRIS scaled radiance for water sample locations as marked on image before TAFKAA

Fig 4.3b. AVIRIS reflectance for water sample locations as marked on image after TAFKAA

Fig 4.3c. AVIRIS reflectance for water sample locations as marked on image after TAFKAA

Fig 4.3d. AVIRIS reflectance for land sample locations as marked on image after TAFKAA

Fig. 4.3 (**a–d**) Results of application of Tafkaa on AVIRIS spectra of land/water sample points within the study area

The effect of aerosol scattering in the 400–700 nm region with an increasing effect toward shorter wavelengths (Green et al. 1996).

Figure 4.4 represents reflectance spectra measured by OL754, modeled spectra based on bio-optical model and TAFKAA derived spectra for station 1 (see Fig. 1.1) within the Sandy Hook Bay transect. (Note: The in-water measured spectra is produced by a handheld spectroradiometer and TAFKAA derived reflectance spectra is based on AVIRIS data with spatial resolution of 20 m × 20 m).

As expected, reflectance values in the Tafkaa output tend to approach zero at longer wavelengths. The general shape of the Tafkaa derived reflectance spectra and the range of values seems to be realistic for 450–750 nm. Although normally the spectral maximum is observed around 550–570 nm, it is slightly skewed to the right. Thus algorithms that are based on phytoplankton optical properties in the red

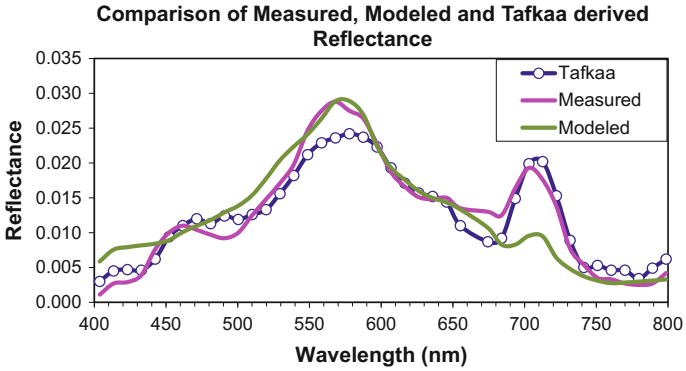

Fig. 4.4 Comparison of reflectance spectra measured by the field spectroradiometer (OL754), modeled spectra based on bio-optical model and Tafkaa derived AVIRIS spectra for sampling station 1 (Fig. 1.1 and Table 3.1)

wavelength region (near 675 nm coinciding with the 2nd chlorophyll absorption peak) are preferred since they provide better basis for remote monitoring of phytoplankton blooms in Case 2 waters. This is due to minimum interference from color dissolved organic material (CDOM) in the short wavelength region (e.g., around 440 nm coinciding with the 1st chlorophyll absorption peak).

Overall, as depicted, the chlorophyll dip is more or less obvious and the 700 nm peak (result of chl absorption) is also nicely reproduced by Tafkaa. Green peak is at the right wavelength (bit skewed to the right), with some difference in peak height. Blue slopes are similar. Although a certain amount of spectral mismatch is evident in the results (e.g., around the 780 nm), overall the Tafkaa derived spectra are reasonable for those locations sampled in situ and marked on Fig. 1.1.

ENVI software was used for image processing including georeferencing of the AVIRIS and band ratio analysis. Satellite remote sensing (i.e., CZCS, SeaWIFS and MODIS) data and associated reflectance (R) ratios have been applied to monitor chlorophyll in case 1 waters (IOCCG 1999). In inland water, Hoogenboom et al. 1998 determined that the ratio of AVIRIS bands around 705 nm with the band at 677 nm was the most sensitive for detecting chlorophyll-a and it is applicable for retrieval of chlorophyll concentrations in a wide range of case 2 waters. The advantage of using the ratio of spectral radiance reflectance is that all of the backscattering coefficients can be ignored. In other words, the ratio can be expressed by using only absorption coefficients, which are more stable for measurement than backscattering coefficients, emphasizing the band selection (Oki 2010).

Using similar band ratio (702 nm and 675 nm) and the equation cited below as in (Hoogenboom et al. 1998), chlorophyll concentration was calculated for Tafkaa derived AVIRIS data of Sandy Hook Bay area. The model was parameterized using

measured IOPs of Hudson/Raritan estuarine waters (Bagheri et al. 2005) representing the optical characteristics of the estuarine waters.

$$\text{Estimated Chlorophyll} = 90.035\,(\mathrm{R}(0)_{675}/\mathrm{R}(0)_{702}) - 70.108$$

The two wavelengths selected were close: one within the absorption range of chlorophyll-a, and the other one outside of the absorption range in order to estimate the chlorophyll-a concentration more accurately. The wavelengths selected found to be close to the published literature and are calibrated with shipboard data collected in this geographic location. The establishment of the—wavelengths in band ratio technique is important for better estimation when the chlorophyll concentration is relatively low. Figure 4.5 is a thematic map of ratio image which depicts the spatial distribution of chlorophyll concentration. The concentrations for given pixels of the

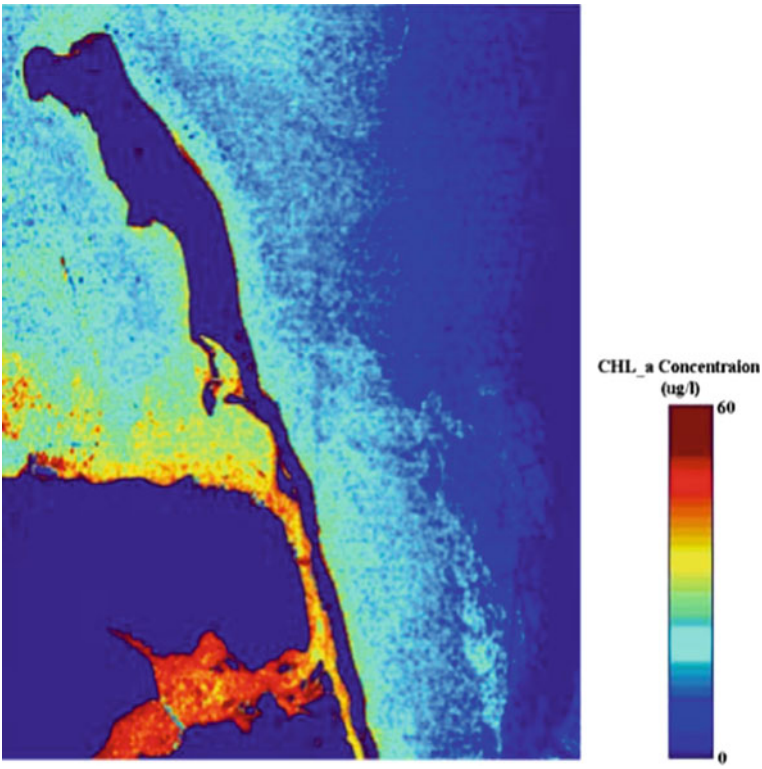

Fig. 4.5 AVIRIS ratio image map of spatial distribution of Ch1 concentration in Sandy Hook Bay transect of the study area acquired on 5/5/2000

Tafkaa derived AVIRIS data are consistent with in situ data supporting the validity of the approach.

The ratio image map (Fig. 4.5) shows maximum values of chlorophyll concentration in the Shrewsbury River and its confluence with the estuarine water (Fig. 1.1, Chap. 1). These maps are important input into a geographic information system (GIS) for better monitoring and management of water resources. Overall, Tafkaa produced more acceptable output result for atmospheric correction when likewise, the regression analysis identified a strong relationship ($R^2 = 0.98$) between the estimated chlorophyll concentrations derived from the AVIRIS band ratio (Fig. 4.5) and laboratory measured values (for sample stations Shrewsbury River and Sandy Hook as shown on Fig. 1.1). Figure 4.6 is a comparison of the model spectra for 3 sampling stations with different chlorophyll concentrations versus Tafkka derived AVIRIS spectra for transect covering the 3 sampling stations. The statistical summary and graph (Fig. 4.6) of the regression analysis as shown below indicate that the modeled is most useful in the vicinity of the (x, y) value on the regression line:

Intercept = −6.08
Slope = 1.08
Variance of the Error = 6.372219 Root Mean Square Error = 1.12891 *P*-value = 0.001365
Correlation Coefficient = 0.9783.

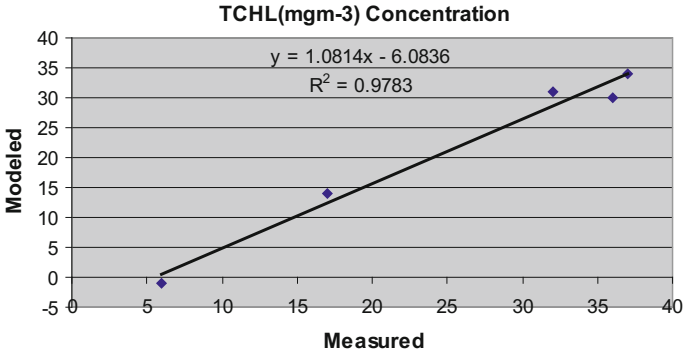

Fig. 4.6 Trend line of in situ chlorophyll plotted versus calculated chlorophyll concentration for Shrewsbury River and Sandy Hook Bay within the study area

References

Bagheri S, Stamnes K, Wei L (2001) Application of radiative transfer theory to atmospheric correction of AVIRIS Data, 10th JPL AVIRS Workshop

Bagheri S, Stamnes K, Lee W (2003) Application of radiative transfer theory to atmospheric correction of AVIRIS Data. In: Proceedings of 10th AVIRS Workshop, Pasadena, CA

Bagheri S, Peters S, Yu T (2005) Retrieval of water quality constituents concentrations from AVIRIS data in Hudson/Raritan Estuary. Int J Remote Sensing 26(18):4013–4027 20

Bagheri S (2011) Nearshore water quality estimation using atmospherically corrected AVIRIS data. Open Remote Sensing J. http://www.mdpi.com/2072–4292/3/2/257/

Carrere V, Briottet X, Jacquemoud S, Marion R, Bourguignon A, Chami M, Dumont M, Minghelli-Roman A Weber C, Lefevre-Fonollosa M-J, Mandea M (2013) Hypxim: a second generation high spatial resolution hyperspectral satellite for dual applications white paper June 2013

Frette O, Stamnes JJ, Stamnes K (1998) Optical remote sensing of marine constituents in coastal waters: a feasibility study. Appl Opt 37:8218–8326

Frette O, Erga SR, Stamnes JJ, Stamnes K (2001) Optical remote sensing of waters with vertical structure. Appl Opt 40:1478–1487

Gao B-C, Davis CO (1997) Development of a line-by-line based atmosphere removal algorithm for airborne and spaceborne imaging spectrometers, in Imaging Spectrometry III. In: Descour MR, Shen SS (eds) Proceedings of SPIE 3118, pp 132–141

Gao B-C, Montes MJ, Ahmad Z, Davis CO (2000) Atmospheric correction algorithm for hyperspectral remote sensing of ocean color from space. Appl Opt 39(6):887–896

Galeazzi C, Varacalli G, Longo F, Lopinto E, Garramone L, Capentiero R (2009) Overview of the PRISMA mission. In: Proceedings of 6th EARSel SIG Workshop on Imaging Spectroscopy, Tel Aviv, Israel

Green RO (2007) Overview of HyspIRI Mission. International Spaceborne Imaging Spectroscopy Working Group, 16 Nov 2007

Green RO (1996) Summaries of the 6th annual JPL airborne earth science jerkshop. Mol. 1, JCL AVIRIS Jerkshop. Pasadena, CA

Hoogenboom HJ, Dekker AG, Haan JF (1998) Retrieval of chlorophyll and suspended matter from imaging spectrometry data by matrix inversion. Can J Remote Sens 24(2):144–152

IOCCG (1999) Status and plans for satellite ocean color missions: considerations for complementary missions, Report Number 2. Dartmouth, Canada, p 42

Jin Z, Stamnes K (1994) Radiative transfer in nonuniformly refracting media such as the atmosphere/ocean system. Appl Opt 33:431–442

Kaufmann H, Segl K, Chabrillat S, Hofer S, Stuffler T, Müller A et al (2006) EnMAP hyperspectral sensor for environmental mapping and analysis. IGARSS, Denver, pp 1617–1619

Lucke RL (2011) Hyperspectral Imager for the Coastal Ocean (HICO): instrument description and first images. Appl Opt 50:1501–1516

Montes MJ, Gao B-C, Davis CO (2001) A new algorithm for atmospheric correction of hyperspectral remote sensing data. In: Roper WE (ed) Proceedings SPIE, Geo-Spatial Image and Data Exploitation II, vol 4383, pp 23–30

Montes MJ, Gao B-C, Davis CO (2004) "Tafkaa Users' Guide", Remote Sensing Division, Naval Research Laboratory

Oki K (2010) Why the ratio of reflectivity is effective to estimate the chlorophyll-a concentration in lake water. Remote Sens 2:1722–1730. doi:10.3390/rs2071722

Pearlman JS, Barry PS, Segal CC, Shepanski J, Beiro D, Carman SL (2003) Hyperion, a space based imaging spectrometer. IEEE Trans Geosci Remote Sens 41(6):1160–1173

Thomas GE, Stamnes K (1999) Radiative transfer in the atmosphere and ocean. Cambridge University Press

USGS Specroscopy Laboratory: http://speclab.cr.usgs.gov/spectral-lib.html

Chapter 5
Forward Bio-optical Modeling and Calibration

Abstract Utilization of remotely sensed data can provide greater economy in many types of hydrologic surveys than using conventional methods. This is possible because certain biological and geochemical constituents of surface/near surface water produce changes in reflectance that can be measured by ocean color remote sensing. To develop analytical algorithms for Case2 waters, an optical (forward) model needs to link the water quality parameters (WQPs) to the inherent optical properties (IOPs), linking these in turn to the subsurface irradiance reflectance R(0−) for retrieval of constituent concentrations using (inverse) modeling. The goal was to establish a monitoring system for retrieval of water constituent concentrations using remote sensing ocean color data. Subsequently, chlorophyll concentration can be used as an indicator for high biomass nuisance blooms, as well as an indicator for super-eutrophic conditions connected to oxygen depletion and dead zone formation.

Keywords Water leaving radiance · Remote sensing reflectance · Bio-optical model · Forward model · Inverse model · Suspended matter · Super eutrophic · Spectral bands · Simulated spectra · Constituent concentration · Absorption coefficient · Backscatter coefficient · Volume scattering function · Ocean optics-2000

5.1 Introduction

Global approaches of the past two decades for deriving water quality parameters (i.e., phytoplankton chlorophyll concentrations) are inadequate in nearshore/estuarine waters (e.g. Salama 2012), yet these waters are often the most significant in terms of national interests and vulnerability to climate change as the population pressure increases and the threat of global warming becomes real. The long-term goal of the research was to establish a monitoring system for retrieval of water constituent concentrations using remote sensing ocean color data. Subsequently, chlorophyll concentration can be used as an indicator for high biomass nuisance blooms, as well as an indicator for super-eutrophic conditions connected to oxygen

S. Bagheri, *Hyperspectral Remote Sensing of Nearshore Water Quality*,
SpringerBriefs in Environmental Science, DOI 10.1007/978-3-319-46949-2_5

depletion and dead zone formation. Remotely sensed data give information on the interaction between solar radiation, sea water and the different substances contained within it. The main processes involved are absorption, scattering and transmission of electromagnetic energy (Aguirre-Gomez et al. 1995). Absorption of light within the marine environment is carried out by four main optically active components: the water itself, phytoplankton pigments, coloured dissolved organic matter (CDOM) and total (inorganic + organic) suspended matter (TSM).

Utilization of remotely sensed data can provide greater economy in many types of hydrologic surveys than using conventional methods. This is possible because certain biological and geochemical constituents of surface/near surface water produce changes in reflectance that can be measured by ocean color sensors.

The presence of several non–correlated active constituents makes coastal/estuarine (Case2) waters optically more complex than most oceanic (Case1) waters. The color of Case1 waters quantified by e.g. remote sensing reflectance, or water leaving radiance which is predominantly a function of absorption and scattering by algal pigments, algal detritus and water itself. In Case2 waters, backscattering from particles is the dominant scattering factor. In those waters the combined effects of particulate backscattering and high absorption introduce complex interacting relations between the water constituents and subsurface reflectance. Therefore, retrieval of constituent concentrations from the reflectance requires an analytical approach (Doerffer 1989). In the analytical approach the retrieval is based on a bio-optical model which describes the relation between the reflectance and the concentrations of the constituents. The analytical approach seeks to model the remote sensing reflectance or the reflectance R(0+) just above the water surface in terms of the water inherent optical properties through radiative transfer modeling (Dekker et al. 2002). The measurement of subsurface reflectance R(0−) is therefore the key modeling parameter for deriving water constituents in terms of total chlorophyll, colored dissolved organic matter and total suspended matter from atmospherically corrected remote sensing data (Kirk 1994; Dekker et al. 1997). To develop analytical algorithms for Case2 waters, an optical (forward) model needs to link the water quality parameters (WQPs) to the inherent optical properties (IOPs), linking these in turn to the subsurface irradiance reflectance R(0−) for retrieval of constituent concentrations in (inverse) modeling. The approach described here yields results and algorithms that should be spatially and temporally transferable. Thus, it will offer a cost-effective management tool in estuarine/coastal environments that are most vulnerable to intensive pollution and concentration of high biomass nuisance blooms, as indicator for super-eutrophic conditions and in some cases the outbreak of HABs.

5.2 Forward Model—Calibration of Gordon's Model

The "forward" model simulates R(0+) from water IOPs using a bio-optical model and an approximation of the radiative transfer equation called the reflectance approximation (Morel and Prieur 1977; Zaneveld 1995) or through direct solution of

radiative transfer equation (RTE) using variety of models including Hydrolight (Mobley 1994). The R(TOA) can then be modeled from the R(0+) using radiative transfer calculations for the atmosphere through codes such as 6S, DISORT (Thomas and Stamnes 1999) or MODTRAN (Berk et al. 1989). The 'inverse' models first solve the R(0+) from R(TOA). Inverse (in water) optical modeling breaks the reflectance down into scattering and absorption components (IOPs) which can be further broken down into concentrations if the specific inherent optical properties of the optically active components are known (Park and Ruddick 2005).

The analytical approach is generally complex and requires field measurements and knowledge of local/regional (S)IOPs to develop a robust forward and inverse model (Mathews 2011). The two inherent optical properties measured were the spectral absorption and scattering. Spectral beam attenuation (c) and spectral absorption (a) were obtained using Ocean Optics-2000 spectrometer. (Note: Use of Ocean Optics-2000 for measuring IOP was experimental in this project). From these measurements, the spectral scattering (b) was deduced via subtraction of spectral absorption from the spectral beam attenuation ($b = c - a$). Absorption spectra of seston (phytoplankton and total suspended material) were determined using the filterpad method of Truper and Yentsch (1967). Several bio-optical models for ocean, coastal, and inland waters were investigated by Gordon et al. (1975), Morel and Prieur (1977), Whitlock et al. (1981), Kirk (1991), and Dekker et al. (1994). To test the applicability of geophysical forward and inverse modeling, the Gordon's model (Eq. 5.1) was used Note that this is the simplified version of the model which originally is a polynomial equation where, for turbid waters the second term of the polynomial is also relevant but often omitted (Lee et al. 1998). The model was used to spectral characteristics of the inland waters in the Netherlands and was adapted to the field measurements and laboratory analysis of the data for the Hudson/Raritan Estuary of NY–NJ:

$$R(0-) = r\ (b_b/(a + b_b)) \tag{5.1}$$

where

a is the total absorption coefficient absorption coefficient.
b_b is the backscatter coefficient backscatter coefficient.
r is a factor based on the geometry of incoming light and volume scattering in the water body.

To establish values for r and b_b for a specific location, knowledge of the volume scattering function is required. Vos et al. (1998) demonstrated that a practical solution for estimating the volume scattering function is to estimate r and b_b by matching modeled R(0−) to measured R(0−) values.

According to Kirk (1991), the factor r for a large number of water bodies measured varied between 0.34 and 0.39 depending on the solar zenith angle and atmospheric conditions. Dekker et al. (1997) reported that the r values ranged from 0.12 to 0.56

with an average of 0.29 for four inland water types in the Netherlands. These water types were: shallow eutrophic lakes, shallow mesotrophic lakes, deep lakes and river and canals. In this study, the values for factor r varied between 0.30–0.38 and were based on the field data obtained in the estuary during the course of the project (1999–2001) and calculations made by fitting measured R(0−) spectra to measured inherent optical properties. The inherent optical properties a and b_b were assumed to be linear functions of the constituent concentrations. This allowed the specific inherent optical properties (SIOP) to be introduced that link the concentrations of all optically active components to the subsurface irradiance reflectance. The inherent optical properties per unit concentration, e.g. the specific inherent absorption by phytoplankton, a*ph, was the absorption caused by 1 mg m^{-3} CHL. Using Beer's law, the total absorption coefficient—a—can be written as sum of the absorption by phytoplankton pigments, absorption by total suspended matter (bleached seston absorption), by coloured dissolved organic matter and water. The concentrations of the constituents are given by CHL, TSM (seston), and $CDOM_{440}$ (the absorption of colored dissolved organic matter at 440 nm). It should be noted that specific absorption for CDOM could not be calculated because no concentrations of DOC or POC were measured therefore, the CDOM absorption measured at 440 nm was taken as measure of concentration. A complete description of the water IOPs requires, in addition to the absorption coefficient, also the scattering coefficient as well as the Volume Scattering Function (VSF) or at least the backscattering coefficient. As part of insitu measurements, the ac-9 which provides extinction and absorption coefficients was used simultaneously with AVIRIS overflight during the field campaign of 2001. Use of the ac-9 complements the laboratory measurements of organic/inorganic constituent concentrations in the water. Comparison of the backscattering coefficient (VSF) determined from the laboratory-based spectrophotometer with that determined from the ac-9, was used to tune the index of refraction needed in the ac-9 method until the best agreement was obtained. This allowed us to check how well the backscattering coefficient and VSF can be determined from the ac-9 alone in the future by assuming that the index of refraction varies within reasonable bounds. It should be mentioned that use of ac-9 was experimental and limited to one sampling station coinciding with the AVIRIS overflight.

The backscattering (b_b) is used here which is based on the conversion of the scattering coefficient to the backscattering coefficient. The volume scattering function of Petzhold (Kirk 1994) is assumed to be valid, therefore b_b was obtained as 0.019b. For pure water, this ratio is 0.5 but for seston measurements depends on the composition (mainly grain size) (Morel and Prieur 1977). The values for absorption coefficient (a_w) and the scattering coefficient (b_w) of pure water were taken from Bukata et al. (1995).

$$a = a_w + a^*_{TSM}\mathrm{TSM} + a^*_{ph}\mathrm{CHL} + a^*_{CDOM}\mathrm{CDOM}_{440} \tag{5.2}$$

$$b_b = 0.5 \cdot b_w + b^*_{bTSM}\mathrm{TSM} \tag{5.3}$$

where

a_w	absorption of pure water.
a^*_{ph}	specific absorption of the phytoplankton.
a^*_{TSM}	specific absorption of TSM.
a^*_{CDOM}	specific absorption of CDOM.
b_w	scattering of pure water.
b^*_{bTSM}	specific backscatter of TSM.
0.5	backscatter to scatter ratio of pure water.

NOTE: *The asterisks denote that a and b_b are specific inherent optical properties per unit concentration denoted by the subscript.*

Table 3.1 shows the list of the sampling stations surveyed during 1999–2001 for data collection in conjunction with AVIRIS overflights. The specific absorption and scattering coefficients of the main water quality parameters of all sample points for August 1999 measured in the laboratory were averaged to produce one set of representative values and were used as the input values in bio-optical modeling (Fig. 5.1). The next step was to parameterize the bio-optical model by relating measured concentrations of CDOM, TSM and algal pigment concentrations to light absorption and scattering. Using the bio-optical model, R(0−) spectra were simulated for the measured concentrations (using measured IOP). The subsequent comparison between simulated and measured R(0−) provides a means to validate the bio-optical model and the accuracy of the field spectroradiometer measurements. Upon successful evaluation of this optical closure analysis, the in situ

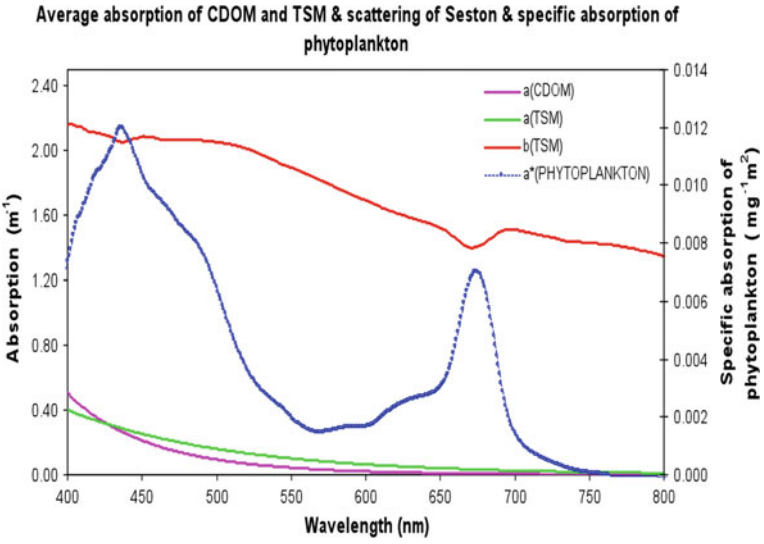

Fig. 5.1 Average absorption of CDOM and TSM, scattering of seston and specific absorption of phytoplankton as measured in situ during August'99 field campaign

measured R(0−) spectra can also be used to validate atmospherically corrected remote sensing observations of reflectance spectra. The shape of the phytoplankton absorption curve (Fig. 5.1) reflected the composition and concentration of different species of phytoplankton found in the estuary as mentioned in Chap. 2. The average absorption coefficient spectra of the seven sampled stations collected in August 1999, exhibited several distinctive spectral features—peak near 440 nm is the first chlorophyll-a absorption maximum, and the peak near 675 nm is the red chlorophyll absorption. There is a trough near 550 nm in which absorption of all photosynthetic pigments is minimal (Bukata et al. 1995). The average spectral scattering showed a slight decrease toward the longer wavelengths. Figure 5.2 depicts the distribution of measured SIOP that used as an input into the forward Gordon model to simulate spectra at two sampling stations (stations 1 and 3) for comparison with AVIRIS spectra in earlier publication (Bagheri et al. 2005).

Both Figs. 5.1 and 5.2 demonstrate that TSM absorption decreased steadily toward longer wavelengths. The measured TSM absorption at 440 nm varied between 0.13 and 0.50 m^{-1}. The colored dissolved organic material (CDOM) absorption showed a strong exponential decrease toward the longer wavelengths. The absorption at 440 nm varied between 0.12 and 0.49 m^{-1}. The specific absorption for chlorophyll-a at 676 nm was determined by dividing the value of a $(ph)_{676}$ by sum of the concentrations of chlorophyll-a and pheaopigment and varied between 0.0058 and 0.0078 mg^{-1} m^2. These values were lower than the values

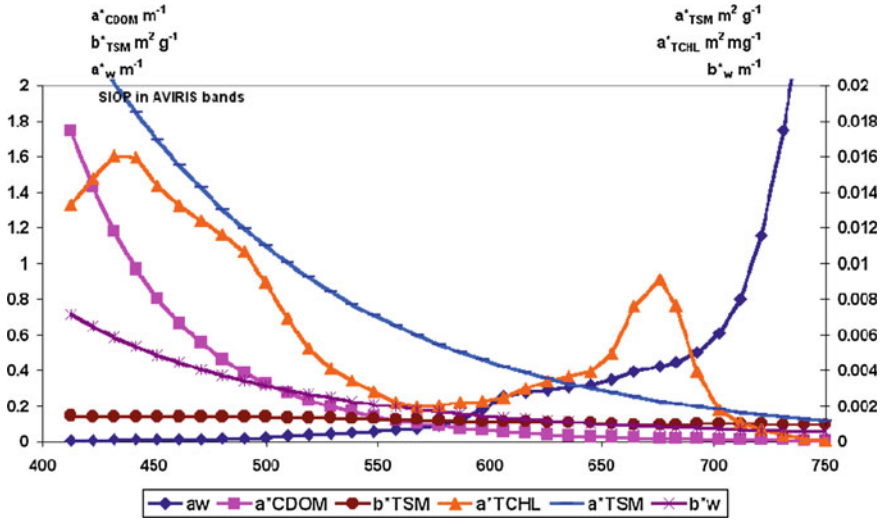

Fig. 5.2 Measured SIOP were input into the forward Gordon's model to simulate spectra for comparison with AVIRIS spectra (Bagheri et al. 2005)

measured in shallow eutrophic/mesotrophic (0.0180–0.0102 mg^{-1} m^2) waters of the Vecht lakes in the Netherlands (Dekker 1993) and the values (0.007–0.013 mg^{-1} m^2) calculated for healthy marine phytoplankton culture (Haardt and Maske 1987).

Using Eq. 5.1, the modeled R(0−) were generated, which represented the spectra for chlorophyll-a concentration 22 mg m^{-3} as calculated for Horseshoe Cove—the sampling station 3 (Table 3.1). Figure 5.3 depicts the measured R(0−) and the modeled R(0−) for Station 3 as sampled within estuarine waters simultaneously with AVIRIS overflight (5/15/2000). The modeled spectra matches the measured spectra reasonably well with a distinctive chlorophyll absorption dip occurred at 676 nm. The reflectance features are prominent supporting earlier research results that information extraction in estuarine/nearshore waters using remotely sensed data should be limited to green—infra red part of the spectrum (Gordon and Morel 1983) but the information in the blue part of the spectrum is needed for CDOM determination.

The modeling approach in estimating the concentrations of the different components is based on establishing the unit contributions of the different water constituents by field and lab measurements giving the specific inherent optical properties measurements and then for any given pixel in the image, estimating the concentrations that would explain the observed reflectance. Accordingly, reflectance spectra calculated from both specific absorption and specific backscattering coefficients together with their concentration ranges can be computed. The approach is described in detail in Jupp et al. (1994).

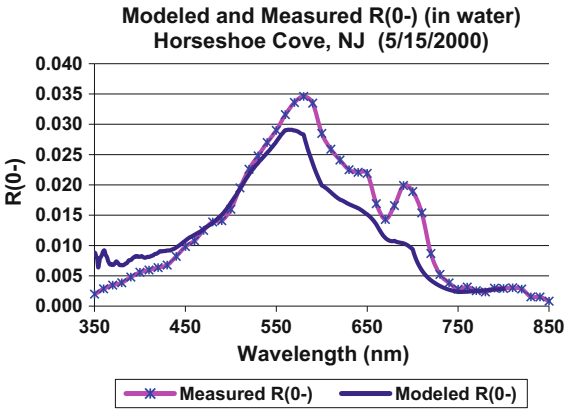

Fig. 5.3 Comparison of reflectance spectra measured by the field spectroradiometer (OL754), modeled spectra based on bio-optical model for Horseshoe Cove (station 3—Fig. 5.1)

5.3 Calibration of R(0−) from AVIRIS Calibrated Radiance

Bio-optical models were constructed and used in conjunction with forward modeling to quantify the effects of chlorophyll, colored dissolved organic matter as well as inorganic material on the measured radiance through inverse modeling as discussed in the next chapter. Simply stated, the inverse modeling consists of determining the water constituents as well as the atmospheric parameters that in combination give rise to the radiance spectra measured by the ocean color sensors. Algorithms were developed and used to quantify the effects of the atmosphere on the radiance measured by the remote sensing sensor. To test the retrieval algorithm the configuration of the NASA/AVIRIS bands were used as discussed in the next chapter. Figure 5.4 depicts the performance of the bio-optical model for different range of chlorophyll concentrations as compared with atmospherically corrected AVIRIS spectra using Tafkka radiative transfer code at three sampling stations surveyed during AVIRIS data acquisition in May 15, 2000. Here the modeled spectra fits reasonably well with the Tafkka derived AVIRIS spectra. Detailed descriptions on the atmospheric correction and inverse modeling are given in Chaps. 4 and 6 respectively.

Overall, The optical closure experiments show that the bio-optical model is sufficiently accurate for this application. At the same time its formulation and parameterization is relatively simple so it can be inversed using relatively straight forward inversion methods such as matrix inversion (see next chapter). Because of the many spectral bands of AVIRIS the system of equations is overdetermined and

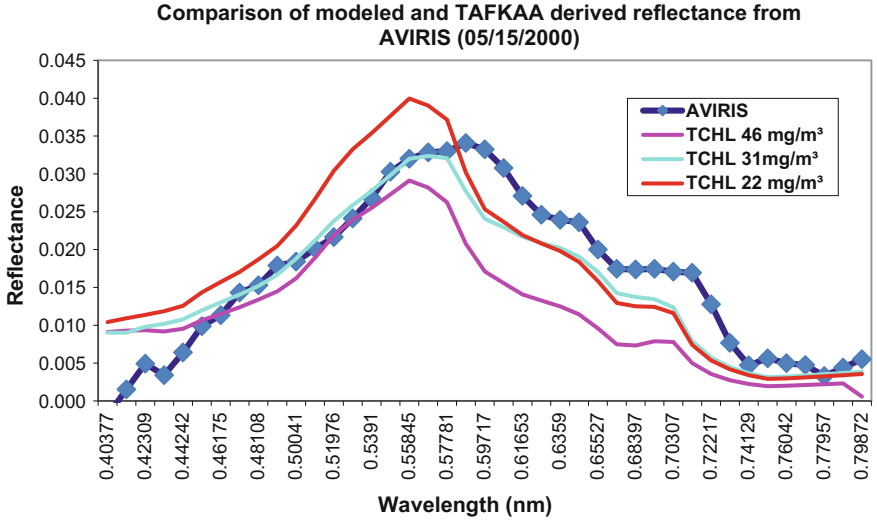

Fig. 5.4 Comparison of modeled spectra for different concentration values and atmospherically corrected AVIRIS spectra for 3 sampling stations surveyed during May 15, 2000 AVIRIS data acquisition

techniques like singular value decomposition can be used. AVIRIS does capture important spectral features such as phytoplankton absorption around 676 nm and SPM backscattering (around 550 nm and above 700 nm).

In brief, bio-optical modeling has the ability to retrieve various optical properties of water quality parameters simultaneously from the remote sensing reflectance. Their theoretical basis on sound solutions to the radiative transfer equation makes them potentially the most reliable approach. The bio-optical model can further be used to simulate spectra at locations where some (general) knowledge exists of the concentrations of optically active water constituents (e.g. very dark and thus clear water locations on the image). This may lead to additional possibilities to calibrate the atmospheric correction of remote sensing observations. It will also help to evaluate the performance of sensors such as AVIRIS at challenging low reflectance conditions. The inversion of the calibrated bio-optical model can be used to characterize the estuarine waters in terms of TCHL concentration, CDOM and TSM (Figure 5.5 depicts the spatial distributions of optical water quality parameters as AVIRIS image maps).

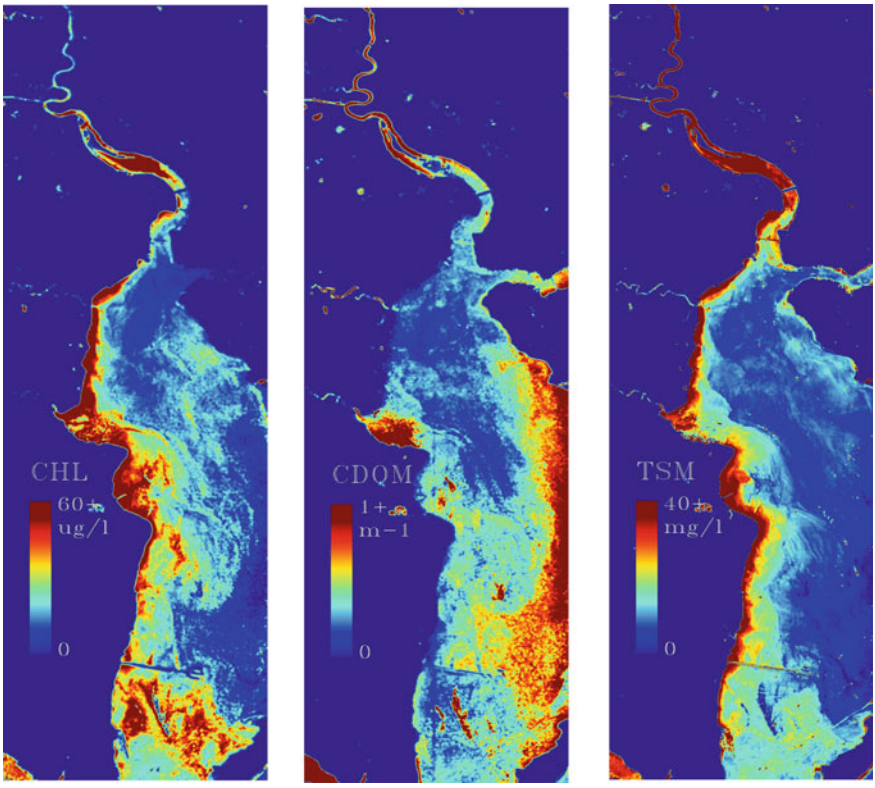

Fig. 5.5 AVIRIS image maps representing the spatial distributions of water quality parameters (i.e., TCHL, CDOM and TSM) along a AVIRIS transect covering southern part of Hudson/Raritan estuary

Global assessments of the quality, quantity and changes occurring in nearshore/estuarine waters from remote sensing are likely to become commonplace within the next few years. Hyperspectral satellite remote sensing (i.e., HyspIRI) will play a vital role in determining the growing impact that global change will have on these limited and increasingly valuable resources.

References

Aguirre-Gomez R, Boxal1 SR, Weeks AR (1995) Identification of algal pigments using high order derivatives. In: IEEE proceedings, pp 2084–2086

Bagheri S, Peters S, Yu T (2005) Retrieval of water quality constituents concentrations from AVIRIS data in Hudson/Raritan estuary. Int J Remote Sens 26(18, 20):4013–4027

Berk A, Berstien LS, Robertson DC (1989) MODTRAN: A moderate resolution model for LOWTRAN7. Report GL-TR-89-0122, US Air Force Geophysical Laboratory, Hanscom, Massachusetts

Bukata RP, Jerome JH, Kya Konratyev, Pozdnyakov DV (1995) Optical properties and remote sensing of inland and coastal waters. CRC Press, Boca Raton

Dekker AG (1993) Detection of optical water quality parameters for eutrophic waters by high resolution remote sensing. Ph.D. Thesis, Vrije Universiteit, Amsterdam, 222 pp ISBN:90-9006-234-3

Dekker AG, Bonze M (1994) Imaging spectrometry as a research tool for inland water resources analysis. In: Hill J (ed) Dordrecht, Kluwer AP, The Netherlands

Dekker AG, Hoogenboom HJ, Goddijn LM, Malthus TJM (1997) The relationship between inherent optical properties and reflectance spectra in turbid inland waters. Remote Sens Rev 15:59–74

Dekker AG, Vos RJ, Peters SWM (2002) Analytical algorithms for lake water TSM estimation for retrospective analyses of TM and SPOT sensor data. Int J Remote Sens 23:15–35

Doerffer R (1989) Imaging spectroscopy for detection of chlorophyll and suspended matter. Imaging spectroscopy: fundamentals and perspective applications. Kluwer, AP, pp 215–258

Gordon HR, Morel AY (1983) Remote assessment of ocean color for interpretation of satellite visible imagery, a review, in lecture notes on coastal and estuarine studies. Springer Verlag, New York, pp 144

Gordon HR, Brown OB, Jacobs MM (1975) Computed relationships between Inherent and apparent optical properties of a flat homogeneous ocean. Appl Opt 14:417–427

Haardt H, Maske H (1987) Specific in vivo absorption coefficient at 675 nm. Limnol Oceanogr 32(3):608–619

Jupp DLB, Kirk JTO, Harris GP (1994) Detection, identification and mapping of cyanobacteria—using remote sensing to measure the optical quality of turbid inland waters. Aust J Mar Freshw Res 45:801–828

Kirk JTO (1991) Molume scattering function, average cosines, and the underwater light field. Limnol Ocean 36(3):455–467

Kirk JTO (1994) Light and photosynthesis in aquatic ecosystems. University Press, Cambridge, UK, p 401

Lee Z, Carder KL, Mobley CD, Steward RG, Patch JS (1998) Hyperspectral remote sensing for shallow waters. I. A semianalytical model. Appl Opt 37(27):6329–6338. Retrieved from http://www.ncbi.nlm.nih.gov/pubmed/18286131

Matthews Mark William (2011) A current review of empirical procedures of remote sensing in inland and near-coastal transitional waters. Int J Remote Sens 32(21):6855–6899

Mobley CD (1994) Light and water: radiative transfer in natural waters. Academic Press, London, p 592

Morel A, Prieur L (1977) Analysis of variations in ocean color. Limnol Oceanogr 22:709–722
Park YJ, Ruddick K (2005) Model of remote-sensing reflectance including bidirectional effects for case 1 and case 2 waters. Appl Opt 44(7):1236–1249. Retrieved from http://www.ncbi.nlm.nih.gov/pubmed/15765704
Salama MS (2012) Current advances in uncertainty estimation of earth observation products of water quality. In: Rustamov RB, Salahova SE (eds) Earth observation: e-book, InTech, Rijeka, pp 229–254. ISBN 978-953-307-973-8
Stamnes K, Li W, Yan B, Barnard A, Pegau WS, Stamnes JJ (Submitted) A new ocean color algorithm: Simultaneous retrieval of aerosol optical properties and chlorophyll concentrations. Appl Opt
Thomas GE, Stamnes K (1999) Radiative transfer in the atmosphere and ocean. Cambridge University Press, UK
Truper HG, Yentsch CS (1967) Use of glass fiber filters for the rapid preparation of in vivo absorption spectra of photosynthetic bacteria. J Bacteriol 94:1255–1256
Vos RJ, Dekker AG, Peters SWM, Rossum GV, Hooijkaas LC (1998) RESTWAQ2, part II. Comparison of remote sensing data, model results and in-situ data for the Southern Frisian Lakes. Report No NRSP-2 98-08b, Remote sensing Board (BCRS), Programme Bureau, Rijkswaterstaat Survey Department, Netherlands
Whitlock CH, Poole LR, Usry JW, Houghton WM, Witte WG (1981) Comparison of reflectance with backscatter and absorption parameters for turbid waters. Appl Opt
Zaneveld (1995) A theorretical derivation of the dependence of the remotely sensed reflectance of the ocean on the inherent optical properities

Chapter 6
Inverse Modeling and Validation

Abstract The 'inverse' model solves the IOPs (or concentrations of optically active water constituents) from reflectance measured at the top of the atmosphere by remote sensors or from in situ measurements of reflectance. Inversion approaches for the retrieval of water-quality parameters from remotely sensed data are typically divided into two categories—empirical and model based (IOCCG 2002). Empirical methods derive a relationship between optical measurements and constituent concentrations based on observations from experimental data sets. Model-based techniques exploit bio-optical models that capture the connection between water constituent and spectra of water-leaving radiance/reflectance and a radiative transfer model that describes light propagation through the water and the atmosphere. Model-based solutions have the ability to retrieve simultaneously various optical and biogeophysical parameters from the remote-sensing reflectance. Their theoretical basis on sound solutions to the radiative transfer equation makes them potentially a more expedient approach (Matthews 2011).

Keywords Inverse modeling · Reflectance spectra · Upwelling radiance · Downwelling irradiance · Zenith · Total chlorophyll (TCHL) · Linear matrix inversion · Inversion matrices · Least square (LS) method · Singular value decomposition (SVD) method · Tikhonov method · MERIS bands (MB) · NIR/Red bands · Maximum a posteriori (MAP) Gibbs sampling · Probability distribution

6.1 Inverse Modeling

As discussed in Chap. 5, the research was based on data from AVIRIS imaging spectrometer, field spectrradiometers and water samplings. Based on these measurements, optical water quality models were constructed linking the water constituent concentrations to (i) the inherent optical properties (IOP), using the specific inherent optical properties (SIOP), and (ii) to the subsurface (ir)radiance reflectance (Bagheri and Dekker (Invited Paper); Bagheri et al. 2000, 2001). The model then was validated with the R(0−) measured in the study site. The validation of

S. Bagheri, *Hyperspectral Remote Sensing of Nearshore Water Quality*,
SpringerBriefs in Environmental Science, DOI 10.1007/978-3-319-46949-2_6

subsurface irradiance reflectance measured by the spectroradiometer is an important step for establishing the optical properties of the Hudson/Raritan estuarine waters. Modeling of reflectance spectra based on the IOP will explain the variability in water quality concentrations and inverse modeling can be used for monitoring water quality conditions in the estuarine waters using remotely sensed data. Since no single method is yet available to accurately derive concentrations of all optically active water quality constituents under variable conditions, we used several inversion techniques as discussed in this chapter for retrieval of constituent concentrations using the in situ data collected by OL754—high resolution/close-range spectroradiometer for subsequent comparison with atmospherically corrected AVIRIS spectra. To retrieve the concentrations of water quality parameters quantitatively, several inverse modeling algorithms (Hoge and Lyon (1996), Hoogenboom et al. (1998) and Peters (2001) were applied to the data set of the study area collected on May 5, 2000 and July 13, 2001) in conjunction with AVIRIS overflights. Results of applications of additional retrieval algorithms, including the two-band three-band algorithms and Bayesian modeling, are also presented in this chapter briefly. For details on the latter, the readers are referred to (Bagheri 2011; Michalopoulou et al. 2010).

6.1.1 Linear Matrix Inversion (Model #1)

The linear matrix inversion model developed by Hoge and Lyon (1996) was selected which describes the generation of upwelled water-leaving spectral radiance caused by backscatter and absorption of incident downwelling solar irradiance. This model is based on bio-optical model developed by Gordon et al. (1988):

$$L_w(\lambda) = F_0 \cdot t(\theta_0) \cdot \cos(\theta_0) \cdot M \cdot R/Q \tag{6.1}$$

L_w water-leaving radiance
F_0 extraterrestrial solar irradiance
t diffuse transmittance of the atmosphere
θ_0 solar zenith angle
M 0.55 for nominal sea conditions
R measured reflectance at sample points
Q ratio of the upwelling radiance to upwelling irradiance toward zenith

It was determined (Gordon et al. 1988) that *R/Q* can be directly related to the total absorption a and the total backscatter b_b by $R/Q = (l_1X + l_2X^2)$, where $R = E_u/E_d$, E_u and E_d are the upwelling and downwelling irradiances, respectively, just beneath the surface. Q is the ratio of the upwelling radiance to the upwelling irradiance toward zenith, l_1 = 0.0949 and l_2 = 0.0794 were calibrated as constants parameters [Gordon et al. 1988]. Note: R = R(0−) is subsurface irradiance reflectance. E_u and E_d are both measured under water and X is the single scattering albedo.

The inversion matrices were used for solving for three unknowns $a_{ph}(\lambda_i)$, $a_d(\lambda_i)$ and $b_{bt}(\lambda_i)$ at any wavelength λ_i:

$$\begin{bmatrix} 1 & 1 & v(\lambda_1) \\ D_{21} & e^{[-S(\lambda_2-\lambda_1)]} & (\lambda_1/\lambda_2)^n v(\lambda_2) \\ D_{31} & e^{[-S(\lambda_3-\lambda_1)]} & (\lambda_1/\lambda_3)^n v(\lambda_3) \end{bmatrix} \cdot \begin{bmatrix} a_{ph}(\lambda_1) \\ a_d(\lambda_1) \\ b_{bt}(\lambda_1) \end{bmatrix} = \begin{bmatrix} h(\lambda_1) \\ h(\lambda_2) \\ h(\lambda_3) \end{bmatrix} \tag{6.2}$$

where

$$h(\lambda) = -(a_w + b_{bw} v)$$

a_w absorption coefficient of pure water
b_{bw} backscatter coefficient of pure water
λ different wavelengths
s spectral slopes
n total constituent backscattering spectral exponent
g phytoplankton Gaussian model spectral width
a_{ph} absorption coefficient of the phytoplankton
a_d absorption coefficient of CDOM
b_{bt} total constituent backscattering coefficient
V a factor to separate absorption and scattering components of water
D the data-model matrix (D matrix contains radiance data and model parameters)

$$D_{21} = e^{(\lambda_2-\lambda_1)^2/-2g^2} \quad D_{31} = e^{(\lambda_3-\lambda_1)^2/-2g^2} \tag{6.3}$$

The $a_{ph}(\lambda_i)$, $a_d(\lambda_i)$ and $b_{bt}(\lambda_i)$ at all wavelengths are computed using the following:

$$a_{ph}(\lambda_i) = a_{ph}(\lambda_g) \cdot e^{[(\lambda_i-\lambda_g)^2/(-2g^2)]} \tag{6.4}$$

$$\begin{aligned} a_d(\lambda_i) &= a_d(\lambda_d) \cdot e^{[-s(\lambda_i-\lambda_g)]} \\ b_{bt}(\lambda_i) &= b_{bt}(\lambda_b)(\lambda_b/\lambda_i)^n \end{aligned} \tag{6.5}$$

To calibrate the model, the algorithm was applied to the in-water measurements collected by the field spectroradiometer in the estuary to retrieve the IOPs (from which the constituent concentrations were obtained). Using the following, the concentration was obtained from the specific absorptions of water quality parameters (i.e., TCHL):

$$C = a_{ph}(\lambda_1)/a^*_{ph}(\lambda_1) \tag{6.6}$$

where

$a^*_{ph}(\lambda_1)$ is the chlorophyll-specific absorption at λ_1.

The result of the matrix inversion method to retrieve the IOPs (from which the constituent concentrations (TCHL and CDOM) can be obtained) are shown in Fig. 6.1a, b using the following values:

$$\lambda_1 = 440, \lambda_2 = 500, \lambda_3 = 560\,\text{nm}, \text{S} = 0.025, \text{n} = 1.2, \text{g} = 30.$$

It should be noted that a modified ***n*** was chosen for Hudson/Raritan Estuary using the least Square algorithm for better retrieval results. Similarly, the CDOM spectral slope—***s*** and phytoplankton Gaussian spectral width—***g*** had to be modified based on the in situ measurements. Further to validate the results of the inversion methods, the following statistical solutions were used to solve the above system including: Least-squares (LS), and the singular value decomposition (SVD) methods (Blank 1980). The SVD method is a good analytical tool and allows a quantitative evaluation of singularities. However, the SVD solutions may become extremely unstable when one or more of the singular values is small. In order to make the solution more stable, the Tikhonov regularization technique was used. The Tikhonov method gives larger weight to larger singular values in the SVD solution and gives lower weight to small singular values. Here, all the three methods were applied for validation.

As shown in Fig. 6.2a, b the output from the three methods were used to compare modeled and measured absorptions of phytoplankton and CDOM were very similar with the SVD method yielding a better result (Yu 2005). But the methods failed to retrieve the phytoplankton peak around 665 nm which could be because of the weights or alternatively it could be that the radiometer has sensitivity problems in this region of the spectrum. Further analysis is needed to justify this result.

Note that in the modified version of Hoge's linear matrix inversion model, the following values were assigned: ***n*** = 1.8, ***s*** = 0.03 and ***g*** = 30.

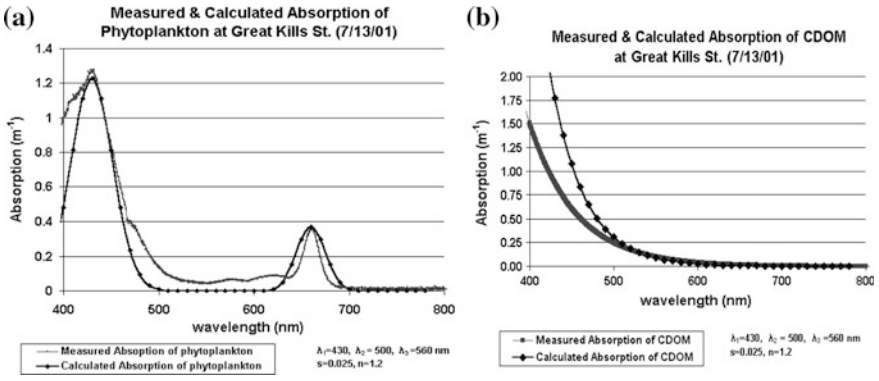

Fig. 6.1 Measured and retrieved phytoplankton and CDOM absorptions at Great Kills Station (see Table 6.1)

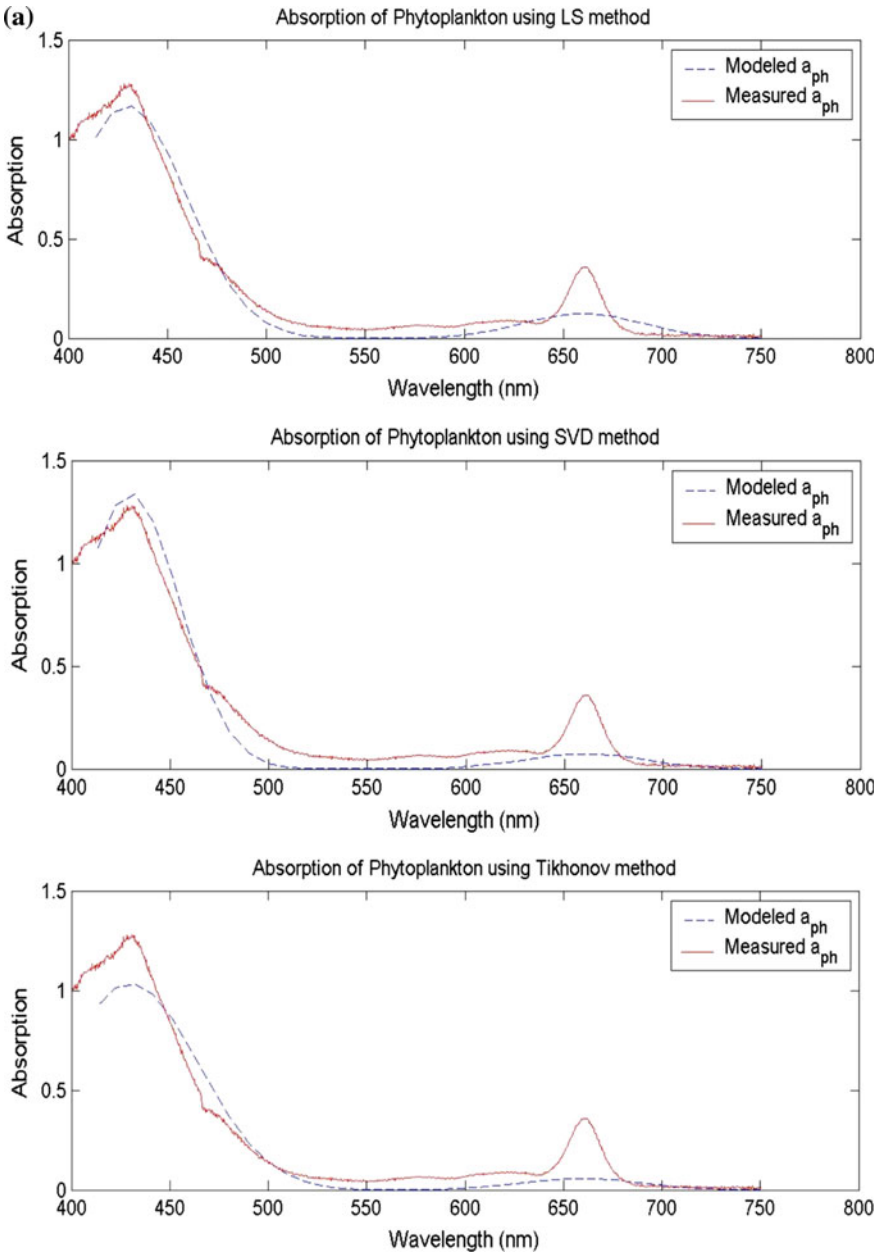

Fig. 6.2 **a** and **b** Comparison between measured and modeled absorptions of phytoplankton CDOM using LS, SVD and Tikhonov methods

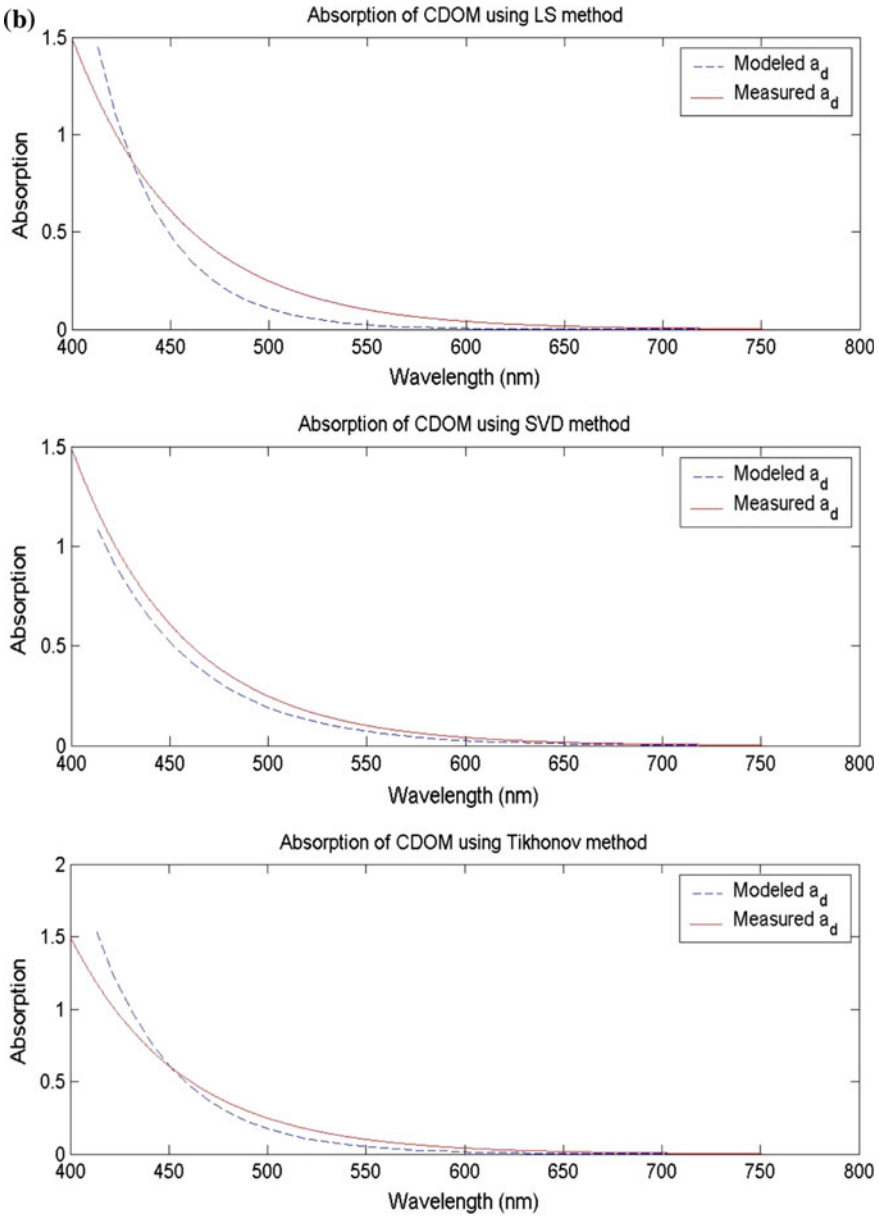

Fig. 6.2 (continued)

6.1.2 Matrix Inversion Method (Model #2)

An alternate form of the bio-optical model was obtained by substituting Eq. (6.7) into Eq. (6.8) and by taking the correlation between TSM and TCHL into account (Hoogenboom et al. 1998):

$$R(0-) = r(b_b/(a + b_b)) \tag{6.7}$$

where

a total absorption coefficient
b_b backscatter coefficient
r a factor based on the geometry of incoming light and volume scattering in the water

$$\begin{aligned} a &= a_w + a^*_{TSM} TSM + a^*_{ph} CHL + a^*_{CDOM} CDOM_{440} \\ b_b &= 0.5 \cdot b_w + b^*_{bTSM} TSM \end{aligned} \tag{6.8}$$

where

a_w *absorption of pure water*
b_w *scattering of pure water*
a^*_{ph} *specific absorption of the phytoplankton*
$b_b{}^*_{TSM}$ *specific backscatter of TSM*
a^*_{TSM} *specific absorption of TSM*
$_{0.5}$ *backscatter to scatter ratio of pure water*
a^*_{CDOM} *specific absorption of CDOM*

Application of such alternate matrix inversion model (MIM) to the dataset of the study area provided a good estimate of the constituent concentrations (Table 6.2). Validation of the concentration estimates by optical means and the AVIRIS atmospherically corrected data is based on in situ measurements of spectra and concentrations. Accordingly, the total TSM is equal to TSM of phytoplankton and TSM of suspended solids ($TSM_{tot} = TSM_{ph} + TSM_{ss}$) values. The total TSM includes the part of the dry weight determined by the biomass of phytoplankton which is correlated to TCHL concentration. The correlation coefficient can vary between 0.02 and 0.1 for fresh water algae (Gons et al. 1992). An average value of 0.07 ($TSM_{ph} = 0.07$ CHL) was used here based on the work of Buiteveld (1990):

$$\begin{aligned} &[a^*_{ph} + 0.07 a^*_{TSM} + 0.07 b^*_{bTSM} X] CHL + [a^*_{TSM} + b^*_{bTSM} X] TSM_{ss} \\ &= -a_w - a^*_{CDOM} CDOM_{440} - b_{bw} X \end{aligned} \tag{6.9}$$

where

$$X = 1 - \frac{f}{R(0-)}$$
$$TSM_{ss} = TSM_{tot} - TSM_{ph} = TSM_{tot} - 0.07CHL$$

Evaluating Eq. (6.9) for every wavelength of interest yields a set of equations for input into a matrix equation:

$$Y = \begin{pmatrix} A_{m1} \\ A_{m2} \end{pmatrix} \begin{pmatrix} CHL \\ TSM_{ss} \end{pmatrix} \tag{6.10}$$

where

$$A_{m1} = a^*_{ph}(\lambda_m) + 0.07a^*_{TSM}(\lambda_m) + 0.07b^*_{bTSM}(\lambda_m)\left(1 - \frac{f}{R(\lambda_m)}\right)$$
$$A_{m2} = a^*_{TSM}(\lambda_m) + b^*_{bTSM}(\lambda_m)\left(1 - \frac{f}{R(\lambda_m)}\right)$$
$$y_m = -a_w(\lambda_m) - a^*_{CDOM}(\lambda_m)CDOM_{440} - b_{TSM}(\lambda_m)\left(1 - \frac{f}{R(\lambda_m)}\right)$$

Matrix A (6.10) is a two by two matrix which can be inverted analytically yielding the following expressions for the concentrations:

$$CHL = \frac{A_{22}y_1 - A_{12}y_2}{A_{11}A_{22} - A_{12}A_{21}} \quad \text{and} \quad TSM_{ss} = \frac{-A_{21}y_1 + A_{11}y_2}{A_{11}A_{22} - A_{12}A_{21}} \tag{6.11}$$

Table 6.1 lists the measured and modeled concentration values for all the stations as computed by the above inversion techniques. There is a reasonable match over majority of sampling stations between measured and modeled concentrations using Model #1 and Model #2. Validation of the concentration estimates by optical means is based on in situ measurements of spectra and concentrations. Further details can be found in Bagheri et al. (2005).

Figure 6.3a depicts the trend line for given CHL-a concentrations calculated by matrix inversion methods plotted versus in situ CHL-a measured in Hudson/Raritan Estuary. Figure 6.3b is the trend line for given TSM concentration computed by the matrix inversion and Hakvoort's numerical model (Hakvoort et al. 2000).

Table 6.1 Comparison of measured - modeled concentrations based on MIM: #1 (Hoge and Lyon 1996), #2 (Hoogenboom et al. 1998), and #3 (Peters 2002), Bagheri et al. (2005)

St	Location	Measured TCHL (mg m^{-3})	Modeled TCHL(#1) (mg m^{-3})	Modeled TCHL(#2) (mg m^{-3})	Modeled TCHL(#3) (mg m^{-3})	Measured TSM (g m^{-3})	Modeled TSM(#2) (g m^{-3})	Modeled TSM(#3) (g m^{-3})
1	Comptons/PewsCreek	**15**	4	29	22	**6**	27	3
2	Keyport Harbor	**32**	–	–	28	**26**	–	13
3	Traid Bridge	**17**	12	2	9	**13**	9	10
4	Crookes Pt Staten Isl.	**37**	19	39	30	**16**	11	15
5	Coney Isl. Pt.	**6**	2	5	3	**11**	14	41
6	Sandy Hook Tip	**22**	–	–	29	**12**	10	27
7	Shrewsbury River	**48**	50	151	68	**21**	21	10

Note All measured data were collected during outgoing tides

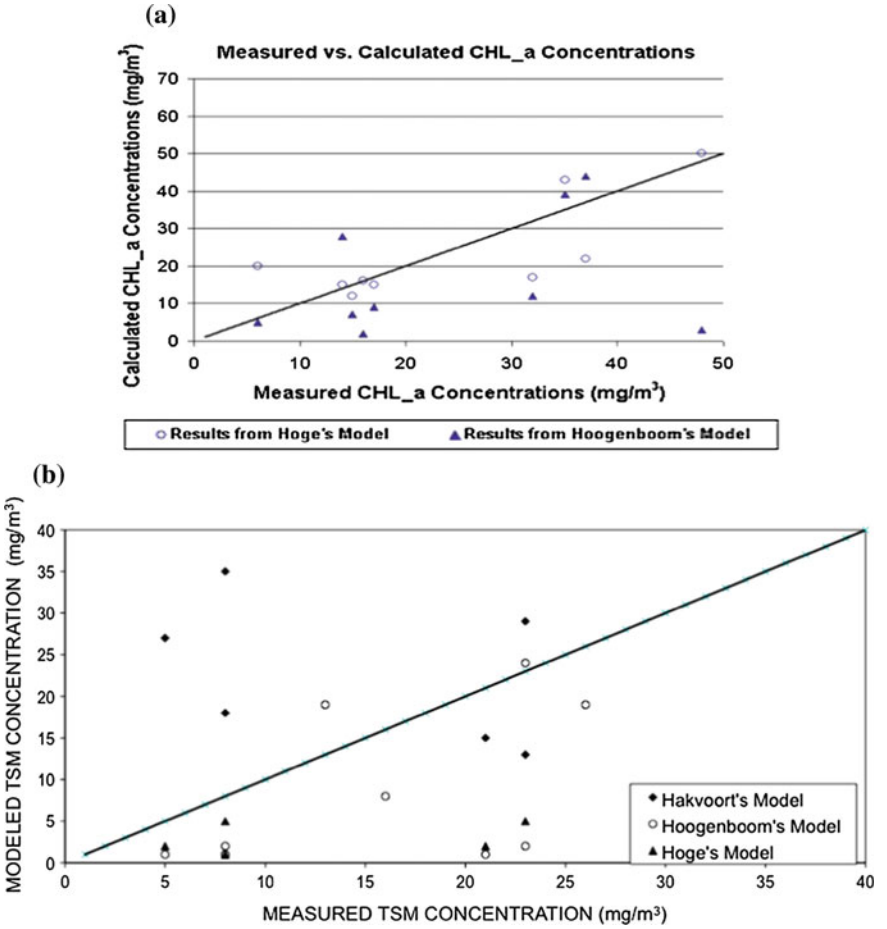

Fig. 6.3 **a** Comparison of measured and calculated TCHL concentration using inversion methods (Hoge and Lyon 1996; Hoogenboom et al. 1998) **b** Comparison of measured and calculated TSM concentrations using inversion and numerical methods (Hoge and Lyon 1996; Hoogenboom et al. 1998; Hakvoort et al. 2000)

6.1.3 Ratio Matrix Inversion (RMI) (Model #3)

To retrieve TSM concentration, we used a one-band semi-analytical algorithm based on the Gordon model (6.1) in which fixed values for CDOM and TCHL were used (Peters 2002):

$$TSM = \frac{-(a_w + a^*_{TCHL} TCHL + a^*_{CDOM} CDOM)\frac{R}{f} + b_{bw}\left(1 - \frac{R}{f}\right)}{a^*_{TSM}\frac{R}{f} - a^*_{bTSM}\left(1 - \frac{R}{f}\right)} \tag{6.12}$$

A ratio of the reflectance at about 702 nm over 675 nm can be related to the concentration of CHL (Peters 2002). Ratio matrix inversion algorithms have proven to be successful for estimating CHL. Needless to say that in many inland waters the reflectance, and thus the ratio of two bands, is significantly influenced by TSM and CDOM. As a result, the ratio algorithm may give ambiguous estimates of the concentration of CHL depending on the water composition in different geographic locations. Using the band ratio technique AVIRIS Image ratio map was generated to depict distribution of Chlorophyll-a Concentration in Raritan River and southern portion of the study area (Fig. 6.4).

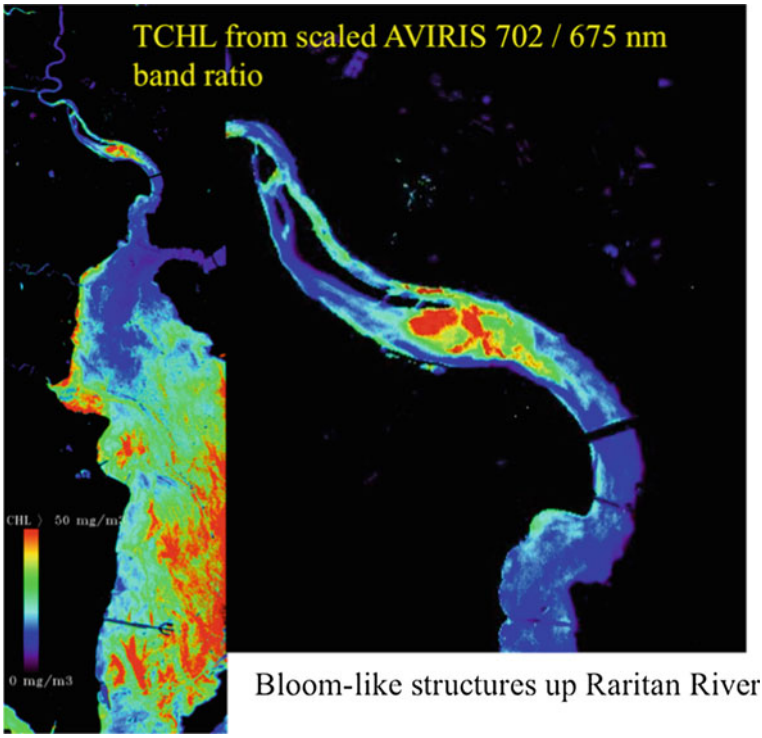

Fig. 6.4 AVIRIS band ratio map (702/675) depicting distribution of chl-a concentration along Raritan River and southern portion of Hudson/Raritan Estuary. *Note Right image* is the enlargement of the *upper segment* of the *Left image* representing the entire AVIRIS transect of the southern portion of the estuary (Raritan River to the *left* and Sandy Hook Bay to the *right* (Fig. 1.1)

6.1.4 *Other Retrieval Methods*

A. **Maximum A Posterior (MAP) Gibbs Sampling**

A novel Maximum A Posteriori (MAP) Gibbs Sampling approach was developed for estimation of phytoplankton absorption/concentration in Hudson/Raritan estuarine waters (Michalopoulou et al. 2009).

The method provides complete probability distributions instead of point estimates typically provided by conventional estimation approaches. The retrieval technique combines an analytical bio-optical model with statistical modeling for the formulation of posterior probability distributions of phytoplankton absorption, backscatter and CDOM absorption. Because of the computational burden entailed in calculating posterior distributions in a multi-dimensional parameter space, a Gibbs Sampler is employed for optimization. In contrast to other methods that typically provide point estimates of the unknown parameters, the proposed method, computing estimates of posterior distributions of the parameters, quantifies the uncertainty present in the problem and reveals correlation patterns among parameters. Maximization of the posterior distribution allows the calculation of a MAP estimate for phytoplankton absorption (aph). In practice, integration needs to be performed over more than two parameters: wavelengths at which phytoplankton absorption peaks are located, slope of CDOM absorption and backscattering. By selecting a statistical model for reflectance data and prior probability distributions in all unknown parameters, we computed the Posterior Probability distributions of the unknowns given data observations. The method was tested successfully on synthetic reflectance data and real in situ data measured in Hudson/Raritan Estuary of New York/New Jersey (Michalopoulou et al. 2009) (Figs. 6.5, 6.6 and 6.7).

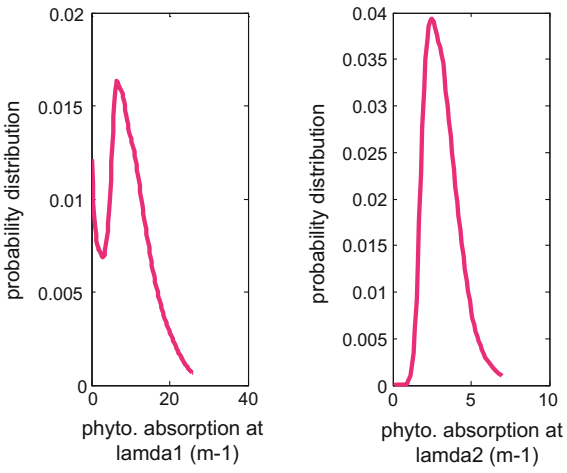

Fig. 6.5 Probability distributions of phytoplankton absorption

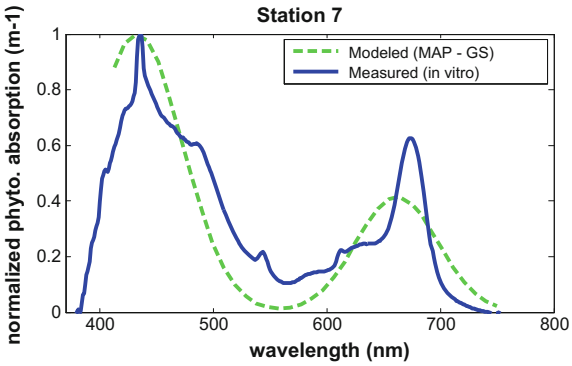

Fig. 6.6 Comparison of MAP-GS results to in vitro absorption estimates

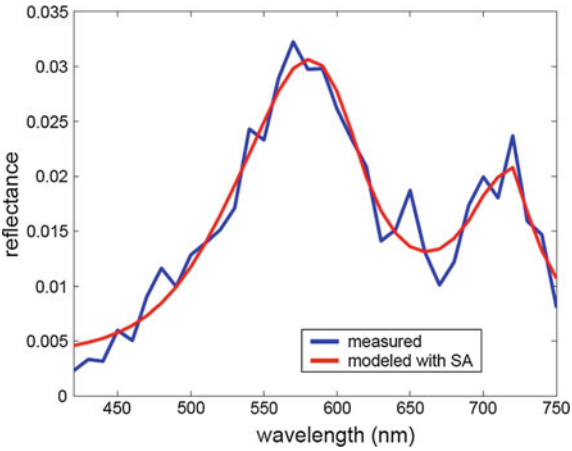

Fig. 6.7 Measured versus Modeled R(0−) for Station 7 in the study area (Fig. 1.1) with MAP-GS

B. The two-band and three-band algorithms

As part of the validation of retrieval techniques, the potential of universal applicability of the algorithms that use Red and NIR spectral bands (further NIR/Red algorithms) to estimate chl-a concentration in the Hudson/Raritan Estuary of NY/NJ was tested. To accomplish this goal, the following Eqs. (6.13) and (6.14) as well as advanced (recalibrated for this geographic location) models (Eqs. 6.15 and 6.16) were tested using a set of in situ measured reflectance and analytically determined chlorophyll-a concentration from water samples collected in the Hudson/Raritan Estuary. The details can be found in Bagheri et al. (2012).

Two-band algorithm with MERIS spectral band settings:

$$\text{Chl-a} = 25.28 \times (2\text{BM})^2 + 14.85 \times (\text{MERIS } 2\text{BM}) - 15.18 \quad (6.13)$$

Three-band algorithm with MERIS spectral band settings:

$$\text{Chl-a} = 315.50 \times (\text{MERIS } 3\text{BM})^2 + 215.95 \times (\text{MERIS } 3\text{BM}) + 25.66 \quad (6.14)$$

The following presents a case for using the NIR-Red algorithms as tools for estimating chl-a concentration in the Hudson/Raritan Estuary without the need for re-parameterization of the algorithms. This will be as a great asset in the real-time remote monitoring of chlorophyll-a concentrations in this region. The spectral locations and resolutions of the NIR and Red channels of MERIS proved to be adequate to capture the spectral variations in reflectance of optically complex turbid productive waters in a wide range of chl-a concentrations. Two-band and three-band NIR-Red algorithms have proven highly reliable for estimating chl-a concentration in turbid productive waters (Moses et al. 2009; Gitelson et al. 2011) (Fig. 6.8). They have yielded consistently accurate estimates of chl-a concentration when using MERIS data in different geographic locations including the Azov Sea and the Taganrog Bay, and field spectrometer/close range data with simulated MERIS bands taken over the Chesapeake Bay, Lake Kinneret (Yacobi et al. 2011), as well as several lakes in Nebraska (Gurlin et al. 2011).

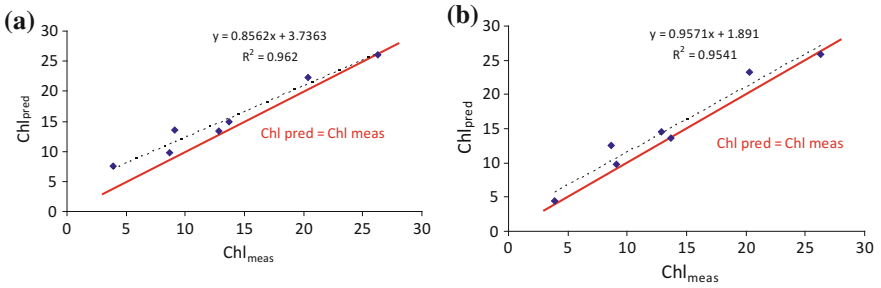

Fig. 6.8 Chlorophyll-a concentrations predicted by two- (**a**) and three-band (**b**) models calibrated using MERIS data taken over Azov Sea (Moses et al. 2009) plotted versus analytically determined chlorophyll-a concentrations in the Hudson/Raritan Estuary

Steps to reach such conclusion are as follows:

Firstly, the NIR-Red models with spectral bands (7, 9 and 10) of MERIS were calculated using measured reflectances in Eqs. 6.13 and 6.14. Then, they were compared with actual in situ chl-a concentrations. The relationships were very close for both models with determination coefficient above 0.94.

In second step, we predicted chl-a concentration in the Hudson/Raritan Estuary using algorithms established and calibrated with data taken over Nebraska lakes (Eqs. 6.13 and 6.14). Chl_{pred}, compared well with analytically determined, Chl_{meas}.

Both models estimated chl-a concentrations accurately (Table 6.2). 2-band model had the lowest MAE and RMSE.

In third step we predicted chl-a concentration in the Hudson/Raritan Estuary using algorithms established and calibrated for MERIS data taken over Azov Sea (Eqs. 6.15 and 6.16). Chl_{pred}, compared well with analytically determined, Chl_{meas}. Both algorithms predicted chl-a concentrations remarkably accurate (Table 6.2) and, as it was the case with Nebraskan Lakes, calibrated algorithms, two-band algorithm performed better than three-band algorithm.

Table 6.2 Mean normalized bias, mean absolute error, root mean square error of Chl-a estimation

Algorithm	MNB (mg m^{-3})	MAE (mg m^{-4})	RMSE (mg m^{-5})	Author
2 band NE	2.76	2.76	3.08	Gurlin et al. (2011)
3 band NE	2.82	2.82	3.46	Gurlin et al. (2011)
2 band MERIS	0.90	1.20	1.70	Moses et al. (2009)
3 band MERIS	−1.70	2.70	3.40	Moses et al. (2009)
2 band advanced	1.78	1.83	2.37	Gilerson et al. (2010)
3 band advanced	1.31	1.47	1.99	Gilerson et al. (2010)

Finally, we predicted chl-a concentration in the Hudson/Raritan Estuary using advanced models (Eqs. 6.15 and 6.16). Both models worked very accurately; 3-band model had slightly lower MAE (Fig. 6.9).

$$\text{Chl} - a = [35.75 \times 2BM - 19.3]^{1.124} \tag{6.15}$$

$$\text{Chl} - a = [113.36 \times 3BM + 16.45]^{1.124} \tag{6.16}$$

It is significant that the best fit functions between predicted and measured chl-a concentration (dashed lines) for both models were very close to 1 by 1 line (solid line) indicating that $Chl_{pred} = Chl_{meas}$. It is important to note that these advanced

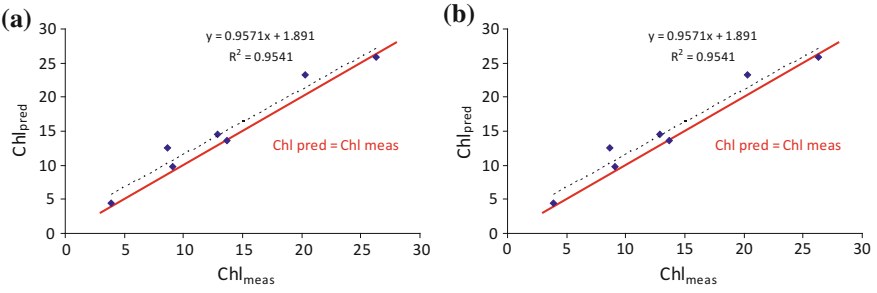

Fig. 6.9 Chlorophyll-a concentrations predicted by advanced two- (**a**) and three-band (**b**) models plotted versus analytically determined chlorophyll-a concentrations in the Hudson/Raritan Estuary

models, based on inherent optical properties of water constituents and water absorption, do not require any additional knowledge about inherent optical properties of water constituents. These results significantly promote the use of these MERIS-based two-band and three-band NIR-Red algorithms as potentially universal tools for estimating chl-a concentration in coastal and inland waters worldwide.

In conclusion, calculating Chl-a in turbid waters is one of the most difficult tasks in remote sensing research especially when concentrations of TSM and CDOM are high making such measurements more challenging. It is also quite difficult to measure accurate spectra given the equipment and their calibration under different conditions. Based on the literature search and research experience, the more advanced methods (matrix inversion etc) often fail because the measurements are difficult and the actual specific phytoplankton absorptions (SIOPs) are often unknown or difficult to measure. In addition to that, small errors in the SIOP readings may lead to significant errors in estimation of the retrieved (modeled) chlorophyll concentration. As long as we don't know this specific phytoplankton absorption for specific geographic location and time, the most reliable output can be obtained using simple methods (i.e., two-band and three-band algorithm) as briefly discussed above. This is a starting point in remote sensing analysis and can be expanded to more complicated methods if and when necessary and possible. The application of advanced methods requires understanding of the actual phytoplankton absorption spectrum much better combined with high standards in measurement systems, calibrations, protocols and quality control procedures.

The objective of this chapter was to present the results of applications of retrieval methods currently being used in order to estimate concentrations of optical water quality parameters. The proceeding chapters provides details on the establishing of the IOPs for this particular geographic location—Hudson/Raritan Estuary which is the prerequisite for any retrieval techniques.

References

Bagheri S, Dekker A. Optical Measurements of Nearshore Water Quality Conditions. In: International Conference on Coastal and Ocean Space Utilization, 11/4/2000. Cancun, Mexico (Invited Paper)

Bagheri S, Rijkeboer M, Pasterkamp R, Dekker AG (2000) Comparison of the field spectroradiometers in preparation for optical modeling. 9th Aviris Workshop, JPL, Pasadena CA, 2/23-2/27/2000

Bagheri S, Stamnes K, Li W (2001) Application of radiative transfer theory to atmospheric correction of AVIRIS data. In: Proceedings of the 10th JPL AVIRS Workshop, Pasadena, CA, pp 35–40

Bagheri S (2011) Nearshore water quality estimation using atmospherically correcected AVIRIS data. Remote Sens 3:257–269. doi:10.3390/rs3020257

Bagheri S, Rijkeboer M, Gitelson A (2012) Utility of field spectroradiometer data in chlorophyll-a estimation. Open Remote Sens J 5:90–95. doi:10.2174/1875413901205010090

Bagheri S, Peters S, Yu T (2005) Retrieval of marine water constituents from AVIRIS data in the Hudson/Raritan Estuary. Int J Remote Sens 26(18):4013–4027

Blank L (1980) Statistical procedures for engineering, management, and science. McGraw-Hill, Inc., New York, p 749

Buiteveld H (1990) A model for calculating secchi depth and extinction (in Dutch), Report 90.058. Rijkswarestaat. GIZA 23

Gilerson A, Gitelson A-A, Zhou J, et al (2010). Algorithms for remote estimation of chlorophyll-a in coastal and inland waters using red and near infrared bands. Opt Express 18: 24109–24125.

Gitelson A-A, Gurlin D, Moses W, Yacobi Y (2011) Remote estimation of chlorophyll-a concentration in inland, estuarine, and coastal waters. In: Weng Q (ed) Advances in environmental remote sensing: sensors, models, and applications. CRC Press, Taylor and Francis Group, Boca Raton, pp 449–478

Gons HJ, Burger-Wiersma T, Outten JH, Rijkeboer M (1992) Coupling of phytoplankton and detritus in a shallow atrophic lake (Lake Loosdrecht, The Netherlands), hydrobiology 23: 51–59

Gordon HR, Brown OB, Evans RH, Brown JW, Smith RC, Baker KS, Clark DK (1988) A semianalytic radiance model of ocean color. J Geophys Res 93:10909–10924

Gurlin D, Gitelson AA, Moses WJ (2011) Remote estimation of chl-a concentration in turbid productive waters—return to a simple two-band NIR-red model. Remote Sens Environ 115:3479–3490

Hakvoort JHM, De Haan H, Jordan RWL, Vos RJ, Peters SWM, Rijkeboer M (2000) Towards airborne remote sensing of water quality in the Netherlands: validation and error analysis. Second EASEL workshop on Imaging Spectroscopy

Hoge FE, Lyon PE (1996) Satellite retrieval of inherent optical properties by linear matrix inversion of oceanic radiance models: an analysis of model and radiance measurement errors. J Geophys Res 101:16631–16648

Hoogenboom HJ, Dekker AG, de Haan JF (1998) Retrieval of chlorophyll and suspended matter from imaging spectrometry data by matrix inversion. Can J Remote Sens 24(2):144–152

IOCCG (2002) Remote sensing of ocean colour in coastal, and other optically-complex, waters

Matthews MW (2011) A current review of empirical procedures of remote sensing in inland and near-coastal transitional waters. Int J Remote Sens 32(21):6855–6899

Michalopoulou Z-H, Bagheri S, Axe L (2009) Bayesian Estimation of Optical Properties of Nearshore Estuarine Waters: A Gibbs Sampling Approach. IEEE Trans Geosci Remote Sens. November 16, 2009 at 20:02 from IEEE Xplore

Michalopoulou Z-H, Bagheri S, Axe L (2010) Bayesian estimation of optical properties nearshore estuarine waters: A Gibbs Sampling Approach. IEEE Transactions on Geoscience and Remote Sensing 48(3): 1579–1587. doi:10.1109/TGRS.2009.2028689

Moses W-J, Gitelson A-A, Berdnikov S, Povazhnyy V (2009) Satellite estimation of chlorophyll-a concentration using the red and NIR Bands of MERIS—the Azov Sea case study. IEEE Geosci Remote Sens Lett 6:845–849

Peters SWM (2001) Analytical inversion methods for water quality parameter determination from remotely observed spectra. Institute for Environmental Studies, Vrije Universities, Netherlands

Peters SWM (2002) Analytical inversion methods for water quality parameter determination from remotely observed spectra. Institute for Environmental Studies, Vrije Universiteit, Netherlands

Yacobi YZ, Moses WJ, Kaganovsky S, Sulimani B, Leavitt BC, Gitelson AA (2011) NIR-red reflectance-based algorithms for chlorophyll-a estimation in mesotrophic inland and coastal waters: Lake Kinneret case study. Water Res 45:2428–2436

Yu T (2005) Utility of remote sensing data in retrieval of water quality constituent concentration in coastal waters of New Jersey. PhD dissertation, Department of Civil and Environmental Engineering, NJIT

Chapter 7
Conclusion

Abstract Considering the significance of water quality for drinking, irrigation and industry, availability of accurate and sufficient water quality data is necessary for water quality management decisions. Remotely sensed data can help to derive water quality variables such as the type and size of suspended particles, toxic algal blooms, and other phytoplankton species that serve as a marker of eutrophication. With increasingly sophisticated sensors, better data and improved algorithms, water quality parameters—phytoplankton can be accurately determined using ocean color data. Information on the role of phytoplankton in the exchange of carbon dioxide between ocean and atmosphere is important since algae have the potential both as an energy source and as a way to deal with global warming.

Keywords Climate Change · Sea level rise · Carbon cycle · Harmful algal bloom · SeaWIFS · MODIS · AVIRIS · HyspIRI · TIR · VSWIR

Balancing environmental and socioeconomic goals is an extremely challenging task and is more complicated by impacts of climate change including sea-level rise, increasingly strong storms, and a host of emerging threats. Climate change affects temperature, precipitation, surface radiation, humidity, winds and sea levels. These changes could affect runoff, groundwater levels and snowmelt, as well as the quantity and quality of water available for drinking, recreation, agriculture and industrial and energy production. The warmer temperatures associated with climate change are predicted to decrease dissolved oxygen levels, increase contaminant load to water bodies, reduce stream and river flows, foster algal blooms, and increase the likelihood of saltwater intrusion near coastal regions.

Climate change impacts to water quality are occurring over a very dynamic range. Increases in temperature due to global climate change can contribute to important changes in water quality parameters—phytoplankton which play an important role in the exchange of carbon dioxide between ocean and atmosphere. This is considered to be a major pathway of carbon cycling in the ocean and thus essential to global change studies. Since global temperatures are strongly correlated with green house gas concentrations, remote sensing data can be used to investigate

S. Bagheri, *Hyperspectral Remote Sensing of Nearshore Water Quality*,
SpringerBriefs in Environmental Science, DOI 10.1007/978-3-319-46949-2_7

the role of phytoplankton in the exchange of carbon dioxide between ocean and atmosphere. Because of its use of CO_2, phytoplankton may play an important role in mediating the Earth's climate in general and in particular the consequences of changes in NY/NJ metropolitan area can be significant. Since phytoplankton depends upon specific conditions for growth, they frequently become the first indicator of a change in their environment. Phytoplankton, as revealed by ocean color images, frequently show scientists where ocean currents provide nutrients for plant growth and where subtle changes in the climate-warmer or colder more saline or less saline-affect phytoplankton growth. Considering the significance of water quality for drinking, irrigation and industry, availability of accurate and sufficient water quality data is necessary for water quality management decisions. Monitoring water quality for large number of inland waters and extensive coastal regions has never been possible by shipboard samplings. Such point samplings cannot provide a comprehensive view of water quality throughout the region. Remote sensing images with the synoptic coverage can give information about the coastal zones, estuaries/rivers and inland waters more cost effective and less labor intensive. Remote sensing can help to derive water quality variables such as the type and size of suspended particles, toxic algal blooms, and other phytoplankton species that serve as a marker of eutrophication. When combined with ground truthing remote sensing is effective in detecting and quantifying harmful algal blooms (HABs) including the specific biotic responses to human and climatic perturbations.

Remote sensing data calibrated with in situ data provides information on water quality issues as related to global change. It is worth mentioning that measuring this indicator suite often requires field teams to spend hours on boats to collect data from discrete locations, which ultimately will not provide complete information on the spatial and temporal variations of environmental processes in an estuary or a lake. Although this protocol will continue to be necessary for various reasons, water-quality monitoring using remote-sensing technologies may provide the most practical way to ensure that management practices, at temporal and spatial scales relevant to environmental managers and the general public, are achieving sustainability. With increasingly sophisticated sensors, better data and improved algorithms, water quality parameters—phytoplankton can be accurately determined using remote sensing ocean color data. Information on the role of phytoplankton in the exchange of carbon dioxide between ocean and atmosphere is important since algae have the potential both as an energy source and as a way to deal with global warming. Currently, both governments and private companies are exploring the use of algae as an alternative fuel. Since algae are among the fastest growing plants in the world, with about 50 % of their weight being oil, algae has the potential both as an energy source and as a way to deal with global warming. This research is timely since biofuels made from algae are the next big thing on the alternative energy horizon (Science 2/3/09).

The intent of this monograph was to test the utility of remote sensing—ocean color data in visualization and their integration with bio-optical and statistical methods to enhance our understanding of ecosystem responses and estimation of water quality conditions to manage eutrophication. The long term goal is to

ultimately link global scale processes with local environmental and resource problems to assess the impacts of climate change on freshwater/estuarine systems in NY/NJ metropolitan areas. The results of this research demonstrate that the high spatial/spectral resolution of the AVIRIS data was advantageous for coastal water quality retrieval, because coastal waters usually have high spatial and temporal variations. The AVIRIS hyperspectral data provided an opportunity to develop algorithms based on the different spectral reflectances characterizing aerosol and water constituents. This can be used as a basis for distinguishing between atmospheric and oceanic effects and to set the estimated turbidity for each region within the image for retrieval of water constituents. Development of a robust algorithm for simultaneous retrieval of atmospheric aerosol optical properties, chlorophyll concentration and colored dissolved organic matter is a very challenging task. Nevertheless, such an algorithm is needed to make progress in this area.

Currently the only ocean color sensors, SeaWiFS and MODIS, deliver repetitive coverage at 1 km spatial resolution do not have the optimal bands for the complex nearshore waters encountered here. Atmospheric correction model—Tafkaa results demonstrate physically realistic reflectance output which represents not only an improved atmospheric correction, but also a more appropriate foundation to address issues of water column correction and spectral analysis of the nearshore water properties. Although satellite sensors with several elements (e.g., data continuity/consistency, revisiting time, costs) would better support global climate change studies than airborne sensors but the coastal zones monitoring requires spatial/spectral resolution that satellite do not always provide. The airborne (i.e., AVIRIS) applications provide other elements that support the exploitation of remote sensing of coastal zones. E.g., scheduled overflights in times of the years where harmful algal blooms (HABs) are expected to assess the spatial distribution patterns and pigment composition, or algorithms development in order to be ready when water color sensors (i.e., HyspIRI) with higher spatial resolution will be available. The data from HyspIRI will be used for a wide variety of studies primarily in the Carbon Cycle and Ecosystem and Earth Surface and Interior focus areas. The HyspIRI mission includes a global mapping imaging spectrometer and multispectral thermal instrument. The imaging spectrometer delivers complete measurements from 380 to 2500 nm at 10 nm sampling at high SNR for the entire terrestrial and coastal regions of the Earth every 19 days with 60 m sampling. The multispectral thermal instrument measures the same area at the same spatial scale in 8 bands between 3 and 12 microns every 5 days. A real-time direct broadcast of a subset of measurements are provided by the intelligent payload module The combined use of HyspIRI TIR and VSWIR will provide significant insight on biological and biogeochemical controls by small-scale physical processes, and how these translate into small-scale ecosystem changes, globally (NASA/JPL).

Hyperspectral observations from mini-satellites and drones is a real possibility in the future especially data collection from drones which will greatly benefit from the experience we have had with airborne hyperspectral instruments such as AVIRIS. Using library spectra of different phytoplankton pigments will explore the extent to which phytoplankton species differentiation can be retrieved. The library spectra

can be used as a management tool for monitoring water resources and provides a baseline on the characteristics of algal blooms important in climate/global change studies.

The results of this work will be applicable to other coastal areas where the majority of the global population lives and the health of the coastal water quality is becoming a challenging issue to be recognized and dealt with. The final products in form of image maps representing the spatial and temporal distributions of water quality parameters (i.e., chlorophyll concentration as indication of algal blooms) comprise an integral part of the geographic information system (GIS) for monitoring and management of the water quality of the estuary.

Reference

HyspIRI (http://hyspiri.jpl.nasa.gov)

Index

S. Bagheri, *Hyperspectral Remote Sensing of Nearshore Water Quality*,
SpringerBriefs in Environmental Science, DOI 10.1007/978-3-319-46949-2